The development and application of a unmanned aerial vehicle laser scanning system for forest management

by

Luke Oliver Wallace

BSurvSpSc (Hons)

School of Land & Food

Submitted in fulfilment of the requirements for the Degree of Doctor of Philosophy

University of Tasmania
April, 2014

This thesis contains no material which has been accepted for a degree or diploma by the University or any other institution, except by way of background information and duly acknowledged in the thesis, and to the best of my knowledge and belief no material previously published or written by another person except where due acknowledgement is made in the text of the thesis, nor does the thesis contain any material that infringes copyright.

Luke Wallace

2 April 2014

Statement of Co-Authorship

The following people and institutions contributed to the publication of the work undertaken as part of this thesis:

Luke Wallace, School of Geography and Environmental Studies, University of Tasmania
Arko Lucieer, School of Geography and Environmental Studies, University of Tasmania
Christopher Watson, School of Geography and Environmental Studies, University of Tasmania
Darren Turner, School of Geography and Environmental Studies, University of Tasmania
Robert Musk, Forestry Tasmania

Author details and their roles:

Conference Paper 1 (Ch. 2): Wallace (80 %), Lucieer (10 %), Turner (5 %), Watson (5 %)
All authors contributed to the idea and its development; Wallace performed all data processing, analysis and writing; Lucieer and Watson contributed editorial advice.

Paper 2 (Ch. 3a): Wallace (85 %), Lucieer (5 %), Watson (5 %), Turner (5 %)
All authors contributed to the idea and its development; Wallace and Turner conducted the field work; Wallace performed all data processing, analysis and writing; Lucieer and Watson contributed editorial advice.

Conference Paper 2 (Ch. 3b): Wallace (90 %), Lucieer (5 %), Watson (5 %)
All authors contributed to the idea and its development; Wallace conducted the field work; Wallace performed all data processing, analysis and writing; Lucieer and Watson contributed editorial advice.

Paper 3 (Ch. 4): Wallace (90 %), Lucieer (5 %), Watson (5 %)
All authors contributed to the idea and its development; Wallace conducted the field work; Wallace performed all data processing, analysis and writing; Lucieer and Watson contributed editorial advice.

Paper 4 (Ch. 5): Wallace (85 %), Musk (10 %), Lucieer (5 %)
All authors contributed to the idea and its development; Wallace conducted the field work; Wallace performed all data processing, analysis and writing; Lucieer and Musk contributed editorial advice.

Paper 5 (Ch. 6): Wallace (90 %), Watson (5 %), Lucieer (5 %)
Wallace contributed to the idea and its development; Wallace conducted the field work; Wallace performed all data processing, analysis and writing; Watson and Lucieer contributed editorial advice.

We the undersigned agree with the above stated "proportion of work undertaken" for each of the above published (or submitted) peer-reviewed manuscripts contributing to this thesis:

Candidate: **Luke Wallace** (7/10/2013)

Arko Lucieer (7/10/2013)

Darren Turner (7/10/2013)

Christopher Watson (9/10/2013)

Robert Musk (10/10/2013)

Luke Wallace

2 April 2014

Abstract

Airborne Laser scanning (ALS) has emerged as an important tool for providing cost-effective characterisation of the 3D structure of forests over large areas. As data resolution is often inversely proportional to coverage area, laser scanning from alternative platforms has been a recent subject of investigation. This thesis advances this exploration by investigating the use of Unmanned Aerial Vehicles (UAVs) as a laser scanning platform (UAVLS) for forest inventory purposes. The design of a small laser scanning system consisting of an automotive laser scanner, a Micro-Electro-Mechanical Systems based Inertial Measurement Unit (IMU), a dual frequency Global Positioning System (GPS) receiver and a downward pointing video camera for use on-board an Oktokopter multi-rotor platform is described. A novel algorithm was developed for the direct georeferencing of laser returns utilising a vision aided GPS-IMU sigma-point Kalman smoother. Evaluating improvements due to the inclusion of vision, both stochastically and in practice, it is demonstrated that an accuracy similar to modern ALS systems and adequate for forest inventory measurements can be achieved (34 cm horizontal, 14 cm vertical RMSE).

Two 4 year old Eucalyptus plantations in south east Tasmania were selected as the primary study area in order to assess the utility of the UAVLS system to map and assess change in key inventory metrics. Analysis of the point clouds captured with different flying parameters indicated that the flying height should be restricted to less than 50 m above ground level and scan angle restricted to $\pm 30^{\circ}$. A survey method within these restraints and utilising overlapping transects was designed to provide cost-effective and repeatable observations of the 3D structure of the plot sized areas (500 m^2). It was found that the maximum deviations of plot level descriptive statistics captured in repeat multiple flights were less than 3%.

Investigating the accuracy and repeatability of individual tree level metrics derived from the high density UAVLS point clouds (up to 300 points/m^2) using five different automatic tree detection and delineation methods highlighted that increased data resolution provided more detail in the characterisation of individual trees. The best performing method, which utilised both the CHM and the point cloud, resulted in 98% of trees being repeatedly and correctly delineated from the point cloud. Tree height (absolute mean deviation of 0.35 m), location (0.48 m), crown area (3.3 m^2) and canopy closure (2.3%) extracted from the delineated tree segments were observed with higher repeatability and better efficiency than that currently achieved using modern field techniques. Subsequent

analysis of change following the application of sequential silvicultural treatments showed that UAVLS is capable of detecting pruning rates of between 96 and 125% of the true pruning rate.

This thesis demonstrates that UAVLS offers unprecedented temporal and spatial resolution, enabling the determination of highly accurate forest inventory metrics and their change over time. In comparison with in situ field techniques, UAVLS offers more efficient and detailed characterisation of the 3D structure of forests.

Acknowledgements

Firstly, I thank my supervisors Dr Arko Lucieer, Dr Christopher Watson, Dr Robert Musk and Dr Jon Osborn. I am grateful for the opportunity under the supervision of people with both knowledge and passion for the subject area. Both Chris and Arko provided guidance, knowledge, enthusiasm, patience and advice at all stages of the preparation of this thesis. Although I probably did not draw on Jon and Rob's knowledge as much as I should have, they were always available when I required any guidance or advice.

I also thank Darren Turner and Tony Veness. I am indebted to both for providing the technical expertise in order to make this thesis fly (well the laser scanning system anyway). I acknowledge Forestry Tasmania for providing field support and access to the study areas used in this project. In particularly David McElwee who provided support in the collection of all in-situ field data. I would also like to aknowledge the Winifred Violet Scott Trust for funding support. The Australian Antarctic Division is acknowledged for providing workshop time in constructing the sensor mount.

Thank you to my parents Stephen and Valerie, the support and privileges that you have given me until this day can not be stressed enough as without them the opportunities I had leading up to and undertaking this project would not have be possible. Thanks also to my other family members, friends and colleagues.

Finally, I thank my wife Daisy for everything. You have supported and encouraged me through all stages of my Ph.D, both good and bad. I feel greatly privileged to have you as both a friend and a partner and I look forward to whatever is next in our lives together.

Table of Contents

List of Tables

List of Figures

1 | Introduction

1.1 Background

1.1.1 Silviculture of *Eucalyptus* forests

To achieve sustainability in the provision of timber and veneer products from *Eucalyptus* plantations, forest managers are required to evaluate the short and long term economic and ecological consequences of silvicultural actions based on knowledge of current and predicted forest conditions. Decisions on the timing and extent of treatments are influenced by current forest characteristics, site quality, and responses throughout a rotation (Forrester et al. 2013a). The impact of an incorrect application of a treatment can lead to economically non-viable production of solid wood products in *Eucalyptus* plantations (Innes et al. 2008).

Typical management for timber and veneer production in Australian plantations involves consistent planting densities and the application of fertilisers as well as pruning and thinning treatments (Wood et al. 2009). The high cost and potential adverse impacts of silvicultural treatments within *Eucalyptus* forests has led to significant and ongoing research into best practice for the management of many species (Medhurst and Beadle 2001; Pinkard 2002; Cassidy et al. 2012; Alcorn et al. 2013; Forrester et al. 2013b). The overall aim of these studies has been on improving product quality and yield and reducing rotation periods while managing the impact on other associated values.

Thinning and pruning can have a significant impact on *Eucalyptus* plantation growth, as well as on the log and wood properties (Forrester et al. 2013b). Thinning, for example, can on some sites double the growth of selected crop trees relative to those in un-thinned stands (Medhurst and Beadle 2001). Typical planting rates of *Eucalyptus* forests are therefore significantly higher than the targeted rate at final harvest. In Tasmania, for instance, *Eucalyptus nitens* and *globulus* are planted at a rate of 1100 stems/ha for a final harvest rate of 300 to 350 stems/ha (Wood et al. 2009). The application of thinning treatments at various stages throughout the rotation encourages growth and allows the use of the thinned stems as pulp, contributing to the economic value of the activity.

As many *Eucalyptus* plantation species have little natural pruning ability, the production of quality timbers requires timely pruning of green branches for knot-free (clear) wood

production (Gerrand et al. 1997). Ideally, pruning should be carried out without reducing overall stem growth and it has been demonstrated that this can be achieved while removing as much as 40% of the green crown length (Pinkard and Beadle 1998). The timing of pruning is, however, crucial in achieving this outcome. For instance, Pinkard (2002) showed that pruning in *Eucalyptus nitens* should occur at the time of canopy closure. Pruning prior to closure was shown to significantly reduce volume growth, while pruning after closure allows branch decay to occur, which reduces the overall quality of the timber.

In order to mitigate potential risks and optimise sustainability outcomes, decisions on pruning and thinning need to be informed using the most complete, accurate and current information on the state of the forest. Current practice to inform these activities involves the use of growth models or limited observations of individual trees and subjective estimates of overall stand characteristics such as canopy closure. Furthermore, the ability to ensure that plantation management activities are performed as prescribed is limited due to the cost of surveys and limited availability of technology to aid in this monitoring.

1.1.2 Remote sensing of forested environments

Forest inventory supports strategic and operational forest management, extending to ecological conservation, fire risk mitigation, and carbon accounting (Wulder et al. 2012; Rosenqvist et al. 2003). These activities require inventories to be informed with increasingly timely and accurate forest inventory information. To achieve these requirements, modern inventories draw on data from a variety of sources, including field observations, growth and mortality models, and remote sensing.

Modern remote sensing tools and techniques provide foresters with a variety of methods and data sources to determine forest inventory metrics at a variety of scales (i.e. measurements of individual trees or estimates at the stand and forest levels). The ability to provide accurate inventory estimates across large areas has proved paramount to addressing the increasing environmental concerns as well as achieving and evaluating effective sustainable forest management strategies (Gillis 2001; Corona et al. 2003).

A wide range of sensors have been evaluated and deployed to capture forest information. Imagery captured from airborne, satellite or terrestrial platforms, for example, is routinely used to evaluate forest extent, health, as well as species and age composition

(Clark et al. 2005; Larsen et al. 2011). The choice of sensor and platform is dependent on the spatial scale of interest (i.e. tree, plot or stand level), the cost of acquisition, and the characteristics of the sensor, such as resolution (including temporal, spatial, radiometric and spectral aspects) and spatial extent (Coops et al. 2007).

Laser Scanning is a remote sensing technology that has been rapidly adopted for use within the forest industry. The motivation for this adoption is the ability of laser scanners to provide more accurate information on the biophysical properties of a forest through the direct measurement of inherent three dimensional structures (Maclean and Martin 1984; Næsset 1997; Hyyppä et al. 2008). Airborne Laser Scanning (ALS) has been the primary mode of data capture, resulting in the development of automatic routines to extract detailed forest attributes from this data source. Internationally and within Australia the forest industry has been an early adopter of the ALS technology. This is highlighted by recent studies into the use of new ALS technologies that have the ability to collect full waveform (Xing et al. 2010) or multispectral data (Morsdorf et al. 2009) developed specifically for use in forests.

Research into the use of ALS data for forestry purposes has primarily focused on characterisation of entire forest stands to produce relevant management outcomes (Wulder et al. 2012). The use of area-based analysis, involving the use of statistical inference based on the height and density distributions of ALS returns, has allowed forest conditions to be characterised across many forest types (Næsset 2002; Holmgren and Persson 2004; Magnussen et al. 2012; McRoberts et al. 2012). The proven accuracy of area-based techniques allows the derived forest metrics to be routinely adopted as a standard source of inventory information. To achieve this accuracy, however, field measurements are required for training and model calibration purposes (Wulder et al. 2012; Hyyppä et al. 2012a). These measurements are required to represent the full range of variability within the forest and be from plots that are sufficiently large to avoid edge effects and to minimize georeferencing errors (Magnussen et al. 2010; Frazer et al. 2011).

Improvements in the precision and resolution of ALS data has allowed high resolution sampling strategies to be considered, and the individual tree to become a more feasible object of analysis. The focus of current research efforts into tree level analysis is the development of repeatable and accurate automatic extraction of individual tree metrics through the development of new algorithms (Reitberger et al. 2009; Li and Guo 2012; Ferraz et al. 2012). Although some of these techniques have produced encouraging results, the accuracy of metrics such as tree location, height, and crown width is highly dependent on the resolution of the captured dataset as well as the spatial distribution

of the trees (Hyyppä et al. 2008; Vauhkonen et al. 2008). As such, individual tree level analysis from ALS data is not commonly deployed within the forest industry because the required accuracies are not reliably met (Peuhkurinen et al. 2011; Vastaranta et al. 2011).

ALS provides a means to collect rich and reliable vegetation metrics over large areas, however, high survey deployment costs, the continued requirement for field measured calibration plots and short flying seasons in some areas has restricted the on-demand use of ALS surveys in support of key management decisions. Consequently static and mobile terrestrial laser scanners have been investigated for their potential to collect high resolution forest information. In contrast to the data collected by airborne sensors, the woody components of the canopy are often visible within the data collected by terrestrial sensors, allowing for the objective and reproducible measurement of a number of key tree-level metrics, such as DBH and crown length, used in the assessment of timber properties. Static Terrestrial Laser Scanners (TLS) provide an unprecedented level of detail in describing the stem, branch and leaf distribution of individual trees. TLS instruments are, however, highly affected by occlusions and multiple viewing points are required in order to capture an area of interest.

Deploying the laser scanner on-board a moving vehicle or using hand-held instrumentation overcomes the small area restriction of TLS. Mobile Laser Scanners (MLS) have shown potential in deriving individual tree level parameters (Lin et al. 2012). In comparison to airborne systems, MLS requires an unobstructed adequate sky-view for data collection and point cloud georeferencing. The development of sampling strategies for the collection of vegetation structure with MLS technology therefore still requires further investigation. The terrain in many production forests is often characterized by steep slopes and thick understory, which may be expected to limit the use of this technology to urban based forestry, as demonstrated in Holopainen et al. (2013).

1.1.3 UAV remote sensing of forested environments

The use of Unmanned Aerial Vehicles (UAVs) as remote sensing platforms is becoming increasingly popular for environmental monitoring purposes (Anderson and Gaston 2013). There are a wide variety of UAV platform designs, such as small fixed-wing planes, single rotor and multi-rotor helicopters, being deployed to collect remotely sensed information. Although many UAV classification schemes exist, distinctions between platforms can primarily be based on weight, range, and payload carrying capacity (see Watts et al. (2012)

for example). Large and medium UAVs (500 km range and 10 to 200 kg payload) operate in a similar spectrum to manned aircraft with large upfront costs and requiring complex ground operations. Mini-UAVs (< 10 km range and up to 5 kg payload) provide low and slow flight capabilities and allow for the capture of highly detailed information. Multi-rotor UAVs in this category are the focus of this thesis.

Mini-UAVs represent a low-cost platform that, when equipped with high quality sensors, can produce data with an unrivalled combination of spatial and temporal resolution. The fine-scale data captured by mini-UAVs is being used in a growing number of environmental monitoring applications (e.g. Berni et al. 2009; Anderson and Gaston 2013). Investigations into the use of UAVs for forest measurement purposes has involved the deployment of a variety of sensors (Horcher and Visser 2004; Dunford et al. 2009; Jaakkola et al. 2010; Dandois and Ellis 2013). The use of multi- and hyper- spectral imagery captured from these platforms has the potential to provide tree level mapping of tree species and health. Berni et al. (2009) used UAVs as a platform for monitoring vegetation health in orchards using thermal and multispectral sensors, highlighting that UAVs allow the optimum spatial and spectral resolutions for most crop stress-detection applications as well as overcoming issues with high frequency revisit times.

Deriving inventory metrics relies on measuring three dimensional vegetation structure. Recently developed image processing techniques such as Structure-from-Motion (SfM) present opportunities to capture vegetation structure from high spatial resolution imagery. Dandois and Ellis (2013) highlighted the application of this technology to the forest industry, showing that 3D structural parameters such as tree height and spectral characteristics can be estimated from SfM point clouds. One drawback of the SfM technique is that the 3D structure of the forest is not fully described particularly with increased stocking rates. Dandois and Ellis (2013) showed that, in densely vegetated areas, observations of terrain height can differ by up to 5 m. These errors directly propagate into the derivation of forest metrics and so the use of this technique in plantation forests is therefore unlikely to be feasable if accurate terrain information from an alternate source is not available.

To capture a more complete description of the 3D structure of plantation forests from a UAV, the deployment of a laser scanning instrument is required. Several examples of UAV Laser Scanners (UAVLS) have been described in the literature (Nagai et al. 2009; Eisenbeiss 2009; Jaakkola et al. 2010). The Finish Geodetic Institutes's sensei system outlined in Jaakkola et al. (2010) and Lin et al. (2011) highlight the first example of a UAVLS designed specifically to be deployed for the collection of forest metrics. The

potential of such systems is highlighted in Jaakkola et al. (2010), showing increased point density of the UAV derived point cloud enables individual tree heights to be measured with higher accuracy than from full-scale airborne LiDAR.

The platform deployed in Jaakkola et al. (2010) (relatively large single rotor helicopter) has limited ability to perform surveys following predefined flight paths to achieve optimal data capture. The recent miniaturisation of Global Positioning Systems (GPS), Inertial Measurement Units (IMUs) and embedded computers have allowed alternative platforms, such as multi-rotor helicopters, to be considered for the collection of remotely sensed data. Although these platforms typically offer reduced payload capacity, the increased precision in control, combined with reliable low-cost autopilots should allow for more rigorous sampling designs. However, the accuracy of the lightweight sensors that have not been designed for mapping purposes is considerably lower than their full-scale counterparts.

1.2 Problems and objectives

1.2.1 Problem statement

Currently, field observations are used in direct support of managements decisions. Due to the low efficiency and high cost per unit area these observations are often limited in sample size and can vary subjectively based on the experience of the field team. Laser scanners deployed on-board UAV platforms provide an option to meet the demands of high temporal and spatial resolution required for the collection of precise on-demand forest metrics. For forest management purposes, a feasible UAVLS system should provide low-cost surveys that meet or exceed accuracy requirements and data collection efficiency of current field based measurement techniques. Due to technological restrictions, research into UAVLS has focused on sensors deployed on medium sized platforms capable of carrying more accurate sensors. The up-front cost and complex requirements for operational use currently restrict the potential of such platforms for deployment as operational forest measurement tools.

Low-cost, lightweight sensors deployed on mini-UAVs may have the potential to overcome the deficiencies of current field-based sampling and to achieve the spatial and temporal resolution required by forest managers, at an economically viable cost. The integration of these sensors present a number of significant hurdles in the development of a UAVLS system to provide accurate measurements of vegetation structure. Hardware integration and on-board sensor control systems need to be designed in such a way to allow large data streams from each of the standalone sensors to be logged and precisely synchronised. Further, the development of new data processing and observation fusion algorithms is required in order to minimises the typically higher sources of error within these sensors and to achieve high georeferencing accuracies.

The properties of lightweight laser scanners and the low flying height of UAVs is likely to cause significant differences in the properties of the point clouds produced, in comparison to ALS systems. Increases in resolution and changes in the vertical distribution of laser returns are likely to present new challenges in the extraction of forest metrics from UAVLS generated point clouds. Significant investigation and development of existing methods and new algorithms are required in order to ensure that forest metrics are reliably estimated from data collected with UAVLS systems.

1.2.2 Objectives

The aim of the work reported in this thesis is to develop a UAVLS platform and associated methods to extract forest metrics capable of supporting and enhancing forest management practices. The work focuses on the high temporal and spatial resolution of UAV remote sensing and 3D structure characteristics derived from laser scanning data. The specific objectives of the research are:

Objective 1- Assess existing approaches and technologies for collecting georeferenced laser scanner data from a mini-UAV and adapt these methods to provide a workflow for accurately georeferencing the data captured by UAVLS; specifically to:

- develop an error budget based on available technologies for direct georeferencing of UAVLS data in order to determine if the deployment of a UAVLS system on a mini-UAV is feasible considering the payload constraints and accuracy requirements;
- develop and apply a new methodology to overcome any constraints of miniaturised technology identified in the error budget to accurately georeference UAVLS data;
- rigorously assess the geometric accuracy of this methodology in typical field conditions.

Objective 2- Adapt existing and develop new methods for processing very high resolution point clouds generated by a UAV platform to accurately assess the structural attributes of typical Tasmanian *Eucalyptus* plantation forests at the individual tree level; specifically to:

- determine the flying conditions required to optimally collect UAVLS point clouds over forested environments;
- assess existing techniques to delineate individual tree segments from the collected UAVLS data;
- derive key inventory metrics from these segments and investigate the requirements of data resolution for the accurate estimation of these metrics;
- quantify the accuracy and repeatability of these metrics.

Objective 3- Determine the capabilities of the UAVLS for measuring change in forest conditions; specifically to:

- assess if change induced by key silvicultural activities, such as pruning, can be

monitored through changes in metrics measured with UAVLS technology

- assess the accuracy achievable in monitoring these activities.

1.3 Thesis structure

The structure of this thesis is by publication, and therefore Chapters 2-6 comprise publications that have been published in peer-refereed literature or submitted for review. The research objectives are addressed by each of the publications as illustrated in Figure 1.1. Each chapter separately addresses the relevant literature and includes detailed methods, results, discussions and conclusions. A conclusion chapter (ch. 7) summarises the overall outcomes and contributions of the thesis in context of the objectives and provides an overview of limitations and future work.

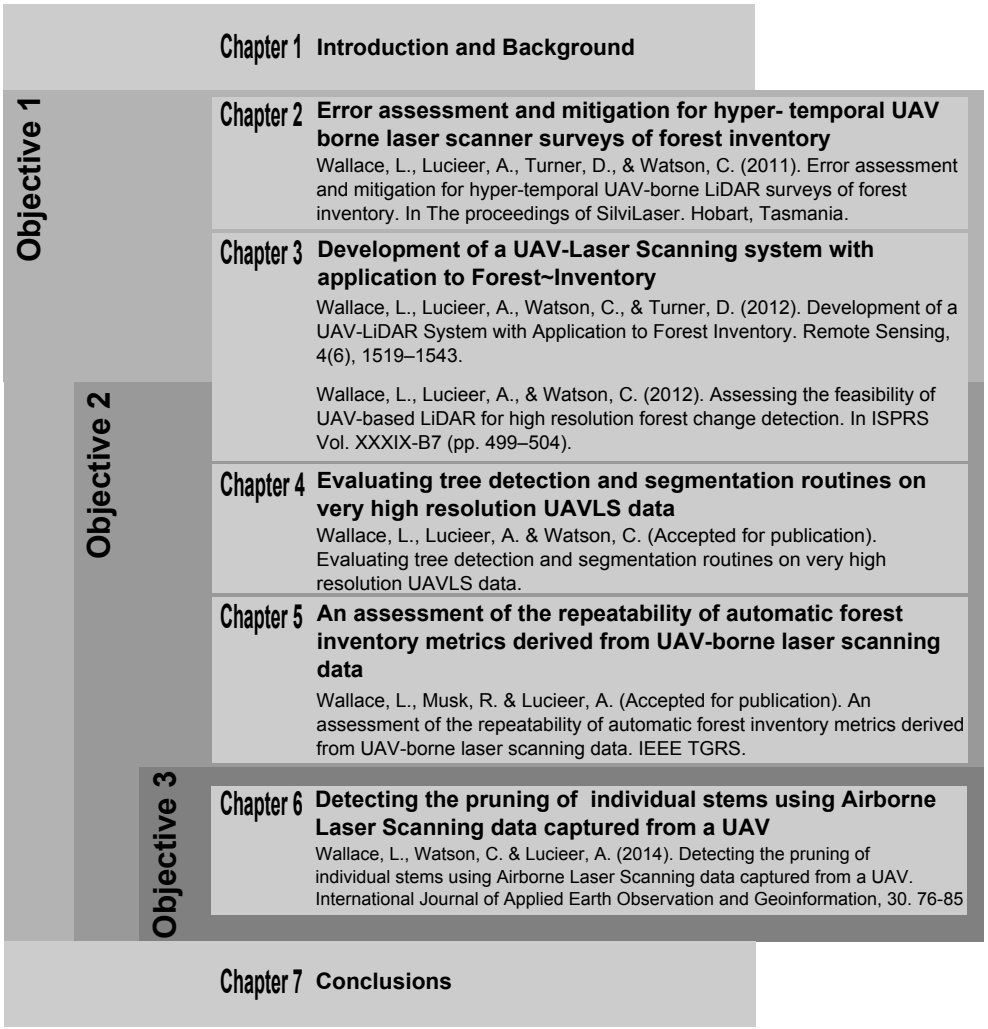

Figure 1.1: Structure of thesis, research objectives and publications.

2 | Error assessment and mitigation for hyper-temporal UAV laser scanner surveys of forest inventory

Chapter 2 focuses on determining the suitability of current technology and data fusion methods for the development of a UAV laser scanner system . The work comprising this chapter is published in the peer-reviewed *proceedings of Silvilaser 2011* (Wallace et al. 2011).

Abstract

Remotely sensed Airborne Laser Scanner (ALS) data has become an important tool in the collection of forest information. Monitoring the high frequency changes within forests with this data has been restricted by the high deployment cost of ALS platforms. The use of Unmanned Aerial Vehicles (UAVs) as a remote sensing platform is a rapidly developing field and these platforms are capable of allowing highly dynamic environmental changes to be monitored. This study investigates the potential of UAVs for the assessment of forest conditions by stochastically examining the achievable accuracy of a newly developed UAV Laser Scanner (UAVLS) system in comparison to a traditional full scale system. In this paper it is highlighted that the major contributions to the error budget of this UAVLS system, when using the traditional ALS processing workflow, can be constrained through the use of a novel UAV specific georeferencing method. Central to this method is the fusion of observations from a low cost Inertial Measurement Unit, a Global Positioning System receiver and a high definition video camera with a Kalman Smoother allowing for greater accuracy in the estimation of orientation. We found that using this workflow and under certain flying conditions, accuracies similar to a modern full-scale system are achievable from this low-cost platform.

2.1 Introduction

2.1.1 Laser scanning: state of the art forest measurement

Airborne Laser Scanning (ALS) has become a well established tool for surveying both natural and man-made environments. Laser scanners emit polarised light and measure the time and intensity of the reflection from different objects to return to the sensor. Modern discrete return laser scanners emit up to 500,000 pulses per second within a 75° field of view and are capable of measuring up to 5 intercepted surfaces per pulse. Each range measurement (or return) is recorded along with the corresponding scan angle observation, simultaneously to observations of position and orientation typically made by a GPS receiver and an Inertial Measurement Unit (IMU) (El-Sheimy 2009). The integration of these observations allow an optimised and accurate estimate of the absolute 3D position of each return to be made.

The coverage area, point density and point distribution of the 3D point clouds produced by these systems are a function of hardware properties; such as scan pattern, laser power, pulse repetition frequency and field of view; as well as the flight altitude and aircraft velocity (Petrie and Toth 2009). Continuous development of laser scanning hardware, including increased pulse repetition rates and higher powered lasers (allowing greater ranging distance), have enabled laser scanners to be used for the collection of information over increased areas without significant loss of data resolution.

Observing multiple returns per pulse from multiple viewing angles, allows ALS systems to penetrate through small gaps within the canopy and record observations relating to the top of the canopy, within canopy structure and the ground surface. The 3D structure present within an ALS point cloud allows an extensive range of data products and information to be derived from the point cloud, including digital elevation models, canopy height models and 3D canopy profiles (Akay et al. 2009). Combined with capacity to provide accurate 3D information over large areas this has lead to ALS becoming a key tool in the observation of forest structure for use in sustainable forest management practices (Hyyppä et al. 2008; Vauhkonen 2010a). Current and future innovations including the collection of full-waveform information, dual wavelength scanners and the simultaneous collection of spectral information are likely to increase the utility of these data products and enhance the use of ALS for forest management purposes.

The application of an ALS point cloud to forest management is typically achieved

through the aggregation of forest into area or tree-level estimation units (Hyyppä et al. 2008). Area level estimation involves determining the properties of the produced point cloud, such as the point density and vertical distribution of the above ground height of returns within a predefined area and using variable imputation techniques to produce metrics which are often strongly correlated to key forest properties (Næsset 2002; Hyyppä et al. 2008). This level of estimation requires only low density point clouds to be collected, allowing greater area to be captured. As such, area based analysis is often preferred within the industry (Vauhkonen 2010a). The estimation of tree level metrics, on the other hand, relies on the properties of each individual tree to be represented within the point cloud and for individual trees to be distinguishable from neighbouring trees. The extraction of accurate tree level measurements such as tree height, crown width, crown volume and species has been shown to be possible from appropriately dense data (Hyyppä et al. 2008; Vauhkonen 2010a).

The inventory metrics derived from both these levels of estimation units can provide forest managers with significantly richer information about their forests than previously available from remotely sensed data sources (Lim et al. 2003; Morsdorf et al. 2009). Nevertheless, in order to perform accurate tree level inventory from ALS data or to monitor change over time, high density data collected in repeat surveys is required. Despite developments in sensor technology, collecting sufficiently high density data requires either a significant decrease in the coverage area or an increase in survey costs. This trade-off, along with short flying seasons in many regions, has limited the collection of high temporal or spatial resolution data for use in investigative purposes only. As such, the intermittent ALS surveys and low density data typically utilised by forest managers, inhibit the ability to assess key forest properties at the tree level as well as the ability to monitor forest dynamics such as growth, defoliation and the rate of canopy closure. Currently, inventory assessment techniques inclusive of ALS data products, still require the use of extensive field plots as well as forest growth models in order to calibrate and maintain area level estimation models.

2.1.2 Mini UAV Laser Scanning technology

Unmanned Aerial Vehicles (UAVs) are fast becoming an important source of remotely sensed information. Anderson and Gaston (2013) provided a classification system for UAVs based on cost, size, payload carrying capacity and operational requirements. Under this system UAVs with high payload capacities (over 50 kg) and the ability to capture data at high to medium altitudes (3 to 20 km) are classified as large or medium. These

UAVs are capable of carrying modern ALS systems and due to their size and range have similar operational requirements to manned aircraft. Similar restrictions therefore exist for the use of these classes of UAVs for the collection of high resolution ALS data for use in forest inventory. Small UAVs (5 to 30 kg payload capacity and a range within line of sight) offer more flexible platforms for remote sensing systems, however, still require significant space for take-off and landing (Anderson and Gaston 2013). Suitable landing zones are not always available within line of sight of the forested environment required to be mapped restricting the suitable of this class of UAV.

Recently, improvements in small scale positioning technology have enabled the use of mini and micro-UAVs (up to 5 kg payload capacity and within line of sight range) as a unique platform for carrying remote sensing systems. This class of UAV offers the ability to capture data at very high temporal and spatial resolutions, with lower operational requirements in comparison to both traditional airborne systems and larger UAV platforms. These UAVs are highly suitable for deployment in forested environments, however, the further reduced payloads and the restriction of within line of site flights decrease the area that these platforms can cover in any individual flight. The potential of micro-UAV laser scanning (UAVLS) systems for use within the forest industry has been demonstrated by Jaakkola et al. (2010). By deploying a rotor wing UAV equipped with a laser scanning system, high-resolution point clouds were produced. Jaakkola et al. (2010) and Lin et al. (2011) have shown that due to the improved density of these point clouds, several metrics, including tree height, can be measured at a finer scale and with higher precision using already developed processing algorithms when compared to traditional ALS platforms.

The availability of laser scanners which meet the payload requirements of mini and micro UAVs is limited. Currently, no laser scanning sensor designed for mapping purposes with a suitable form factor for use with these platforms are available for purchase and sensors need to be adapted from other fields for this purpose. For example comparing the properties of a modern laser scanner and the automotive sensor used in Jaakkola et al. (2010) (as well as this paper) highlights that, due to the intended purpose and low cost nature of the sensor, it has been designed with significantly higher beam divergence (up to 0.8°), shorter overall range (200 m in comparison to 3500 m) and lower accuracies in the measurements of both range and scan angle. The sensor also has a lower scan repetition frequency, however, the innovative use of multiple scanning layers and a small angular increment between pulses allow high density data to be recorded. Further description of this sensor is provided in section 2.2.1.

The payload restrictions of a mini-UAV also reduce the availability of technology for determining aircraft position and attitude. Full scale sensors make use of highly accurate IMUs and dual-frequency GPS systems. Although dual-frequency GPS receivers are available in a form factor suitable to be deployed on-board a mini-UAV, the accuracy of lightweight small form-factor IMUs is significantly less than that of the full scale counterparts. These IMUs have more and higher sources of error. The increases in error due to light weight laser scanners and IMUs have the potential to decrease the positioning accuracy of a UAVLS system to a point were there use for forest management is not realistic.

2.1.3 Objectives

The high spatial and temporal resolution, together with low operation costs, will allow micro-UAVs to provide a more targeted approach to forest mapping and allow for the use of multi-temporal surveys monitoring forest health and canopy closure for instance. Studies such as Jaakkola et al. (2010) and Lin et al. (2011) suggest that the combination of low cost, high resolution data capture, UAV platforms are likely to be the next tool of choice for optimising detailed small area surveys within forests. Despite these developments, a rigorous analysis of the error structure present within low cost and small form factor sensors used onboard micro-UAVs, and how these errors propagate into the final 3D measurements has yet to be undertaken. Such an analysis of error is necessary for use in the mapping of forested environments to determine the feasibility of high density and multi-temporal surveys. This paper presents an analysis of the propagation of error based on the stochastic error model of a UAVLS system under development at the University of Tasmania using lightweight, low-cost sensors. In this analysis, we make use of the well-known error propagation techniques used for ALS systems to determine the achievable accuracy and major sources of error within this system and propose innovative approaches to restrain these errors.

2.2 Methods

2.2.1 Equipment

The sensor package of the multi-rotor UAV (Droidworx/Mikrokopter AD-8) currently under development by the TerraLuma research group at the University of Tasmania will be used as the basis for this study (Figure 2.1). In comparison to other UAV

platforms multi-rotor UAVs offer increased stability and decreased vibration making it the ideal UAV for the collection of laser scanner data. The Mikrokopter UAV is capable of lifting up to 2.8 kg, which when the primary sensor (Ibeo LUX Automotive Laser Scanner, 1 kg), batteries and logging equipment are taken into account allows for only a minimal payload for position and orientation sensors. Based on these requirements (and a desire to minimise cost) a lightweight sensor suite has been designed for positioning and orientation consisting of a Microstrain 3DM-GX2 Micro-Electro-Mechanical Systems (MEMS) based IMU (50 g), a Novatel OEMV-1DF dual-frequency GPS receiver (21.5 g + 113 g antenna) and a ContourGPS digital video camera (150 g).

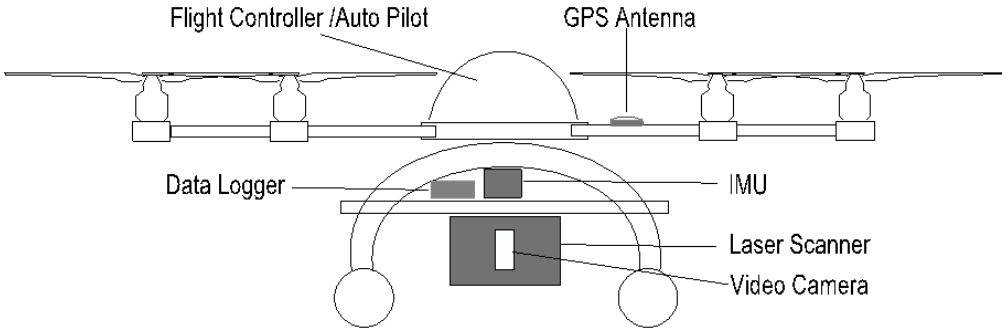

Figure 2.1: Schematic of the UAV remote sensing platform under development at the University of Tasmania.

The sensor payload is mounted on the UAV through a rigid sensor framework designed such that the lever arm offsets between the laser scanner, IMU, GPS and video camera are minimised and constant. The frame also allows for an adequate sky-view for the accurate operation of both the GPS antennas and GPS enabled video camera. The properties of each sensor have been rigorously tested in order to independently determine their standalone accuracy values under flight conditions. The results from these tests are displayed in Table 2.1 along with a brief explanation of the methods used to determine the estimates of instantaneous accuracy. All data logging and time synchronisation is performed using an on-board miniaturised computer (Gumstix Verdex pro) and all other processing is completed offline.

2.2.2 Airborne laser scanner error propagation

The calculation of the ground coordinates from the UAVLS system observations follow the same methodology as used for full scale traditional platforms. Coordinates of points that reflect the outbound laser pulse can be calculated directly from the scan angle and range measurement provided by the laser scanner and estimates of position and orientation from the other sensors on-board the UAV using the well known "LiDAR

Table 2.1: Description of the sensors mounted on-board the UAV and the method used to determine the accuracy of the sensor.

Equipment	Description and Accuracy Determination	Data Rate (Hz)	Standalone Accuracy
Dual-Frequency GPS receiver	Provides 3D positional observation of the helicopter operating under typical short baseline (<3 km) configurations. The GPS receiver has been benched marked against a geodetic grade GPS receiver.	20	**Horizontal** ± 0.03 m **Vertical** ± 0.05 m
Microstrain 3DM-GX2 IMU	A light weight - IMU consisting of s MEMbased accelerometer, gyroscope and magnetometer triads. An independent calibration procedure following the methods of Zhang et al. (2010) has been performed to verify the calibration and accuracy of the sensor.	100	**Orientation** ± 2.0° (+ bias instabilities and noise)
ContourGPS HD video camera	A high definition video camera equipped with a GPS antenna allowing accurate time synchronisation with the other sensors. The video camera has been calibrated and lens distortions removed using the procedure described by Bouget (2010). The accuracy of the orientation, using the algorithm described in section 2.2.3, has been quantified using dense ground control as reference.	30	**Orientation** ± 0.2 - 0.5°
Ibeo LUX laser Scanner	The Ibeo LUX sensor measures points in four scanning layers and in doing so can record up to 22000 returns/sec. The scanner has a measurement range of up to 200 m. The beam divergence of the Ibeo LUX laser scanner is 0.08° horizontally and 0.8° vertically.	880 (points per scan layer)	**Range** ± 0.1 m

equation" (Baltsavias 1999)

$$\begin{bmatrix} x \\ y \\ z \end{bmatrix} = \begin{bmatrix} X \\ Y \\ Z \end{bmatrix} + R_b^m[R_s^b r^s + a^b] \tag{2.1}$$

where $\begin{bmatrix} X & Y & Z \end{bmatrix}^T$ is the position vector as measured by the POS system expressed in the Earth Centred, Earth Fixed (ECEF) cartesian frame; R_b^m is the attitude matrix as measured by the POS and parameterized by the pitch, roll and yaw angles; R_s^b is the boresight matrix describing the angular offset between the body frame and the laser scanner frame; r^s is the observation vector from the Ibeo LUX system and consists of a range observation as well as an encoder angle and a^b is the lever arm offset between the origin of the POS frame and the laser scanner frame.

There has been significant and ongoing research into the various factors that affect the accuracy of coordinates derived from a laser scanner (Schaer et al. 2007). Individual laser scanner systems contain unique factors that affect the overall error (see May and Toth (2007) and Morin (2002) for an overview). However, these factors are mostly captured within 17 error components which will occur in every system, being;

- 3 errors existing in the measurement of the absolute position (σx, σy and σz)
- 3 errors existing in the measurement of aircraft orientation ($\sigma\omega$, $\sigma\phi$ and $\sigma\kappa$)
- 6 errors caused by the inaccurate calibration of the system affecting the boresight angles ($\sigma\omega b$, $\sigma\phi b$ and $\sigma\kappa b$) and lever arm offset (σxL, σyL and σzL);
- 3 Internal laser scanner errors occur in measurements of range (σr) and the two encoder angles ($\sigma\beta$ and $\sigma\gamma$) measured from the UAV; and
- 2 errors due to divergence of the laser beam which propagate in the horizontal direction (σB_h) and in the elevation angle measurement (σB_e) within the laser scanner reference frame. These errors will be modelled as one quarter of the quoted beam divergence of the laser scanner following Lichti and Gordon (2004) and Glennie (2007).

These error components can be propagated through the functional model of the "LiDAR equation" enabling the magnitude of the error in the final coordinates of a point to be determined. Propagation for an individual return can be performed by linearising

equation 2.1, through the truncation of the Taylor series expansion after the 1st term and assuming that each of the error sources are uncorrelated (Schaer et al. 2007). This enables the determination of the 3x3 point covariance matrix C_{xyz}, using equation 2.2 as follows:

$$C_{xyz} = \begin{bmatrix} C_x & C_{xy} & C_{xz} \\ C_{yx} & C_y & C_{yz} \\ C_{zx} & C_{zy} & C_z \end{bmatrix} = F_{ll} C F_{ll}^T \tag{2.2}$$

where F_{ll}^T is the Jacobian matrix of the linearised functional model and C is the stochastic model given by a diagonal matrix containing the magnitude of the 17 summarised error sources.

The covariance matrix, C_{xyz}, can be used a-priori to a laser scanner survey in order to determine the best and worst case point positioning accuracy. The analysis in this report will consider a scenario based on typical UAV flying heights (e.g. 30 to 120 m above ground level (AGL)), with the aircraft flying a flat northern path (i.e. ω, ϕ and $\kappa = 0°$).

2.2.3 Structure from Motion

Structure from Motion (SfM) is a method for the reconstruction of a 3D scene from a set of 2D images. Recent advances in feature extraction and image to image matching routines have allowed the 3D point clouds produced using SfM to have similar density and accuracy to laser scanning (even for images captured using non-metric cameras) (Fonstad et al. 2013). Although originally developed for land based applications, the accuracy of SfM has allowed it to be successfully applied to the generation of 3D models for monitoring and measuring natural environments based on imagery captured from UAVs (Westoby et al. 2012; Niethammer et al. 2012; Lucieer et al. 2014).

The SfM workflow is similar to that of traditional photogrammetry, in that SfM relies on images captured from multiple viewpoints in order to estimate the 3D properties of the scene. Unlike photogrammetry, SfM algorithms make use of recent and automated image matching techniques which are invariant to large changes in viewpoint and scale. Through the use of multi-scale brightness and colour gradients, image matching algorithms, such as SIFT (Lowe 2004) and SURF (Bay et al. 2006), are able to match features across randomly acquired imagery. This allows for ease of use and flexibility in

the capture of imagery used as input for SfM point cloud generation.

The large number of conjugate features extracted by these techniques allow collinearity equations to be solved in a coordinate system with an arbitrary origin and scale without the need for camera position or ground control points (Fonstad et al. 2013). This allows the 3D position of each conjugate point to be determined within this coordinate system and an intermediate point cloud to be produced. This point cloud can then be transformed into an established coordinate system using a seven parameter transformation or a refined bundle adjusted based on the use of ground control points.

Along with determining the 3D position of conjugate points, SfM algorithms also estimate the position and orientation of the exposure point of each image. This information has been exploited for navigation purposes as an alternative to position and orientation from GPS and IMU sensors (Lee et al. 2010). The accuracy of the point cloud and camera position and orientation produced by SfM techniques are dependent on the accuracy of the ground control points and the image matching routines. State of the art image matching algorithms are able to achieve sub pixel accuracy, however, this is dependent on the quality of the imagery and the properties of the scene being captured.

The camera position and orientation provided by structure from motion has the potential to be used to georeference the laser scanning data captured by the UAV. The introduction of a globally constrained estimate of orientation, as provided by SfM, has the potential to overcome the potentially large errors introduced by the use of small MEMs-based IMUs. To achieve this, careful consideration in the choice of matching algorithm is required to avoid the introduction of non-linear errors within the intermediate point cloud. Techniques that improve the robustness of feature matches such as random sampling and consensus (RANSAC) are, therefore, considered in this study.

In this chapter the potential improvements to georeferencing accuracy through the inclusion of SfM observations captured from a downward looking video camera were investigated. An algorithm based on Snavely et al. (2006) has been developed for this purpose. This algorithm makes use of feature identification based on the SIFT and nearest neighbour kd-tree matching. An iterative global RANSAC approach following Nistér (2004) was applied to identify and eliminate outliers from the set of feature matches. This produces a robust set of feature matches for use in the solving the collinearity equations and generating a sparse point cloud and estimates of camera position and location.

2.2.4 UAVLS / ALS comparison

The propagation of error in the positioning of ALS point clouds is usually reported on based on the flying conditions and error expected within a state-of-the-art ALS system at the time of publication. For example, Goulden and Hopkinson (2010) reports on the error within a ALS system based on the Optech 3100 scanner. Table 2.2 highlights that the conditions of a UAV survey are significantly different to that of a full-scale survey due to factors such as reduced flying heights and the greater inaccuracies of the miniaturised sensors. The variables provided in Table 2.2 can also be used as a measure of data quality in forest surveys (Lovell et al. 2005). Given the lower flying height and slower velocity the UAVLS system is able to produce the exceptionally high point density (300 points/m^2) data potentially enabling accurate analysis at the tree level, however, in order to capture large areas the UAVLS is required to utilise greater scan angles and angles of incidence with the terrain. Increases in both of these variables have been demonstrated to produce biases in the determination of forest metrics (Disney et al. 2010).

Table 2.2: A comparison of the key variables between the UAVLS and an Optech ALTM 3100 scanner.

Variable	**UAVLS**	**Full Scale System**
Typical Flying height	50 m	1100 m
Scan Angle Range	âĂŞ60° âĂŞ 50°	âĂŞ25° âĂŞ 25°
Swath width at 25°	47 m	1300 m
Maximum Swath width	146 m	1300 m
Point Density	up to 300 pts/m^2	3-15 pts/m^2
Laser footprint	$0.07x0.70$ m	$0.27x0.27$ m
Max. angle of incidence (flat terrain)	60°	25°

For comparative purposes we propagate error into both the UAVLS system outlined herein and a ALS system based on the Optech 3100 scanner. Table 2.3 provides an initial comparison between the error contribution of each of the 17 components within the UAVLS system and an Optech 3100 system. This table highlights the inaccuracy associated with the measurement of angular quantities in UAVLS systems. The values given in Tables 2.2and 2.3 are used as the basis for the results of this error propagation.

Table 2.3: A-priori standard deviation values of parameters within the UAVLS System in comparison to a full scale system (adapted from Goulden and Hopkinson (2010) and based on an Optech ALTM 3100 scanner)

Parameter	UAVLS Value (1 σ)	Full Scale Value (1 σ)
σ x, σ y	0.03 m	0.03 m
σ z	0.05 m	0.05 m
$\sigma\omega$, $\sigma\phi$	$0.2^\circ - 0.5^\circ$	0.005°
$\sigma\kappa$	$0.2^\circ - 0.5^\circ$	0.010°
$\sigma\omega b$, $\sigma\phi b$ and $\sigma\kappa b$	in $\sigma\omega$, $\sigma\phi$ and $\sigma\kappa$	in $\sigma\omega$, $\sigma\phi$ and $\sigma\kappa$
σxL, σyL and σzL	0.01 m	0.01 m
σ r	0.10 m	0.015 m
$\sigma\beta$	0.125°	0.003°
σB_h	0.020°	0.014°
σB_e	0.200°	0.014°

2.3 Results and Discussion

2.3.1 UAVLS error constraining strategies

The UAV's position and orientation system consists of three sensors (IMU, video, and GPS), providing observations at variable rates up to 100 Hz. This paper will consider three different processing strategies, making use of the observation from these sensors to determine the position and orientation of the laser scanner at the instant of each laser return.

Stand Alone Sensor Observations

The most basic method for processing the data is to make use of the position observation from the GPS and orientation observations as observed by the IMU. This strategy relies on the accuracy and data rate of the individual sensor to be sufficient for the task. As the laser scanner emits up to 11,000 pulses per second, position and orientation are required to be known at this rate. The GPS receiver is only capable of observing at 20 Hz and the IMU at 100 Hz, therefore interpolation is required to determine position and orientation at the instance of each pulse. Interpolation between points would be likely to introduce further error into the observations of position and orientation. Furthermore, due to the low cost nature of the sensor, error within a MEMs based IMU often include significant bias instabilities and noise (which if uncorrected can result in a drift of up to 0.2° per second).

For demonstrative purposes the IMU is considered to provided a drift free observation of orientation with a mean error of 2.0° and both the IMU and GPS are assumed to be measuring at the rate for the laser scanner. Even without considering these error due to drift and interpolation, figure 2.2 suggests that the final pointing accuracy of the UAVLS system would not be feasible for mapping purposes. Under this scenario the error due to poor estimates of orientation contributes up to 98% of the total stand-alone sensor error budget.

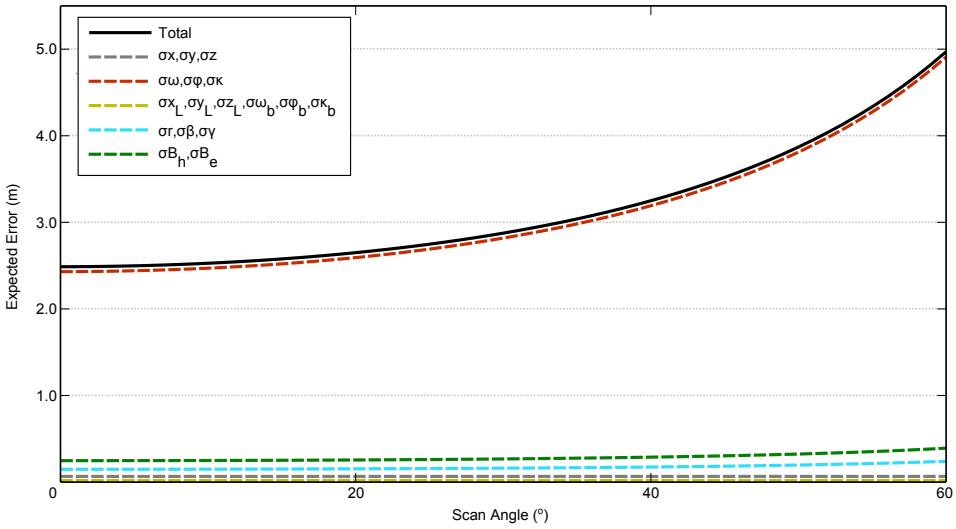

Figure 2.2: The effect of all error sources within the UAVLS system on the point positioning accuracy of the returns, considering the worst case system errors and a flying height of 50 m.

GPS/IMU Kalman Filter

In order to partly overcome the slow observation rate of the GPS and IMU sensors, ALS systems use processing algorithms to optimally combine the observation of the GPS and IMU sensors in determining position and orientation. By optimally combining the observations from both sensors, the overall accuracy of the orientation is improved and position is tracked at the rate of the IMU. The most commonly used algorithm for this purpose is the Extended Kalman Filter (EKF). This type of filter is limited in its complexity and accuracy by the inclusion of a first order linearisation of the functional model (Van Der Merwe and Wan 2004). Other algorithms overcome some of these limitations, for example it has been shown that variants of Sigma-Point Kalman filters (SPKF) consistently outperform the EKF in terms of correctness, robustness and ease of implementation (Kelly and Sukhatme 2009; Van Der Merwe and Wan 2004). It is envisaged that a SPKF strategy will be used with this particular platform, due to the

potentially dynamic sensor set, and is therefore considered in the analysis of this paper. Nevertheless, the improvements in accuracy of such a strategy are likely to be minimal in regards to the stochastic modelling performed and alternate filtering options will be likely to produce similar results.

The use of a well designed integration strategy will constrain the error in the estimation of orientation as well as allow estimates of position to be made at the higher rate of the IMU. Under such a strategy, it has been shown that with a similar IMU the errors in the observations of pitch and roll ($\sigma\omega$ and $\sigma\phi$) can be reduced to 0.5° and to 1.5° in the yaw observation ($\sigma\kappa$) (Du 2010). Figure 2.3 demonstrates that the optimal combination of the IMU and GPS observation would offer a significant reduction in the positioning error of laser returns. Nevertheless, using this processing strategy orientation is still the primary contributing source of error.

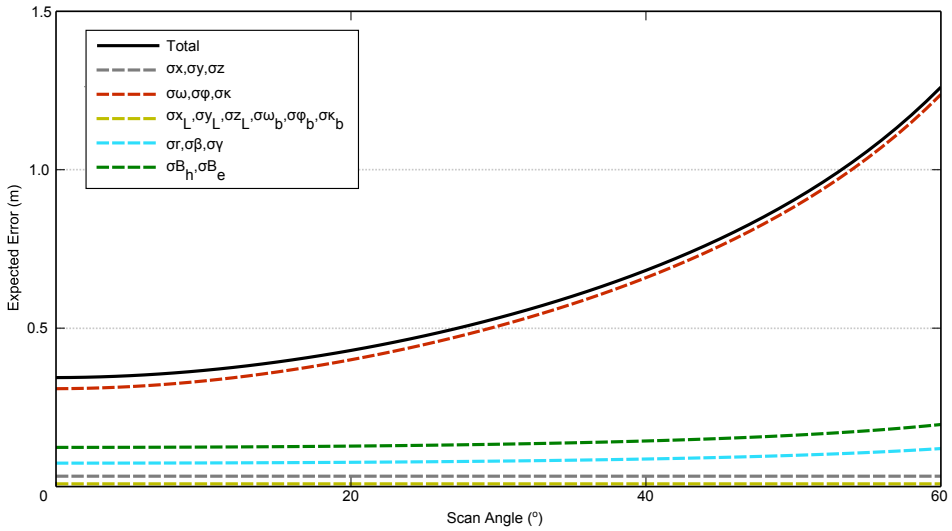

Figure 2.3: The result of a GPS/IMU filtering strategy constraining orientation error, to 0.5° in pitch and roll and 1.5° in Yaw, at a flying height of 40 m resulting in a higher overall point positioning accuracy.

GPS/IMU/SFM Kalman Filter

In order to further constrain the error, SfM based orientation estimates can be included within the filter. Initial experiments of the novel algorithm developed for this research has shown significant improvement in the estimate of yaw and smaller improvements in the estimate of pitch and roll. Based on these initial tests, orientation estimates are expected to be reduced to within a range of 0.2 to 0.5°. Figure 2.4 shows that the contribution of error from orientation is now within a similar range to the contributions

of other system components.

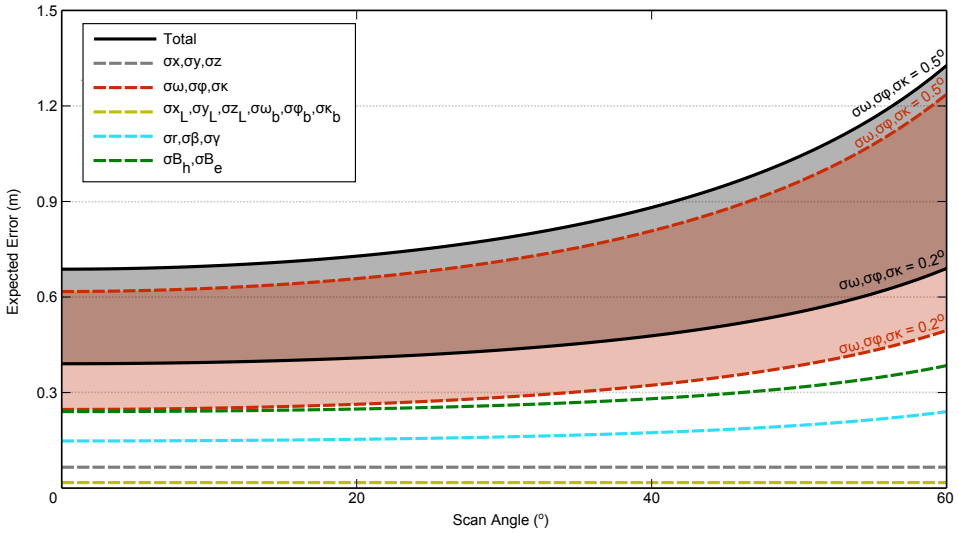

Figure 2.4: The expected result of improved orientation measurements due to the inclusion of HD video and Kalman filtering within the on-the-point positioning accuracy of the UAVLS system.

2.3.2 The effect of flying height

The point positioning error present within the observations made by the UAV platform has been shown to increase with scan angle (Figures 2.2 to 2.4). Considering the high beam divergence of the Ibeo LUX scanner, the other dominant variable affecting the accuracy of a laser scanner return is flying height (demonstrated in Figure 2.5). Increased flying heights also result in significant decreases in the density of the measured point cloud. The magnitude of horizontal error towards the edges of the scan angle range increases by an order of magnitude between flying heights of 30 and 120 m. This effect is least pronounced at the centre of the scan suggesting that if increased flying heights are to be used, the scan angle of the laser scanner should be constrained.

2.3.3 ALS/UAVLS Comparison

The cumulative effect of the errors, as a function of scan angle, within the UAVLS system (flying at 50 m) in comparison to a modern full scale system flying at 1100 m is illustrated in Figure 2.6. The full scale system has a scan angle range of +/-25°. Within this range the accuracy of the UAV system is comparable to the full scale system. However, the use of larger scan angles produce significantly greater error. Based on this

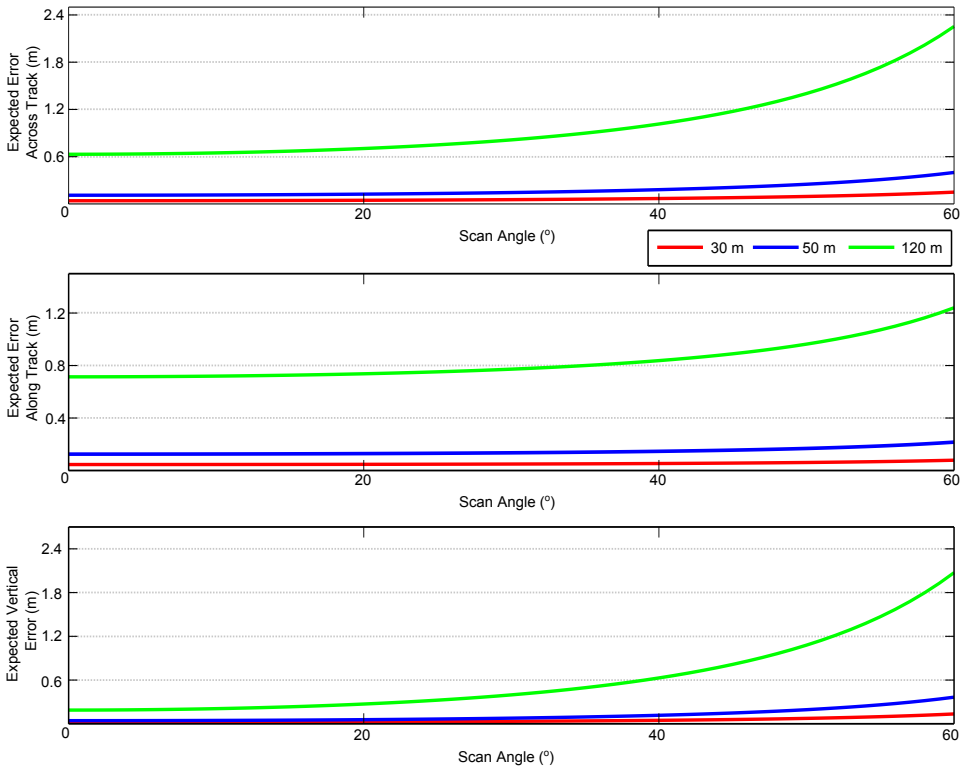

Figure 2.5: The accuracy of the UAVLS system based on the error statistic presented in Table 2.1 ($\sigma\omega$, $\sigma\phi$ and $\sigma\kappa = 0.35°$) and at flying heights of 30 m, 50 m and 120 m.

analysis it is recommended that the UAVLS scan angle be constrained to a similar range to that of modern full scale scanners.

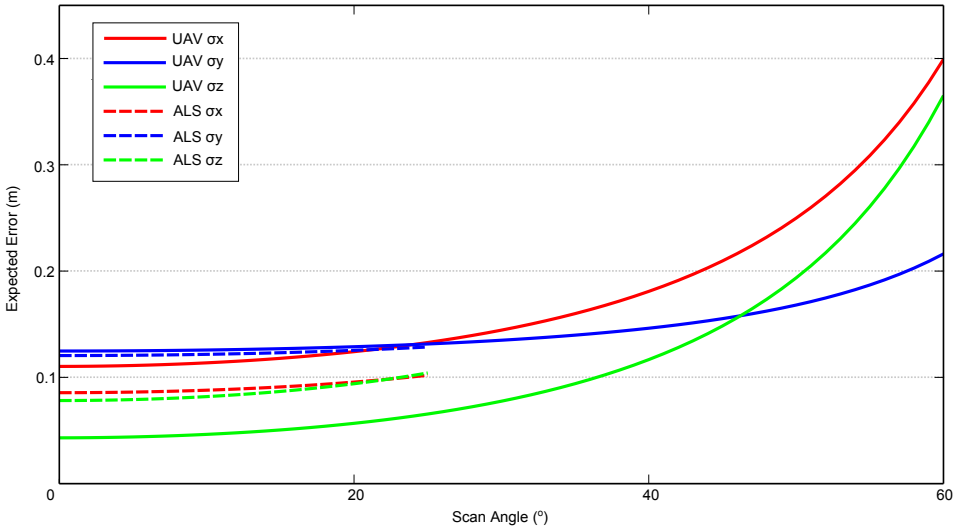

Figure 2.6: Accuracy of the UAVLS system ($\sigma\omega$, $\sigma\phi$ and $\sigma\kappa = 0.35°$) flying at 50 m in comparison to the accuracy of a traditional full scale system flying at 1100 m (full scale system properties adapted from (Goulden and Hopkinson 2010).

2.3.4 Sensor Calibration

The three methods outlined above have assumed that the calibration (boresight angles and lever arms) between all sensors are equivalent in accuracy to the calibration of a full scale system. Due to the low individual accuracy of the IMU and laser scanning sensors, achieving a precise calibration of the boresight angles is problematic, however, errors introduced due to boresight misalignment can be minimised by maintaining a lower flying height. For example a 0.01°misalignment results in an error of 1.31 m at a flying height of 700 m, and only 0.005 m at a typical UAV flying height of 50 m.

Errors in the measurement of the lever arm offset between the center of the position and orientation system and the laser scanner propagate directly into the accuracy of point position and need to be minimised by an appropriate calibration strategy. Conventional procedures for determining calibration parameters of ALS systems require a periodic survey of a well observed site (often an air field). The modularity of a UAV system suggests that the boresight angles are likely to be significantly more dynamic and change between individual surveys as sensors are taken on and off. Therefore, a specific calibration procedure for this UAV, which can be easily preformed in the field and accurately determine leverarms is required. Such a procedure would be required to follow the three traditional stages of calibration for a laser scanner system outlined by Habib et al. (2010) and make use of portable targets of known size and shape.

2.4 Conclusion

The fusion of observations from GPS, IMU and video sensors has been stochastically demonstrated to allow for the significant reduction in the direct geoferencing error of the UAVLS system in comparison to a standard workflow utilising only GPS and IMU sensors. At a typical flying height of 50 m, UAVLS can be expected to produce point clouds with sufficient accuracy for forest mapping. This accuracy, coupled with the increased point density acquired by the UAVLS system, presents a significant advantage for the fine-scale mapping of forests. The use of such a system will most likely result in a reduction in the underestimation of tree height measurements due to the highly dense point cloud being produced. Moreover, the modularity and low cost of the a UAVLS system will enable surveys to be conducted at a higher temporal frequency, allowing canopy closure rates and forest health to be monitored closely. Limitations of the use of a UAVLS system for forest measurement are primarily a result of the restricted flying

heights and scan angles required to produce accurate data, which in combination with expected flight time significantly restricts the potential ground coverage of the system.

The next stage in the development of the UAV is the rigorous in field assessment of the spatial accuracy of the system and the analysis of data over a forested test area. This will allow the capabilities of the system for forest mapping to be fully assessed and a set of survey designs to be developed with the aim of determining key forest metrics to monitor temporal changes in forest conditions. Other future improvements to the system are reliant on advances in laser scanner technology, however, increased uptake of current technology could result in demand for an adaptation of automotive laser scanners into lightweight scanners with smaller beam divergence designed specifically for mapping purposes.

2.5 Thesis Context

This Chapter outlined stochastic modelling of the accuracy achievable using off-the-shelf technology for the development of a UAVLS system. It was highlighted that GPS/MEMs IMU kalman filtering will not provide the required georeferencing accuracy for UAVLS to be suitable for forest inventory purposes and the need for an augmented vision solution. The next chapter uses this theoretical background and outlines the full development of the UAVLS system with a video camera providing the required auxiliary observations of orientation.

3 | Development of a UAV-laser scanning system with application to forest inventory

Chapter 3 focuses on the development of a UAV laser scanner and associated direct georeferencing system. The work comprising this chapter is published in *Remote Sensing* (Wallace et al. 2012b) and in the Proceedings of ISPRS2012 (Wallace et al. 2012b).

Abstract

We present the development of a low-cost Unmanned Aerial Vehicle Laser Scanner (UAVLS) system and an accompanying workflow to produce 3D point clouds. UAV systems provide an unrivalled combination of high temporal and spatial resolution datasets. The TerraLuma UAVLS system has been developed to take advantage of these properties and in doing so overcome some of the current limitations of the use of this technology within the forestry industry. A modified processing workflow including a novel trajectory determination algorithm fusing observations from a GPS receiver, an Inertial Measurement Unit (IMU) and a High Definition (HD) video camera is presented. The advantages of this workflow are demonstrated using a rigorous assessment of the spatial accuracy of the final point clouds. It is shown that due to the inclusion of video the horizontal accuracy of the final point cloud improves from 0.61 m to 0.34 m (root mean square error assessed against ground control). The effect of varying flying parameters on the properties of point clouds collected from UAVLS surveys over an *Eucalyptus* plantation was assessed by performing repeat flights between 30 to 90 m above ground level (AGL). This study demonstrates that flying height is required to be restricted to below 50 m AGL and scan angle should be minimised where possible to avoid occlusions and to ensure repeatable observations.

3.1 Introduction

3.1.1 Background

Airborne Laser Scanning (ALS) remote sensing has become a powerful tool in the management of modern forest inventories (Hyyppä et al. 2008). Ongoing research into the processing and analysis of laser scanner data has allowed for the development of an extensive range of data products from which a wide range of forest metrics can be derived (Lefsky et al. 2002; Akay et al. 2009; Erdody and Moskal 2010). Stand metrics and tree-level statistics have provided forest managers with significantly richer information about their forests (Morsdorf et al. 2009; Lim et al. 2003). It is, however, evident that the full potential of ALS technology for forest measurement and management is yet to be reached. Prohibitive factors, including high survey costs and short flying seasons in many areas, have limited the ongoing application of multi-temporal studies. As such, the assessment of factors such as forest health, defoliation, and rate of canopy closure are not feasible from the current intermittent ALS surveys utilised by forest managers.

Recently, improvements in small-scale technology have enabled the use of Unmanned Aerial Vehicles (UAVs) as an alternative remote sensing platform offering a distinctive combination of very high resolution data capture at a significantly lower survey cost. Current research into the use of UAVs as a 3D data-capture platform includes archaeological surveys (Barazzetti et al. 2010; Chiabrando et al. 2011) and vegetation monitoring (Sugiura et al. 2005; Laliberte et al. 2011; Hunt Jr et al. 2010), for example. These studies use image matching and photogrammetric techniques, which allow high density point clouds to be generated from the very high resolution imagery collected by UAVs. These point clouds have also been evaluated for forest monitoring and management by Tao et al. (2011) and Dandois and Ellis (2010), both showing the advantages of significantly higher density point clouds in comparison to those commonly collected with ALS platforms. The drawback of point clouds generated from imagery is that few points will be measured from within the canopy and from the underlying surface in densely vegetated areas. This within canopy information is vital for many of the techniques which have been developed for deriving stand and tree level metrics, including above ground biomass, from point clouds.

Jaakkola et al. (2010) provided the first example of the potential of UAV Laser Scanner (UAVLS) for use in the forestry research. With the deployment of a rotor wing UAV equipped with a number of navigation sensors, in combination with two on-board laser

scanners, high-resolution data sets were produced offering improved individual tree level mapping. Jaakkola et al. (2010), and more recently Lin et al. (2011), have shown that due to the improved density of a UAVLS point cloud, several metrics can be measured at a finer scale and with higher precision when compared to ALS platforms. Because of their high spatial and temporal resolution, together with low operational costs, UAVs can provide a more targeted approach to forest monitoring and allow for the use of multi-temporal surveys aimed at monitoring forest growth, health and canopy closure for example. Studies such as these suggest that through the combination of low-cost, high resolution data capture, UAV platforms are likely to be the next tool of choice for optimising detailed small area surveys within forests.

Several other UAV-platforms have also been developed for the purpose of collecting laser scanner data (Choi et al. 2009; Nagai et al. 2009; Miller and Amidi 1998; Jaakkola et al. 2010). The majority of these examples have been designed for government or military purposes (Choi et al. 2009; Nagai et al. 2009) or as proof of concept platforms to show that laser scanner data can be collected from UAVs (Miller and Amidi 1998). The drawback of such platforms is that the size and budget is significantly larger than what could be considered useful as an operational tool in forest management. A key reason for this is that the derivation of a spatially accurate point cloud requires careful consideration to be given to the determination of aircraft position and orientation. Even small errors in the observation of orientation and position result in substantial on ground displacements in point measurements (Glennie 2007). The considerations regarding the positioning and orientation payload for UAV systems are confounded by the payload weight and size restrictions, and a trade-off between accuracy and weight must often be made. This has resulted in the majority of UAVLS systems consisting of larger UAVs, capable of carrying heavier payloads (Miller and Amidi 1998; Choi et al. 2009; Nagai et al. 2009), making them difficult to deploy in forested environments. For example, the platform outlined in Nagai et al. (2009) has a take-off weight of 330 kg. The mini-UAV outlined by Jaakkola et al. (2010) uses a combination of a tactical grade IMU and laser scanner. This combination, which weighs over 3 kg, pushes the payload limitations of most commercially available vertical take-off and landing (VTOL) mini-UAVs suitable for forest based research.

Micro-Electromechanical System (MEMS) based IMUs offer an alternative option for positioning and orientation that is both lightweight and low-cost. These IMUs have been deployed for a variety of positioning and orientation tasks, including navigation, obstacle avoidance and land-based mapping (Schwarz and El-Sheimy 2004). This technology can be used as the primary orientation sensor within a GPS/IMU sensor framework to

provide the high rate estimates of position and orientation required for laser scanner mapping. However, due to the high levels of error within MEMS IMUs and based on reported errors of sensor fusion algorithms using such sensors (El-sheimy 2009), it can be shown that estimates of orientation and position would be of an inadequate accuracy for use on-board a UAVLS system (Wallace et al. 2011). Several innovative algorithms fusing GPS and MEMS observations have been shown to improve the modelling of the large stochastic drifts within MEMS IMUs and as a consequence the accuracy of orientation estimates Shin (2004), El-Sheimy et al. (2006), and Chiang et al. (2009). Furthermore, the augmentation of techniques developed within the fields of photogrammetry and computer vision have contributed to improving the accuracies of MEMS-based navigation systems when used for direct georeferencing (Andersen and Taylor 2007; Gajdamowicz et al. 2007; Bryson and Sukkarieh 2011). These developments suggest that a UAV system consisting of a lightweight MEMS based IMU along with GPS and visual observations can provide estimates of position and orientation with the accuracy required for mapping forest metrics using UAVLS systems.

3.1.2 Objectives

The aim of this paper is to present the development of a UAVLS system using lightweight and low-cost sensors, and demonstrate its capability of collecting spatially dense, accurate, and repeatable measurements for forestry inventory applications. This paper outlines and assesses the accuracy of a modified workflow to produce a UAVLS point cloud. Within this workflow, a technique for accurately georeferencing laser scanner returns is presented, which includes a novel inclusion of orientation estimates from HD-video using a modified version of the structure from motion (SfM) algorithm outlined in Snavely et al. (2006). The fusion of these orientation observations with observations from the GPS receiver and the MEMS-IMU within a Sigma Point Kalman Smoother is proposed in order to overcome the presence of large orientation errors which occur in GPS/MEMS-IMU based fusion systems. We evaluate the system in terms of absolute spatial accuracy as well as assess the required survey conditions to accurately measure forest metrics within a *Eucalyptus* plantation.

3.2 Hardware

A multi-rotor UAV (OktoKopter Droidworx/Mikrokopter AD-8) currently being developed as a remote sensing platform by the *TerraLuma* research group at the University of

Tasmania is used for this study (Figure 3.1). Multi-rotor UAVs offer increased stability and decreased vibration in comparison to other platforms. This is a key consideration in the development of a mapping platform as any source of vibration equates to a source of error within measurements of position and orientation. The OktoKopter has 8 brushless motors which operate at different rotor speeds to achieve directional flight. There is however a minimum rotor speed required to achieve flight which will induce vibration. We isolate this vibration by ensuring the sensing payload is mounted in a rigid frame isolated from the OktoKopter airframe through the use of 4 silicon mounts. These mounts have been selected based on the mass of the payload and the minimum frequency vibration expected from the rotors.

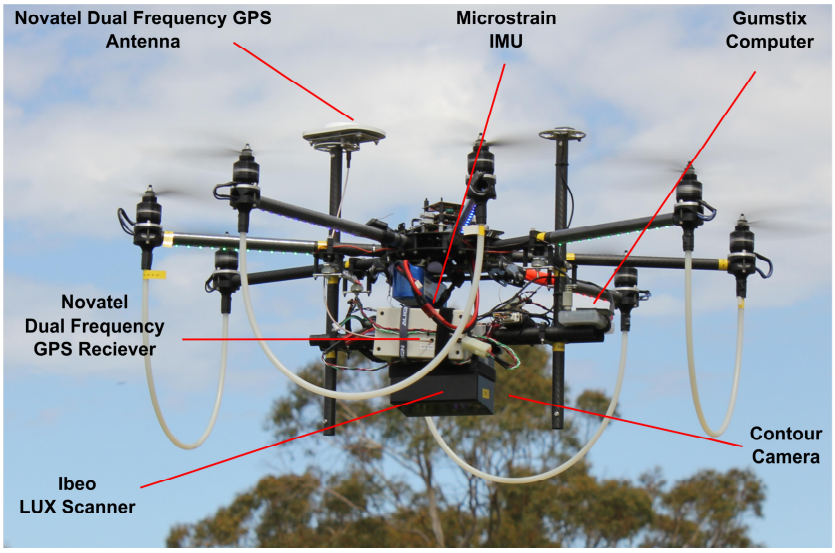

Figure 3.1: The multi-rotor Oktocopter UAV platform with the vibration isolated sensor frame, carrying the laser scanner, MEMS based IMU, GPS receiver and antenna and video camera.

The OktoKopter has a standalone control system including an on-board navigation and autopilot system. This allows predefined flight paths to be followed ensuring maximum use of flight time and repeat surveys to be easily performed. Furthermore, the use of a VTOL UAV within forested environments is of high importance as cleared areas for use as runways are often not present. The main limitation of this platform is the small payload capacity and subsequently the reduced flight time. The electric OktoKopter is only capable of flight times between 3–5 min.

The sensor payload is mounted on the UAV through a custom-designed rigid sensor framework with fixed lever arm offsets and boresight angles between all sensors. The framework also allows for an adequate sky-view for the accurate operation of both the GPS antennas and GPS enabled video camera. The primary sensor on-board the UAV

is an Ibeo LUX laser scanner. The scanner is designed for automotive purposes and has a maximum range of 200 m and scans in 4 parallel layers with a transversal beam divergence of 0.8° allowing complete coverage of the sensor's field of view. The sensor was set to have a scan frequency of 12.5 Hz and an angular resolution of 0.25°. These settings were chosen primarily due to the limitations of the data logging computer. The maximum scanning range of the Ibeo LUX is 110°, although this is restricted to ±30° as large scan angles have been shown to have a significant impact on the derivation of key metrics used for forest investigation (Morsdorf et al. 2006). The LUX records ranges and intensities for up to three echoes per pulse, with a repeatability of 10 cm in the range measurement and a resolution of 4 cm. Although the attributes of the scanner such as the wide beam divergence and low range resolution do not make it an ideal mapping sensor, its low power consumption and lightweight (approximately 1 kg) allow its use on-board UAV platforms.

The remaining sensors contained within the sensing payload belong to the Positioning and Orientation System (POS). The POS consists of a MEMS IMU (microstrain 3DM-GX3 35), a dual frequency GPS receiver (Novatel OEMV1-df) and lightweight antenna (Novatel ANT-A72GA) and a high definition GPS enabled video camera. The IMU contains orthogonal sets of accelerometers, gyroscopes, and magnetometers as well as an internal GPS receiver allowing all observations to be synchronised to GPS time. The IMU, which weighs only 50 g, is set to observe angular rate and acceleration at a rate of 100 Hz. The key properties of the gyroscopes and accelerometers are summarised in Table 3.1. The IMU has been factory calibrated, however, to confirm the results the IMU was calibrated using the methods outlined in (Zhang et al. 2010). The GPS observations, recorded at a rate of 5 Hz, are differentially post-processed in order to achieve the highest possible accuracy. Finally, the HD video camera records 30 frames per second and has a field of view of 110° . The calibration parameters of this camera have been determined using the method outlined in Bouget (2010). Data logging and time synchronisation is performed using an on-board miniaturised computer (Gumstix Verdex pro). All other processing is performed offline. The entire sensor payload weighs 2.4 kg meeting the requirements for use on-board the OktoKopter platform, which has a maximum payload of 2.8 kg.

Table 3.1: Properties of the MEMS based Microstrain 3DM-GX3 35 IMU.

	Gyroscopes	**Accelerometers**
Range	50°/s	1.7 g
Non-linearity	0.2%	0.2%
Bias Stability	0.2°/s	0.003 g

3.3 Methodology

3.3.1 UAVLS workflow

The use of ALS has received significant research attention and operational use as a source of information for forest scientist since its introduction in the mid-1990s. This has allowed a well-defined best practice data collection and processing workflow to be established by data providers. The end product of this workflow is a spatially accurate point cloud with each point given an appropriate classification. The processing of laser scanning data captured using a UAV follows a similar workflow as shown in Figure 3.2. However, considerations need to be given to the miniaturised sensors, reduced flying height and time, as well as the increased point density during each of the stages of processing. For example, during the data collection phase consideration needs to be given to the limited flight time of a UAV and optimal mapping strategies need to be determined. An advantage of the platform used in this study is the on-board autopilot allowing maximum coverage of the targeted area during each flight.

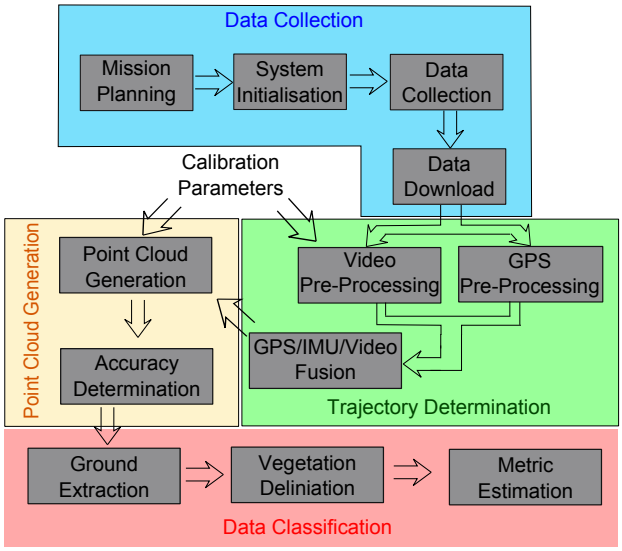

Figure 3.2: The modified laser scanning workflow to be used in producing a point cloud from the UAV system. Signification modifications are highlighted in red to account for the miniaturised sensors and increased resolution when using this workflow to produce a point cloud from data captured from on-board a mini-UAV.

Similarly, modifications need to be made within the trajectory determination and point cloud generation stages due to the use of miniaturised sensors. The underlying requirement of these stages is the determination of all the variables within the direct georeferencing equation at the instance of each pulse, given as follows:

$$\begin{bmatrix} x \\ y \\ z \end{bmatrix} = p_t + R_b^m [R_s^b r^s + a^b] \tag{3.1}$$

The determination of aircraft trajectory, including position, $p_t = \begin{bmatrix} X & Y & Z \end{bmatrix}^T$, and the orientation matrix, R_b^m, are crucial to the final spatial accuracy of the position of each measured laser scanner return $\begin{bmatrix} x & y & z \end{bmatrix}^T$ measured in the mapping frame (North, East, Up). System calibration to determine the boresight matrix R_s^b and lever arm a^b is performed separately, as the reduced accuracy of the laser scanner means traditional techniques such as strip adjustment are not feasible. Further discussion on these issue is provided in Sections 3.3.2 and 3.3.3. Furthermore, the four layer off-nadir scanning properties of the Ibeo LUX laser scanner require the laser scanner observation matrix (r^s) to be modified giving Equation (3.2).

$$r^s = \begin{bmatrix} \cos\Theta_L & -\sin\Theta_L \sin\Theta_E & -\sin\Theta_L \cos\Theta_E \\ 0 & \cos\Theta_E & -\sin\Theta_E \\ \sin\Theta_L & -\cos\Theta_L \sin\Theta_E & \cos\Theta_L \cos\Theta_E \end{bmatrix} \begin{bmatrix} 0 \\ 0 \\ r \end{bmatrix} \tag{3.2}$$

This observation matrix includes the addition of a layer angle, Θ_L, as well as the range r and the encoder angle, Θ_E, used within the common direct georeferencing equation.

3.3.2 Trajectory determination

In order to resolve the UAV's states (position and orientation) from the observation of the multiple on-board sensors, a state based estimator is used. The aim of this estimator is to make use of all information and optimally combine the results. The core algorithm of the state-based estimator used in this work is the Square Root Unscented variant of the Sigma Point Kalman filter (SPKF) outlined in Van Der Merwe and Wan (2004). This variant of the SPKF was chosen over the traditional Extended Kalman Filter (EKF) as it partially addresses the issues of approximation present in the EKF (Wan and Van Der Merwe 2000). Furthermore, the SPKF has been shown to converge faster, thus allowing a greater section of each flight to be used for mapping (Shin 2004). This implementation of a SPKF is a straightforward extension of the sigma-point approach to the recursive estimation of a non-linear discrete time system. Error within the system is estimated by propagating sigma points selected from within an *a-priori* measurement noise distribution. These sigma points are applied to the current augmented state through the kinematic model to determine a corresponding set of updated

sigma-points. A complete overview of the SPKF algorithm can be found in Van Der Merwe and Wan (2004) and for brevity is not included in this paper. The application of the SPKF to the determination of vehicle states does however requires state-based process and observation models to be defined.

Process model

As in most strap-down navigators, the observations of linear acceleration $a = \begin{bmatrix} a_x & a_y & a_z \end{bmatrix}$ and rotational velocity $\omega = \begin{bmatrix} \omega_p & \omega_q & \omega_r \end{bmatrix}$ are made in the body frame by the IMU. The biases and noise within these observations are corrected for using the following models:

$$\bar{a} = a - a_b - n_a \tag{3.3}$$

$$\bar{\omega} = \omega - \omega_b - C_n^b \omega_c - n_\omega \tag{3.4}$$

where $\bar{a}$ and $\bar{b}$ are the corrected observations and n_a and n_ω are estimated noise terms within the measurements of acceleration (a) and angular rate (ω). ω_c is the rotational velocity of the Earth for a given longitude and latitude. The time varying noise terms a_b and ω_b model both the bias and scale factor error terms of the IMU. These noise terms are modelled as a zero-mean Gaussian random variable with the variance set according to manufacturer's specifications. A quaternion representation of orientation is used to avoid singularities which can occur in alternate representations of orientation, following Shin (2004), Crassidis (2006), and Van Der Merwe and Wan (2004). This results in a state vector with 16 elements as follows:

$$x = \begin{bmatrix} p_t & v_t & e_t & a_t & \omega_t \end{bmatrix}^T \tag{3.5}$$

where $p_t = \begin{bmatrix} x & y & z \end{bmatrix}^T$ and $v_t = \begin{bmatrix} v_x & v_y & v_z \end{bmatrix}^T$ are the position and velocity within a fixed mapping frame. $e_t = \begin{bmatrix} q_0 & q_1 & q_2 & q_3 \end{bmatrix}^T$ is attitude quaternion representing the rotation between the body frame and the mapping frame. a_t and ω_t are the three element accelerometer and gyroscope bias vectors. The mechanisation of the corrected IMU observations used as the kinematic process model to transform the measurements made in the body frame into changes in position and attitude in the mapping frame

follows Van Der Merwe and Wan (2004). The discrete time kinematic equations are given as follows:

$$p_{t+1} = p_t + \dot{p_t} \cdot dt \tag{3.6}$$

$$v_{t+1} = v_t + \dot{v_t} \cdot dt \tag{3.7}$$

$$e_{t+1} = exp(-\frac{1}{2}\tilde{\Omega} \cdot dt)e_t \tag{3.8}$$

$$a_{b_{t+1}} = a_{b_t} + r_{w_t} \cdot dt \tag{3.9}$$

$$\omega_{b_t+1} = \omega_{b_t} + w_{b_t} \cdot dt \tag{3.10}$$

where r_{w_t} and w_{b_t} are zero mean Gaussian noise terms and the term $exp(-\frac{1}{2}\tilde{\Omega} \cdot dt)$ is composed of a skew symmetric matrix representing the effective rotations in the body frame:

$$\tilde{\Omega} = \begin{bmatrix} 0 & \bar{\omega}_p \cdot dt & \bar{\omega}_q \cdot dt & \bar{\omega}_r \cdot dt \\ -\bar{\omega}_p \cdot dt & 0 & -\bar{\omega}_r \cdot dt & \bar{\omega}_q \cdot dt \\ -\bar{\omega}_q \cdot dt & \bar{\omega}_r \cdot dt & 0 & -\bar{\omega}_p \cdot dt \\ -\bar{\omega}_r \cdot dt & \bar{\omega}_q \cdot dt & \bar{\omega}_r \cdot dt & 0 \end{bmatrix} \tag{3.11}$$

Based on the proofs provided by Gavrilets (2003) and Van Der Merwe (2004), the matrix exponent and the skew symmetric property can be used in forming a closed form solution as follows:

$$exp(-\frac{1}{2}\tilde{\Omega} \cdot dt) = \left[I(cos(s) + j \cdot dt\lambda) - \tfrac{1}{2}\tilde{\Omega}\tfrac{sin(s)}{s}\right] e_k \tag{3.12}$$

where $s = \frac{1}{2}|| \begin{bmatrix} \bar{\omega}_p \cdot dt & \bar{\omega}_q \cdot dt & \bar{\omega}_r \cdot dt \end{bmatrix} ||$. The term $j \cdot dt\lambda$ serves as a Lagrange multiplier to ensure the unity norm constraint of the quaternion orientation representation, given $\lambda = 1 - |e_k|^2$ and j is the factor that determines the convergence speed of the numerical error.

Observation models

The measurement update step of the Kalman Filter uses the current state of the kinematic system, the independent observations from the GPS receiver and/or the video camera. A cascading filter structure is used as both the GPS and video observations require some amount of preprocessing.

The GPS receiver measurements are post-processed in Novatel's GrafNav software, which provides position p_t^{GPS} and velocity v_t^{GPS} relative to the mapping frame. The antenna reference point is offset from the origin of the body frame by a lever arm $\bar{r}_{GPS}$. This allows the GPS to also provide an observation of orientation through the lever arm effect (Van Der Merwe 2004). Compensating the GPS observations for the lever arm offset gives the following mathematical model:

$$p_t^{GPS} = p_t + C_b^n \bar{r}_{GPS} + n_{p_t} \tag{3.13}$$

$$v_t^{GPS} = v_t + C_b^n . \omega_t \bar{r}_{GPS} + n_{p_t} \tag{3.14}$$

where C_b^n represents the direction cosine matrix from the body frame to the mapping and is a function of the current quaternion attitude. ω_t is the true rotational rate of the vehicle and n_{p_t} and n_{vt} are the stochastic measurement noise terms.

The observations of orientation provided by the video camera are determined using a modification of the Structure from Motion (SfM) technique. The SfM technique allows the construction of the 3D structure of imaged objects as well as the estimation of the exterior camera orientation by analysing motion signals over time (Dellaert et al. 2000). The technique can be applied to a set of overlapping images to obtain a sparse point cloud for a wide range of objects (Snavely et al. 2006). In creating this sparse point cloud, the technique optimally estimates the exterior orientation parameters of the camera in relative space through the use of a bundle adjustment.

The 30 frames per second rate of the video camera, in conjunction with the flight dynamics of the UAV, results in relatively short baselines between the capture of video frames. This is problematic for the recovery of 3D structure within a bundle adjustment due to the poor geometry of the ray intersections used. To include a more complete set of video observations, a modified SfM algorithm was developed for use with this UAV platform. The algorithm first uses a standard SfM algorithm on key frames automatically selected based on the GPS velocity observations such that there is a constant overlap between key frames and a solution with strong geometry is achieved. Each frame is then trimmed to remove a border of 200 pixels from the edge to reduce the effects of lens distortion present in the consumer grade camera.

The first stage of the SfM algorithm is then used to identify projections of the same features in space from two or more views using the Scale Invariant Feature Transform (SIFT) technique developed in Lowe (2004). SIFT key features are identified in each

frame and then matched between frames using an approximate nearest neighbour kd-Tree approach (Snavely et al. 2006). The approach used in the matching of SIFT key features allows preliminary matches that are invariant to large changes in scale and rotation to be made (Lowe 2004). This set of feature matches is likely to contain several incorrect correspondences or outliers. An iterative global RANSAC approach following Nistér (2004) is used to identify and eliminate these outliers and at the same time estimate the frame to frame homographies. The camera's exterior orientation estimates can then be derived from these homographies. The resulting set of feature correspondences and exterior orientation estimates can then be used to predict the three-dimensional locations of each feature in relative space. This information is then used along with initial camera locations within a global bundle adjustment to provide optimal estimates of 3D point location and the camera's exterior orientation within an arbitrary mapping frame.

Once an initial sparse set of 3D points and exterior orientation estimates are known for each of the key frames, the orientation of the non-key frames which are selected to create a 5 Hz dataset to match the GPS observation rate can be determined. A reduced set of points with a strong spatial distribution is selected from each non-key frame based on an initial estimate of that frames geometry. These points are matched to points within the key frames and a spatial resection is performed to determine the exterior orientation of the non-key frames. The initial alignment of the camera was determined based on ground control targets placed near the take-off and landing area. A minimum of three targets was used for this purpose, however, the use of four targets is preferable in order to provide redundancy and avoid gross errors. If the boresight angles (e_b^c) between the camera and body frames are known, the orientation component of each exterior orientation estimate can be transformed into the body frame giving q_c. This provides the observation model used for each video frame. For consistency the orientation is calculated in quaternion space as follows:

$$q_c = e_\phi \cdot (e_b^c \cdot e_k) \tag{3.15}$$

where e_ϕ is the estimate of camera orientation in the camera frame given by the SfM algorithm. e_k is the stochastic measurement noise term within the SfM estimates of orientation. This noise is weighted based on the output of the bundle adjustment and non-key frame observations are attributed a higher noise than the surrounding key frames.

Sigma Point Kalman Smoother

To further improve the accuracy of the system, a smoothing algorithm is used. By applying a smoothing algorithm, an optimal solution is found for the position and orientation of the UAVLS system based on the entire set of flight observations. The smoothing algorithm involves running two independent filters forward and backward in time. The optimal state estimate, for each epoch, is then found by optimally combining the forward and backward estimates and their error covariances. It is well known that these smoothed estimates, which now incorporate all measurements, provide a significantly improved estimate of the vehicles state, see Shin (2004) for an example.

3.3.3 Calibration

The calibration of a laser scanning system is an important step in generating an accurate point cloud. The determination of the calibration parameters is made particularly difficult by the use of a system made up of off-the-shelf low cost component that introduces significantly large errors and has internal coordinate systems not well-defined. The lever-arm offsets between the laser scanner and the navigation system (a^b) and between the GPS and the IMU ($\bar{r}_{GPS}$) have been manually measured to cm level accuracy. The resolution of the boresight angles (R_b^s) between the laser scanner and the IMU are effectively hidden by the resolution and accuracy of the laser scanner as well as the orientation errors of any determined trajectory. A thorough literature search revealed no method which could repeatably resolve these angle, as such they have been assumed to be zero.

The determination of the boresight angles (e_b^c) between the camera and the IMU require careful attention as any error in these angles will introduce errors into the trajectory determination algorithm. A technique, outlined by Hol et al. (2010), which makes use of observations of the gravity vector made by both sensors was employed for this task. This procedure was repeated on 15 separate occasions to ensure that the correct boresight angles were found. Once the calibration parameters have been determined, the repeatability of the individual mounts and the strap-down nature of the system suggest that they will remain constant for future surveys.

3.3.4 Point cloud generation and accuracy assessment

The University of Tasmania's farm was used as the study area to assess the accuracy of the point cloud generated by the UAV platform (Figure 3.3). The 100 × 100 m area provides significant variation in slope as well as an area of significant canopy coverage in the south west. Furthermore, five different planar man-made features are present within the area. This area was surveyed using 8 different flight transects during 4 different flights at an average flying height of 50 m and an approximate horizontal velocity of 3.3 m/s. As previously mentioned, only scan angles of between ±30° were used for mapping. Under these conditions the resultant point cloud has a swath width of 57 m and a point density of approximately 50 points per m^2. The laser footprint at nadir is 0.69 m along track and 0.07 m across track. This results in significant overlap of laser footprints along the track and a gap of approximately 0.06 m across track. The footprint size increases towards the edge of the swath depending on the range and the angle of incidence with the terrain. Each of the four flights was flown using the OktoKopter's on-board autopilot and are summarised in Table 3.2. All flights were flown in very similar conditions, indicating the on-board autopilot provides an adequate solution for following predefined flight paths.

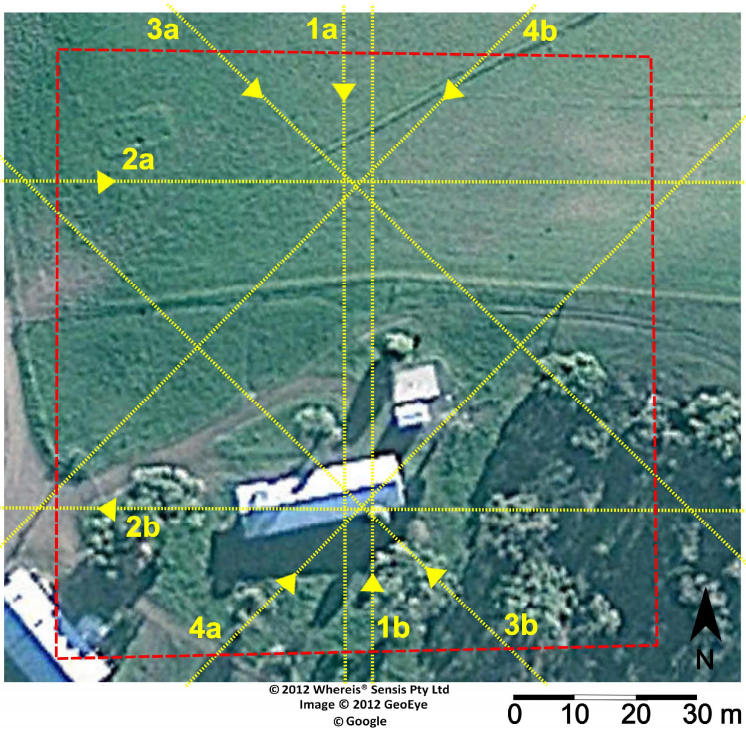

Figure 3.3: The test field (red) used for both the calibration and the determination accuracy of the UAV-platform showing the flight paths (yellow).

Each flight was processed twice to assess the effect of the inclusion or otherwise of SfM

observations. To achieve this assessment, 32 high reflectivity targets were placed across the study site. The 0.3 m^2 target size allowed a minimum of 4 direct observations to be made of each target under the targeted flying conditions. The design of these targets allowed them to be identified within the point cloud based on the return pulse width, which is reported by the Ibeo LUX and can be considered analogous to intensity for this study. A threshold at which these target could be identified was found by examining a histogram of return pulse widths produced for each point cloud. As trees were the only other features within the study producing pulse widths above this threshold, ground control strikes were identified as ground points with a pulse width above this threshold.

Table 3.2: Summary of the four flights flown over the study area.

Flight	**Flight Time (s)**	**Mean Height (m)**	**Mean Horizontal Velocity (m/s)**	**Primary Heading (deg)**	**Key Frames**/s
1	161	48	3.77	180	2.3
2	137	54	3.27	90	1.8
3	130	46	3.16	135	1.9
4	195	44	3.33	225	1.8

The location of ground control targets as measured by the laser scanner was determined to be the mean of all identifiable strike positions. This location was compared to the location of the center point of each target measured using dual frequency differential GPS ($\pm$0.02 m horizontal and $\pm$0.05 m vertical) to determine the accuracy of the UAVLS system. Only ground control with 5 or more identifiable strikes were used in this comparison, resulting in a small number of targets from the edge of the scan being excluded. The mean difference and standard deviation in the North, East and up values were calculated for each transect as well as the absolute horizontal error statistics. Finally, the points obtained over planar surfaces (e.g., building roofs) were extracted from each of the 8 point clouds. After applying a least squares fit of a plane to the extracted data, the standard deviation was calculated. This standard deviation gives an indication of the measurement performance of the laser scanner and the internal precision of the vertical measurements within the point cloud.

3.3.5 Assessing flying parameters for data collection

The optimum parameters for the collection of ALS data over forested environments have been widely studied (Lovell et al. 2005; Morsdorf et al. 2006; Goodwin et al. 2006). Point density, beam divergence, scan angle and the internal properties of the scanner are all

known to have an effect on the derivation of forest metrics in ALS data. Therefore, determining the effect of variations in survey conditions is an important consideration for UAVLS surveys. For instance, the laser scanner used in this system, has a higher beam divergence, a less sensitive diode, a different triggering mechanism and the ability to utilise higher scanning angles (up to 180°) in comparison to traditional ALS systems.

In order to determine the optimum flying conditions for this UAVLS system, data was collected over a 4-year old *Euclyptus* plantation in four flights. Each flight followed the same transect in forward and reverse directions with an average velocity of 4.0 m/s. For each flight the flying height was increased from 30 to 90 m above the take-off point in steps of 20 m. Point clouds were generated separately for the forward and reverse transects resulting in 8 separate point clouds. The point clouds were classified into ground and non-ground points using the filtering technique available in LASTools (Isenberg 2011). The height of each point above the ground was then calculated by subtracting the ground elevation from the absolute point height.

Four 12.62 m radius circular plots were extracted from each point cloud. The slope of the terrain and constant flying height above the take-off point allowed a variety of mean AGL flying heights to be assessed within these plots. Variation in footprint diameter, point density and scan angle were also assessed due to the significant variation caused by increases in flying height. For instance, the footprint diameter at 30 m (0.4 m across track) can be considered similar to the footprint size captured with modern full-scale systems. At 90 m the footprint size (1.4 m) is significantly larger than this. The lowest flying height of 30 m ensured a safe minimum operating distance of approximately 10 m above the trees at the top of the slope.

The high density point clouds collected by the UAVLS were decimated to lower point densities in steps of 10 points/m^2, from full point density to 0.5 points/m^2. The decimation procedure involved creating a grid with a randomly selected starting point and a cell size chosen to match the desired point density. For each cell within the grid the first return closest to the centre of the grid was added to the decimated point cloud. Any second and third returns from the same pulse were also included in the decimated point cloud. This procedure was preferred over other methods as it produced the most visibly similar point clouds to those produce at the higher flying heights.

A set of descriptive statistics were generated for each point cloud to assess variations of the point cloud characteristics captured with different properties. The set of statistics includes above ground height (AGH) quantiles, mean AGH, standard deviation, skew-

ness, kurtosis, and coefficient of variation. These statistics were chosen as they have been shown to represent the key canopy attributes and can be derived directly from the point cloud (Lim and Treitz 2004; Donoghue et al. 2007). These statistics were calculated for only first returns and for all non-ground returns above 1.0 m falling within the plot boundaries and for each cell within a 1.0 m grid covering the plot area.

The point cloud and statistic sets were then qualitatively and quantitatively compared. Initially, all non-decimated point clouds were compared in order to determine the overall effect of UAV flying height on the measurement of forest structure. Following this the decimated point clouds were used in the comparisons with the aim of separating out the individual variations due to point density, scan angle, and footprint size. Point density was separated from the other effects by comparing decimated point clouds from the same flight. The isolation of scan angle was achieved by comparing the gridded statistics of point clouds decimated to the same density. This approach allowed cells with up to 20° differences in scan angle to be compared, however, due to variations in range the footprint size was still a contributing factor to any differences found. A similar approach was taken to isolate footprint size, however, only cells with a scan angle difference of less than 3° were included in this analysis.

3.4 Results and discussion

3.4.1 Trajectory generation

Observations of the on-board position and orientation sensors were made for the entirety of each flight. The vibration isolation properties of the sensor mount allowed a high signal to noise ratio in the IMU observations to be achieved. These observations did not exceed the maximum range of the gyroscopes and accelerometers at any stage. GPS lock was also maintained by all receivers for each flight and a minimum of 5 satellites was observed by the dual frequency receiver at all times. This allowed accurate GPS position and velocity observations to be computed for each of the four flights.

The camera to IMU calibration procedure produced results with 99% confidence intervals of 0.11°, 0.17° and 0.18° for pitch, roll and heading. These results are consistent with the results presented in Hol et al. (2010) and can be considered to have been resolved to an accuracy suitable for this application. The SfM algorithm was able to orient all of the frames from each of the four flights. However, the accuracy of the observations from images dominated by the building in the middle of the study area was reduced due to the

relatively low number of SIFT features detected in these frames (Figure 3.4(a)). Within a forested environment, areas of bare earth will produce a similar reduction in SIFT features. The inclusion of these frames therefore represents a reasonable determination of the spatial accuracy of a point cloud generated in these environments. A high number of SIFT features were detected in frames that included a significant area of vegetation cover, as demonstrated in Figure 3.4(b). These results suggest that when used in densely vegetated environments, the SIFT algorithm should provide a reliable number of features for the SfM technique to operate accurately.

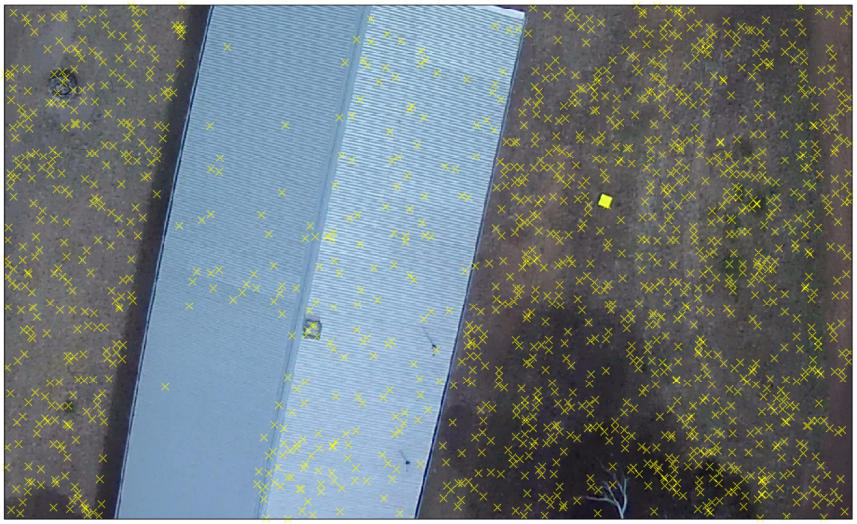

(a)

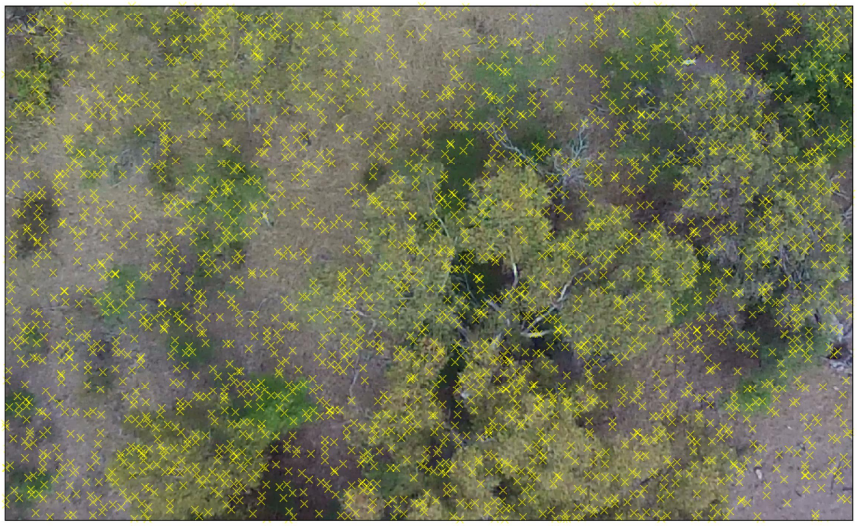

(b)

Figure 3.4: The detection of SIFT features (yellow crosses) within (**a**) a frame dominated by the building in the center of the study area, 1714 SIFT features were found and (**b**) a frame dominated by natural features including trees, 2959 features were found.

Figures 3.5(a) and 3.5(b) provide a comparison between the trajectory estimates from Flight 2 by the SPKS with and without the inclusion of SfM observations. As it was not possible to determine the true pose of the system, this comparison only allows the discrepancy between the two solutions to be observed. In this case, the orientation is varied by the inclusion of the SfM solutions. Considering an error of only 0.5° in an orientation angle can result in an on the ground error of 0.2 m, these differences are highly significant and any improvement will be determined by examining the spatial accuracy of the point cloud. There is only comparatively small differences in the estimation of position which is governed by the GPS observations.

3.4.2 Point cloud properties

Figure 3.6 shows an example of the point cloud generated for Transect 2a. This point cloud has a point density of 42.2 points/m^2. Table 3.3 gives a summary of the point cloud properties for each of the eight transects. The average point density including all three returns over every flight was 43.21 points/m^2. This density is significantly higher than the data that is currently used in forestry management and research (8 points/m^2) (Shrestha and Wynne 2012). The number of second and third returns across the entire study area was low, however, in the areas of dense vegetation the percentage of second returns increased up to 24% and third returns to 4.2%. This increase along with visual inspection of the point clouds is sufficient to suggest that points are being measured from within the canopy for use in the modelling of key forest metrics such as leaf area index and above ground biomass. An average area of 11,288 m^2 was mapped in each flight, which allows multiple transects to be flown over individual forest plots in a single flight.

The internal precision of the point cloud is highlighted by the standard deviations across planar surfaces. The standard deviation from a least squares best fit planes fitted to each surface was found to be 0.04 m, which is within the measurement precision of the Ibeo LUX (0.1 m at 1 σ). This is consistent with the results from (Jaakkola et al. 2010) who reported a similar variation with a Ibeo LUX sensor.

3.4.3 Point cloud accuracy

The results from the point clouds generated from the IMU/GPS only trajectory were first evaluated against the observed ground control targets. The method used to identify

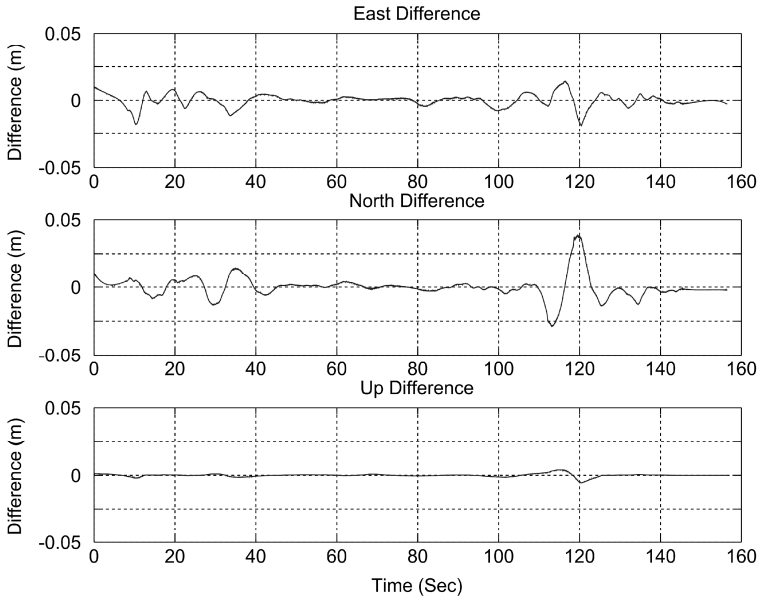

(a)

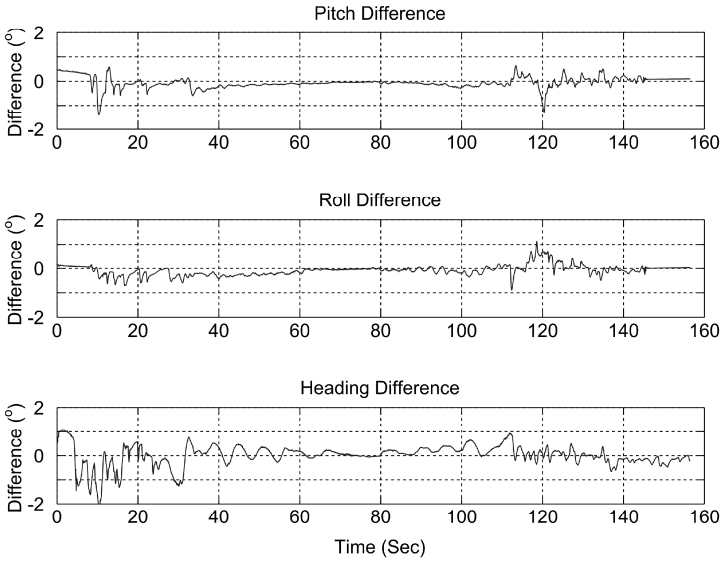

(b)

Figure 3.5: The differences in position (**a**) and orientation (**b**) as estimated by the Sigma Point Kalman Smoother with and without the inclusion of observations of orientation generated by the SfM algorithm. A difference in orientation 0.5° can result in a 0.2 m difference of a measured point at the nominal flying height used in this trial.

the number of points belonging to ground control allowed an average of 14 points per target to be observed. Across the 8 point clouds only 3 targets were rejected as they were observed with five or less points. All 3 of these rejected targets were only partially observed at the edge of the swath. Table 3.5(a) shows that the errors are generally within

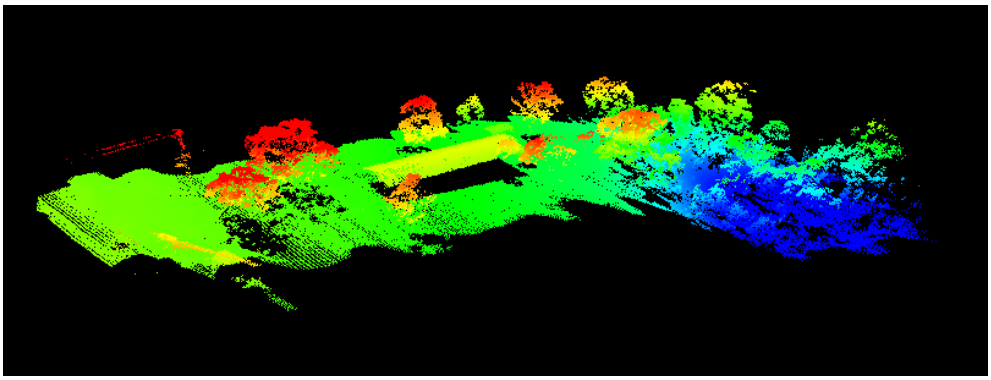

Figure 3.6: An example point cloud produced by the SfM trajectory determination algorithm. This particular point cloud has an average point density of 40 points/m^2 and covers 4,877 m^2.

Table 3.3: Properties of the eight generated point clouds.

Transect	**Area** (m^2)	**Point Density** (**pp**m^2)	**% 2nd Returns**	**% 3rd Returns**
1a	5,931	38.7	4.09	0.35
1b	6,288	37.2	5.88	0.53
2a	5,586	62.6	3.46	0.54
2b	4,922	42.2	13.90	2.05
3a	5,459	35.9	15.01	2.02
3b	4,986	36.5	15.41	2.37
4a	6,176	40.6	2.92	0.25
4b	5,811	52.0	2.63	0.17

the expected values from the stochastic modelling outlined in Wallace et al. (2011). The standard deviation in both North and East measurements are similar. This suggests that they are not dominated by the effect of the beam divergence properties of the Ibeo LUX laser scanner.

The results from the IMU/GPS/SfM solution shown in Table 3.5(b) are close to the expected values from stochastic modelling (Wallace et al. 2011). The horizontal RMSE across all of the 130 measured ground control locations is 0.34 m (expected 0.26 m) and the vertical error is 0.15 m (expected 0.14 m). One source of error which is not included in stochastic modelling can be attributed to the use of large ground control targets and the systematic sampling properties of the laser scanner. This target size is required in order to ensure the ground control target is directly measured and to ensure that these measurements are found. The use of an average position from all identified target strikes relies on either an even point sampling across the target or a significant number of random strikes being recorded. This is potentially biased in the along track direction by the location of scan lines across the target.

Table 3.4: Mean, Standard Deviation and RMSE in the differences between the ground control location measured by the UAVLS system without (**a**) and with (**b**) SfM observations in comparison to the locations measured by a differential GPS survey. The expected values as derived from stochastic modelling are also included as derived in Wallace et al. (2011).

Flight	**No. Targets**	**East (m)**		**North (m)**		**Up (m)**		**RMSE (m)**	
		Mean (m)	**σ (m)**	**Mean (m)**	**σ (m)**	**Mean (m)**	**σ (m)**	**Hor. (m)**	**Vert. (m)**
1a	16	−0.11	0.23	0.26	0.21	0.11	0.23	0.57	0.24
1b	14	0.22	0.40	−0.13	0.31	−0.02	0.07	0.62	0.07
2a	17	0.08	0.59	−0.06	0.33	0.09	0.22	0.66	0.23
2b	16	−0.13	0.42	−0.10	0.21	0.01	0.05	0.48	0.05
3a	16	−0.17	0.55	0.18	0.34	0.27	0.09	0.85	0.29
3b	17	−0.04	0.14	0.30	0.24	0.07	0.10	0.40	0.12
4a	15	−0.06	0.50	−0.05	0.54	0.00	0.17	0.70	0.16
4b	18	−0.13	0.37	0.15	0.42	−0.00	0.20	0.58	0.19
all	130	−0.03	0.41	0.07	0.42	0.06	0.18	0.60	0.19
						Expected		0.54	0.16

(a)

Flight	**No. Targets**	**East (m)**		**North (m)**		**Up (m)**		**RMSE (m)**	
		Mean (m)	**σ (m)**	**Mean (m)**	**σ (m)**	**Mean (m)**	**σ (m)**	**Hor. (m)**	**Vert. (m)**
1a	17	0.02	0.11	−0.12	0.27	−0.02	0.14	0.38	0.15
1b	14	0.13	0.15	−0.05	0.24	0.09	0.08	0.41	0.12
2a	17	−0.03	0.25	0.03	0.06	0.04	0.14	0.35	0.17
2b	16	−0.04	0.12	−0.06	0.07	−0.00	0.03	0.21	0.03
3a	16	−0.19	0.32	0.08	0.08	0.05	0.13	0.34	0.16
3b	17	0.09	0.12	0.17	0.22	0.11	0.14	0.31	0.17
4a	15	0.02	0.30	−0.17	0.24	−0.04	0.09	0.41	0.10
4b	18	−0.03	0.22	0.02	0.26	−0.06	0.15	0.33	0.16
all	130	0.01	0.17	−0.01	0.21	0.03	0.12	0.32	0.14
						Expected		0.26	0.15

(b)

Another effect of the averaging technique used is that the error due to beam divergence is not fully represented in the final error statistics. Beam divergence, which is high in the Ibeo LUX laser scanner, affects predominantly the horizontal accuracy of the point cloud in the along track direction. The standard deviation in flights one (flown north-south) and two (flown east-west) suggest that some of this effect is captured. The effects of these errors are more evident when examining the high intensity returns within the point clouds, in which the footprints of each individual ground control points can measure up to 0.6 m in the across track direction. This averaging will not occur in measured trees for future surveys, therefore, careful consideration will need to be given to tree metrics measured in the horizontal direction such as canopy width. These measurements are likely to be exaggerated and may require adjustment before being applied within any further modelling.

In comparison to the IMU/GPS only solution, the results with the inclusion of SfM observations show significant improvement in the horizontal component. The RMSE for the total 130 ground control targets dropped from 0.61 m without SfM observations to 0.34 m with SfM observations. This improvement combined with the difference in orientation shown in Figure 3.5(b) suggests that the SfM algorithm has resulted in an improvement in the estimation of orientation. As expected, the vertical errors within the point clouds from both solutions are similar. These results suggest that both of the assessed solutions are suitable for use in forest inventory assessment. However, the SfM observations allows the accuracy to improve to a level comparable to that achieved by modern full-scale systems (based on the values reported in Goulden and Hopkinson 2010). This improvement will allow for direct comparison and integration of the two datasets. Furthermore, the improvement in accuracy enhances the reliability and suitability of the platform for use in multi-temporal surveys.

3.4.4 Survey constraints for inventory capture

The distribution of AGH first and last vegetation returns was found to be highly affected by the flying height of the UAVLS as demonstrated in Figure 3.7. For flying heights of below 50 m AGH minimal variation in the AGH distributions was observed. Attenuation in the number of returns in the upper canopy was present when plots were captured at flying heights greater than 50 m. At this altitude there was also a decrease in the proportion of pulses with multiple returns (from 35% at 30 m to 2% at 90 m). This suggests that the energy required to trigger a pulse in the Ibeo LUX scanner is not being reflected from the canopy when the pulse is emitted at these flying heights. As the Ibeo

LUX scanner has a working range of 200 m, the signal attenuation is most likely due to a combination of the canopy structure (i.e. small surface areas and dispersal of the emitted light), the footprint size of the beam, as well as the internal triggering mechanism of the Ibeo LUX laser scanner.

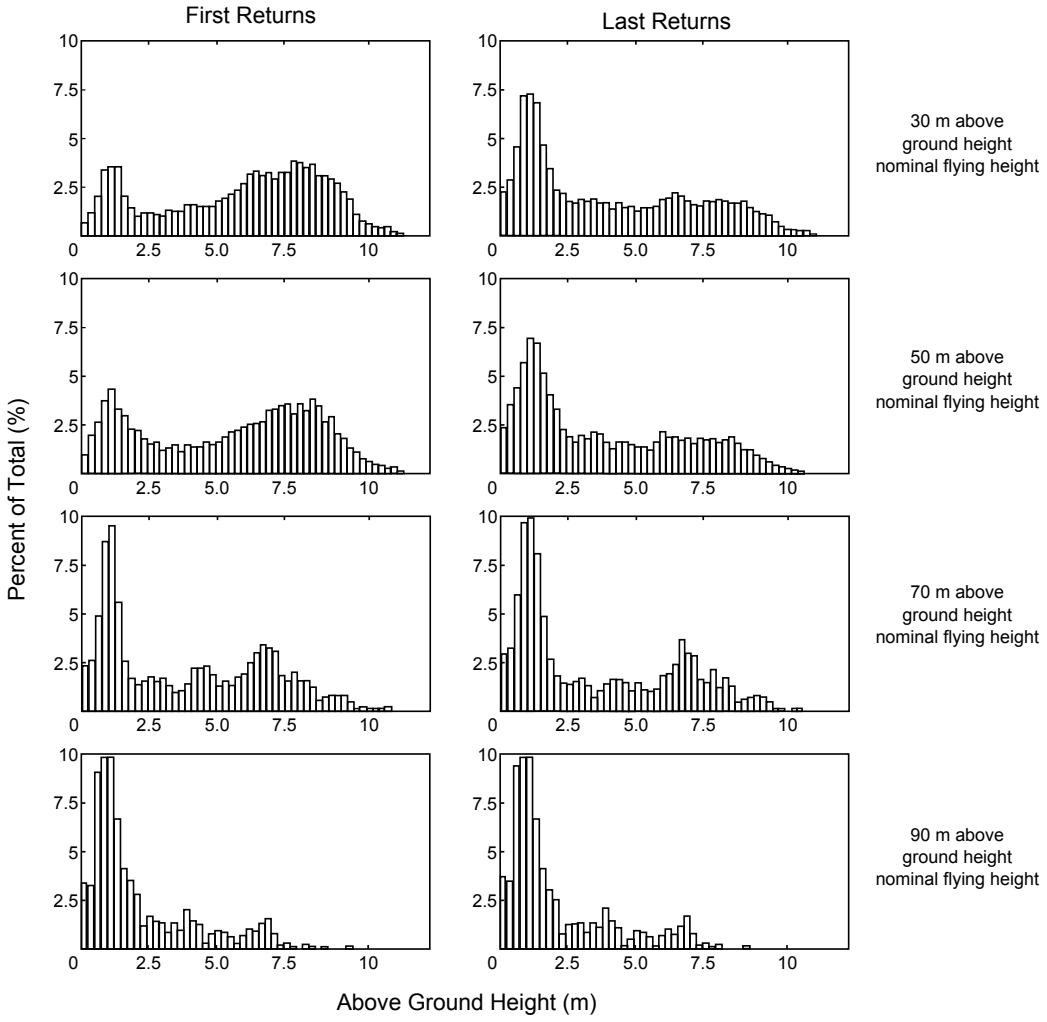

Figure 3.7: Histograms of the above ground height of vegetation returns over a single plot for point clouds captured at above ground flying heights 30 m, 50 m,70 m and 90 m. There is an obvious attenuation of upper canopy returns due to flight altitude.

At flying heights below 50 m all of the distribution statistics were observed with high levels of repeatability. For instance, the absolute deviation comparing forward and reverse transects captured at the same height below 50 m is less than 3%, and less than 7% when comparing all plots captured with mean flying heights of less than 50 m. This variation reached up to 120% when point clouds captured at flying heights greater than 50 m were included in the analysis.

Although not as severe as seen in point clouds captured at flying heights 50 m AGL,

comparing decimated point clouds highlighted that decreases in point density result in a reduction in the proportion of points returned from the very top of the crown. This is illustrated by a decrease of up to 1.2 m in the upper AGH quantiles at the plot level (90^{th} and 99^{th}, when comparing 10 points/m^2 to 77 points/m^2). As the positively skewed canopy height distribution tends toward symmetry there is also a smaller increase in the mid-canopy height quantiles. Nevertheless, a reduction in point density from 77 points/m^2 to 30 points/m^2 was found to have little effect on any of the plot level statistics calculated. Under sampling of the canopy at lower point densities resulted in significant variation of distribution statistics within individual 1 m grid cells. For point densities below 30 points/m^2 there is a significant reduction of up to 10% in the higher quantiles. Furthermore, the percentage of canopy returns varied by up to 50% with large variations in point density ($>$ 20 points/m^2).

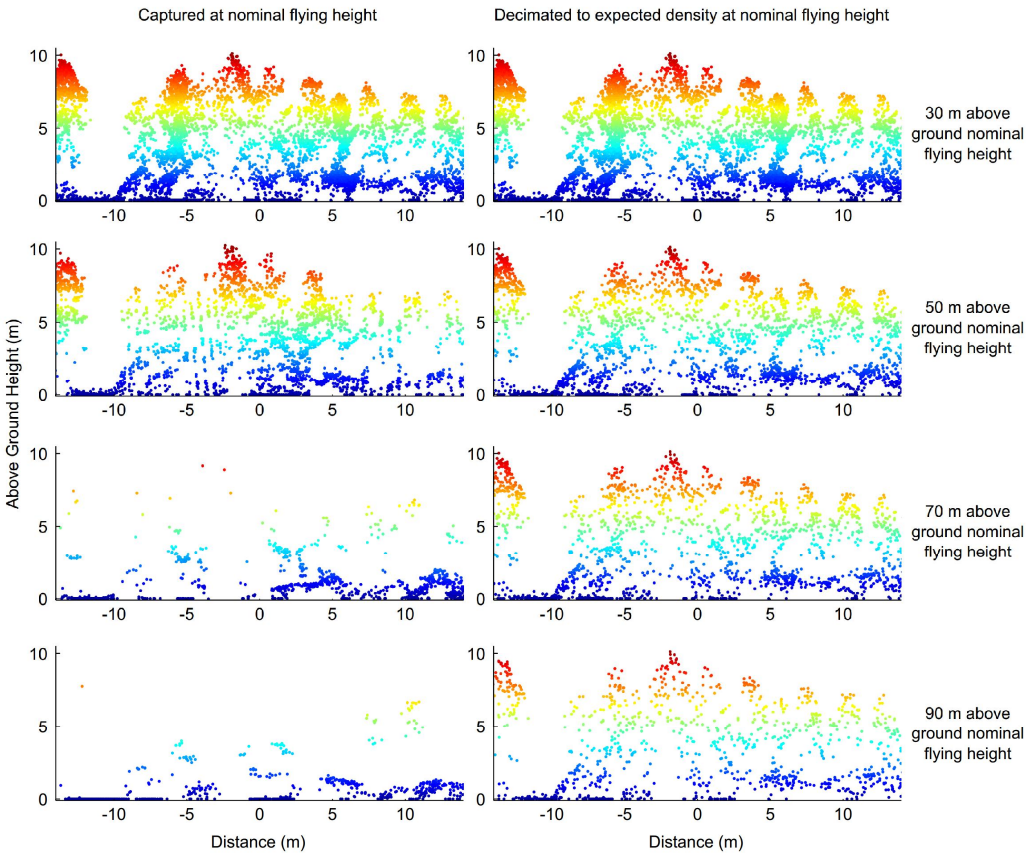

Figure 3.8: Point clouds as captured at four different flying heights in comparsion to point clouds generated from the decimation procedure at the expected density of each nominal flying height.

The use of large scan angles resulted in occlusions and voids occurring in the data (Figure 3.9). Statistics in grid cells with a low number of returns were not calculated, therefore,

the comparison of most statistics from cells with a sufficient number of returns showed only a slight increase in variance for cells with large scan angle differences. There was no significant variation observable due to footprint sizes (over a range of 0.4 to 1.3 m) in data captured at lower than 50 m. Analysis was restricted to comparisons of cells with similar scan angles. Therefore, greater variation towards the edges of the swath due to an increased range of footprint sizes may occur.

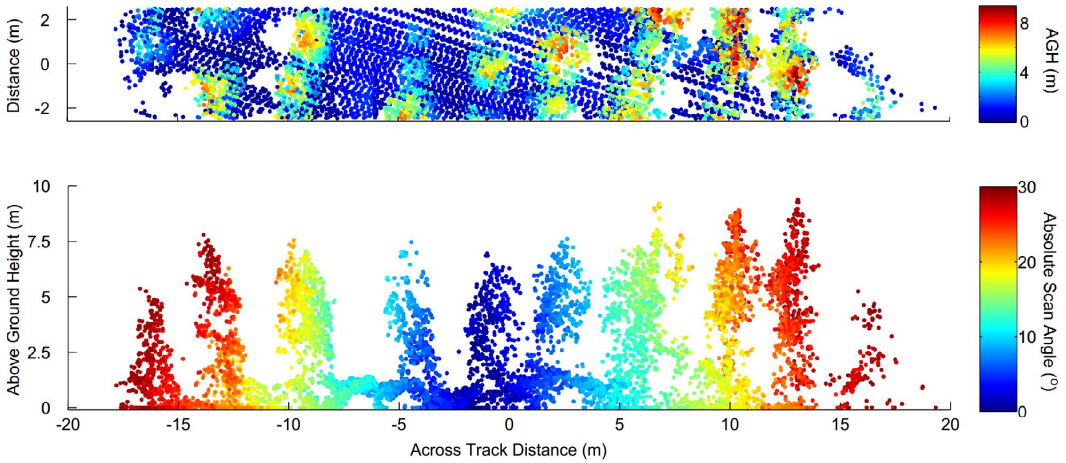

Figure 3.9: Top view and profile plot of a point cloud demonstrating the occlusion and resulting shadowing effect, which increases with increasing scan angle.

3.5 Conclusions and future work

This paper has outlined the development of a low-cost Unmanned Aerial Vehicle laser scanning (UAVLS) system. This included the development of a Sigma Point Kalman Smoother (SPKS) with the aim of optimally combining observations from a Micro-Electromechanical System (MEMS)-based Inertial Measurement Unit (IMU), a GPS receiver and the observations of orientation using High Definition (HD) video and a Structure from Motion (SfM) algorithm to determine an accurate estimate of aircraft position and orientation. This system was assessed with application to forest inventory to determine the spatial accuracy of the resultant point clouds and the repeatability in the measurement of individual tree height, location and canopy width.

We demonstrated that with the inclusion of observations of orientation from video, this system is capable of producing point clouds with root mean square errors of 0.34 m horizontally and 0.14 m vertically for a nominal flying height of 50 m. This represents a 68% reduction in variance within the horizontal component when compared to point

clouds generated with the same SPKS without video observations. This accuracy is similar to that achieved by full scale ALS systems currently used for forest inventory purposes.

Performing multiple repeat flights over of a forest plantation indicated that repeatable point cloud characteristics can be captured from the UAVLS system in this environment. To achieve this, however, the use of large scan angles should be avoided and the flying height of the system needs to be restricted to less than 50 m. At flying heights greater than 50 m there was a significant attenuation of returns from the canopy caused by a decrease in the return intensity from vegetation features.

Future research is aimed at performing forest surveys to further evaluate the UAV's potential within the forestry industry. These surveys will be designed to assess the UAV as a tool, which allows forest managers to make more informed decisions on pruning and thinning regimes, monitoring tree health and defoliation, as well as improving the accuracy of allometric forest growth models. Although future developments of this system (including hardware and battery technology) will increase flight endurance, the current system has been shown to be capable of flying multiple transects capturing data over an individual forest plot in a single flight with restricted flying conditions. These results have confirmed that our UAVLS system is a suitable platform for the generation of high resolution point clouds for assessing forest structure at the individual tree level.

3.6 Thesis context

This Chapter provided the foundations for this thesis, outlining methods for the accurate georeferencing of point clouds captured with the UAVLS system. The positional accuracy of laser return was assessed and found to be suitable for the collection of data for inventory assessment. Furthermore, restrictions on the flying properties for the repeatable measurement of forested environments were tested and will be adhered to in the remainder of this thesis.

4 | Evaluating tree detection and segmentation routines on very high resolution UAV laser scanning data

Chapter 4 focuses on the extraction of Individual Tree segments from the UAVLS data. The work comprising this chapter is in press in *IEEE Transactions on Geoscience and Remote Sensing* (Wallace et al. Accepted for publication[b]).

Abstract

Airborne Laser Scanning (ALS) is becoming an increasingly used tool to support decision making processes within forest operations. Area-based methods that derive information on the condition of a forest based on the distribution of points within the canopy have been proven to produce reliable and consistent results. Individual tree-based methods, however, are not yet used operationally in the industry. This is due to problems in detecting and delineating individual trees under varying forest conditions resulting in an underestimation of the stem count and biases towards larger trees. The aim of this study is to use high resolution laser scanning data captured from a small multi-rotor Unmanned Aerial Vehicle (UAV) platform to determine the influence of the detection algorithm and point density on the accuracy of tree detection and delineation. The study was conducted in a 4-year old *Eucalyptus globulus* stand representing an important stage of growth for forest management decision-making processes. Five different tree detection routines were implemented, which delineate trees directly from the point cloud, voxel space, and the Canopy Height Model (CHM). The results suggest that both algorithm and point density are important considerations in the accuracy of the detection and delineation of individual trees. The best preforming method which utilised both the CHM and the original point cloud was able to correctly detect 98% of the trees in the study area. Increases in point density (from 5 to 50 points/m^2) lead to significant improvements (of up to 8%) in the rate of omission for algorithms which made use of the high density of the data.

4.1 Introduction

Sustainable forest management and decision making processes require timely and accurate forest information. The information derived from Airborne Laser Scanning (ALS) point clouds is increasingly used to support decision making processes within everyday forest operations. A number of the processes and algorithms used to derive information from ALS have reached maturity, and it can now be considered a standard data source for defining the spatial characteristics of a managed forest (Wulder et al. 2008; Hyyppä et al. 2012b).

Forest inventories are able to be derived from ALS data using one of two approaches. The area-based approach, first reported in Nelson et al. (1988), infers forest properties for an area of interest based on the relationship between field measurements and the empirical above ground height (AGH) distribution of canopy returns (Packalén and Maltamo 2007). This approach is used to estimate a variety of forest inventory attributes with high accuracy including biomass, stand volume, and basal area (Næsset 2002; Holmgren 2004; Hudak et al. 2008). The individual tree detection approach, first reported in Hyyppä and Inkinen (1999), segments points representing each tree to determine individual tree properties such as position, height, canopy shape, and species.

The timing of silvicultural activities, such as pruning, thinning and harvesting, is of crucial importance to the management of plantation forests. Due to the high costs of airborne data the inventory information collected from ALS surveys is not often timed to coincide with these key growth stages. As such, decisions made based on these surveys often require input from alternate sources, such as growth models or field inventories to be accurate. Mini-Unmanned Aerial Vehicles (UAV) have recently been proposed as an alternative platform for the capture of laser scanning data (Jaakkola et al. 2010; Wallace et al. 2012b). UAVs have been shown to allow very high spatial resolution data (50 to 120 points/m^2) to be captured at comparatively low survey costs. These low survey costs will allow for high temporal resolution data to be collected in support of key decision making processes.

Data from a mini-UAV is captured without significant occlusion of the top of the canopy and therefore has similar characteristics to full scale airborne data (Wallace et al. 2012a). Nevertheless, the low altitude flight and minimal flight time restrict the area which can be captured in a single flight. This suggests that in order to take full advantage of the unique combination of high spatial data collected at low costs, accurate and robust

delineation of individual trees is essential in order for UAVs to be considered a viable and practical tool within the forest industry. The high density data collected from UAV platforms suggests that UAV Laser Scanning (UAVLS) has the potential to replace laborious and costly field sampling in discrete plots.

Several algorithms have been developed to delineate trees from ALS point clouds (Maltamo et al. 2005; Koch et al. 2006; Wang et al. 2008; Alexander 2009; Reitberger et al. 2009; Vauhkonen et al. 2011a). The majority of these algorithms aim to exploit the fact that tree tops represent the highest part of the landscape and, therefore, attribute local maxima within the data to individual tree tops. This is followed by the segmentation of feature space to produce representations of trees for example using region growing (Brandtberg 2003). Differences between these algorithms typically relate to the amount of smoothing applied to the data to remove false maxima, post-processing of the results (e.g. data smoothing), or the feature space in which the segmentation is employed. For instance, detection and segmentation processes have been performed directly on point cloud feature space (Morsdorf et al. 2003; Li and Guo 2012; Lahivaara et al. 2012) or on a feature spaces which have been derived from the initial point cloud, such as a Canopy Height Model (CHM) (Yu et al. 2011) or voxel space (Vaughn et al. 2012).

Difficulties in detecting and delineating individual trees, often produce an underestimation of the number of stems and a bias towards larger trees (Peuhkurinen et al. 2011). These low stem detection accuracies have been shown to have a significant effect on the accuracy of inventory estimates derived from these approaches (Vastaranta et al. 2011).The extent of this effect is dependent on the accuracy of the reported algorithms which varies significantly. Pitkanen et al. (2004), for instance, achieved a tree delineation accuracy of only 40% in comparison to Heinzel et al. (2011) who achieved accuracies of up to 88%. Directly comparing these results, however, could be misleading due to different dataset properties (i.e. pulse density and number of returns per pulse) and forest conditions (stem density for instance).

In order to provide an objective estimate of the accuracy of different routines several studies comparing the application of these routines under varying conditions have been completed (Hyyppä et al. 2001; Vauhkonen et al. 2011b; Edson and Wing 2011; Kaartinen et al. 2012). Kaartinen et al. (2012) for example, compared 13 different algorithms under boreal forest conditions concluding that the main factor affecting the accuracy of the tree detection and delineation was the algorithm employed. Whereas Vauhkonen et al. (2011b) compared six different algorithms across varying forest structures and suggested that accurate delineation of trees is highly dependent on the properties of the

forest, including stand density and the spatial pattern of the trees.

The focus of these comparative studies, and the development of most algorithms, has been the delineation of individual trees from ALS datasets of typical densities captured during airborne surveys (from 1 to 10 points per square meter (points/m^2)). It has been hypothesised that higher density data, such as that obtained by UAV platforms, is likely to provide a better representation of the features used to delineate trees and therefore improve the accuracy of these methods (Wang et al. 2008).

The aim of this paper is to apply and assess the ability of tree detection algorithms to detect and delineate individual trees within an immature *Eucalyptus globulus* plantation using high density UAVLS data. This paper evaluates the effect of point density on the accuracy of tree detection and delineation using several tree detection algorithms within an immature *Eucalyptus globulus*. A UAV platform is used to collect on-demand high density data, which is subsequently decimated to providing a comparison to densities collected with modern full scale systems. The results from each approach and at each density are subsequently validated against data acquired from field surveys.

4.2 Study area and data collection

The study was conducted in a 4-year old *Eucalyptus globulus* plantation located in Southern Tasmania, Australia (E146 ° 56 ′ 54 ″, S43 ° 05 ′ 18 ″). Trees within the coupe were planted at 2.25 m intervals along rows 4.0 m apart. A field survey of individual trees within six plots with fixed radii of 12.62 m was conducted. Within each plot we recorded position, crown diameter, tree height, the number of overlapping crowns, and the presence of forks and ramicorns for each plantation species. For non-plantation species (representing 2% of the recorded trees), only position of the stem at breast height and tree height were recorded. Plot centres were surveyed using a differential GPS receiver (0.05 m accuracy) and stem heights and locations were measured using a forestor vertex hypsometer and compass bearing to the plot centre (giving an approximate 1.0 m accuracy). Crown diameter was measured as the mean of the largest diameter branch and the diameter of a branch at 90° to this initial measurement. Summary statistics of the field data collected within the six plots are given in Table 4.1. The stem densities of the plot ranged from 680 to 1560 stems per hectare suggesting inconsistent planting and some loss of trees.

Discrete return laser scanning data was collected over each plot with the TerraLuma

Table 4.1: The properties of the six plots for which field data was collected within the *Eucalyptus globulus* plantation.

Plot	Stem Count	Mean Height (m)	Mean DBH (m)	Mean Crown Width (m)	Mean Point Density (points/m^2)
1	49	5.71	0.07	3.01	67
2	34	6.47	0.09	3.79	163
3	59	8.93	0.09	3.60	65
4	78	7.05	0.08	3.17	68
5	46	8.80	0.09	3.07	61
6	42	8.86	0.11	3.05	87

UAVLS system described in Wallace et al. (2012b). An Ibeo LUX laser scanner, which measures up to 3 returns per pulse, was mounted on the UAV and used to collect observations within a scan angle range of ±30 °. Two perpendicular passes were flown over each plot at an approximate flying height of 40 m above ground level (AGL) (and 32 m above mean crown height). The point clouds from the perpendicular flights were merged resulting in final point clouds with point densities of at least 60 points/m^2 covering each plot with a 8 m buffer (Table 4.1). For the purpose of independent validation of horizontal and vertical accuracy, six reflective targets were placed under each flight path and surveyed with RTK GPS. The locations of these targets within the generated point clouds suggested that root mean square errors (RMSE) of better than 0.17 m horizontally and 0.11 m vertically were achieved (consistent with Wallace et al. 2012b). The resultant point clouds were clipped to include a 5 m buffer around the plot area to minimise edge effects in the tree detection and delineation algorithms.

4.3 Materials and methods

4.3.1 Point cloud pre-processing

In order to determine any improvement provided by the use of high density UAV data, the full density point cloud was decimated to produce four further point clouds with densities of 5, 10, 25, and 50 points/m^2 to simulate data collected at different densities. The decimation procedure follows Vauhkonen et al. (2008), which involves selecting an individual pulse from each cell within a grid, with a cell size set to match the desired point density. In this case, a random starting point and orientation were selected for each grid and a random pulse selection was made from the pulses which fell within each cell. Every return from each selected pulse was included in the decimated point cloud.

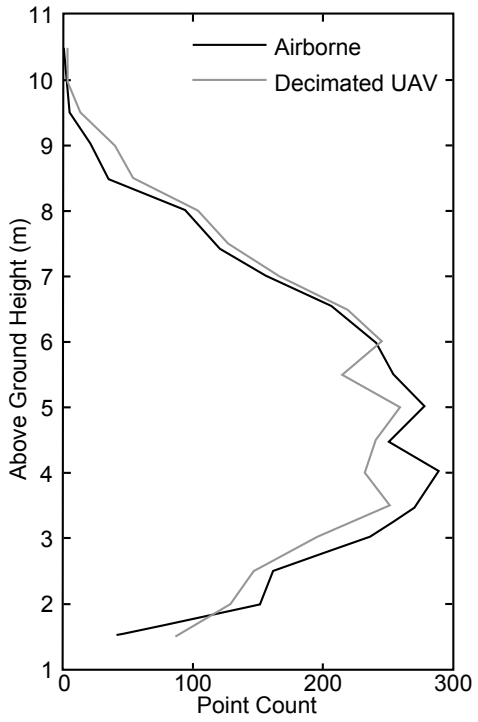

Figure 4.1: AGH distributions of full scale airborne and UAV data decimated to the same density (8 points/m^2) captured over a coincident area. The ALS data was captured with an ALTM Gemini laser scanner with a pulse rate frequency of 70 kHz and an on ground laser footprint of 0.2 m.

This method was preferred over techniques which remove points based on scan lines (i.e. Raber et al. (2007)) as it produces a homogeneous point density and a similar AGH distributions of canopy returns to full scale ALS data (Figure 4.1). This allows the decimated data to be used as a proxy for full scale data.

In order to obtain forest information from a UAVLS point cloud, initial processing requires the extraction of all ground points. This includes the computation of point height above the ground surface. There are numerous algorithms available to distinguish bare ground points from vegetation and other above ground points (e.g. see review in Meng et al. (2010)). In this study, we applied the iterative filtering and thresholding algorithm developed by Axelsson (1999). The approach uses a progressive Triangular Irregular Network (TIN) densification method where new points are iteratively added to a TIN model of ground points if they are within defined angle and distance thresholds. The ground points identified by this algorithm were then used to create a 0.1 m resolution Digital Terrain Model (DTM) using natural neighbour interpolation. The AGH of all non-ground points was then calculated using this surface resulting in a normalised point cloud. This approach was applied to the full and decimated point clouds independently with thresholds for each decision rule set to achieve optimum results at each point

density.

The normalized point clouds were then used to generate Canopy Height Models (CHM) by assigning each pixel with the maximum height of all the points that fall within its boundaries. Missing data and sinks (the result of pulses which have penetrated the canopy) were replaced using a pit filling algorithm outlined in Ben-Arie et al. (2009), in which pits are identified and replaced by median value of the 8 surrounding cells. The cell size of the generated CHM is dependent on the individual tree detection algorithm used as discussed in the following section.

4.3.2 Individual tree detection algorithms

The tree detection and delineation algorithms evaluated in this study were selected to be representative of the three different feature spaces often used in the literature: 1) the original 3D point cloud space, 2) Voxel space, 3) and the Canopy Height Model (CHM) (as depicted in Figure 4.2). One algorithm from each feature space as well as one hybrid algorithm have been evaluated in this study. These algorithms have been selected as they are commonly used in the literature and comparative studies such as Kaartinen et al. (2012) and Vauhkonen et al. (2011b) have indicated that the tree detection accuracies are relatively high. Where necessary, the following algorithms have been adapted to ensure that the increased resolution of the data is fully utilised and to account for the properties of the tree crowns found in the study area.

Point cloud detection and delineation (PDD)

Several algorithms that delineate trees directly from the point cloud have been presented within the literature (Reitberger et al. 2009; Alexander 2009; Li and Guo 2012). The algorithm employed here is an adaption of the technique outlined in Li and Guo (2012). The approach aims to exploit the changes in relative space between individual trees at different heights to determine a tree boundary. Beginning with the highest point in the normalised point cloud as the first tree, all other points are evaluated against a set of criteria to determine if they belong to this current tree. The criteria are:

1. If the point is not a local maxima within a given search radius (i.e. 2 m) it belongs to the current tree if the point is closer to a point within the current tree than any point already classified as a non-tree point.

2. If the point is a local maxima, the point belongs to a tree if it is within a distance

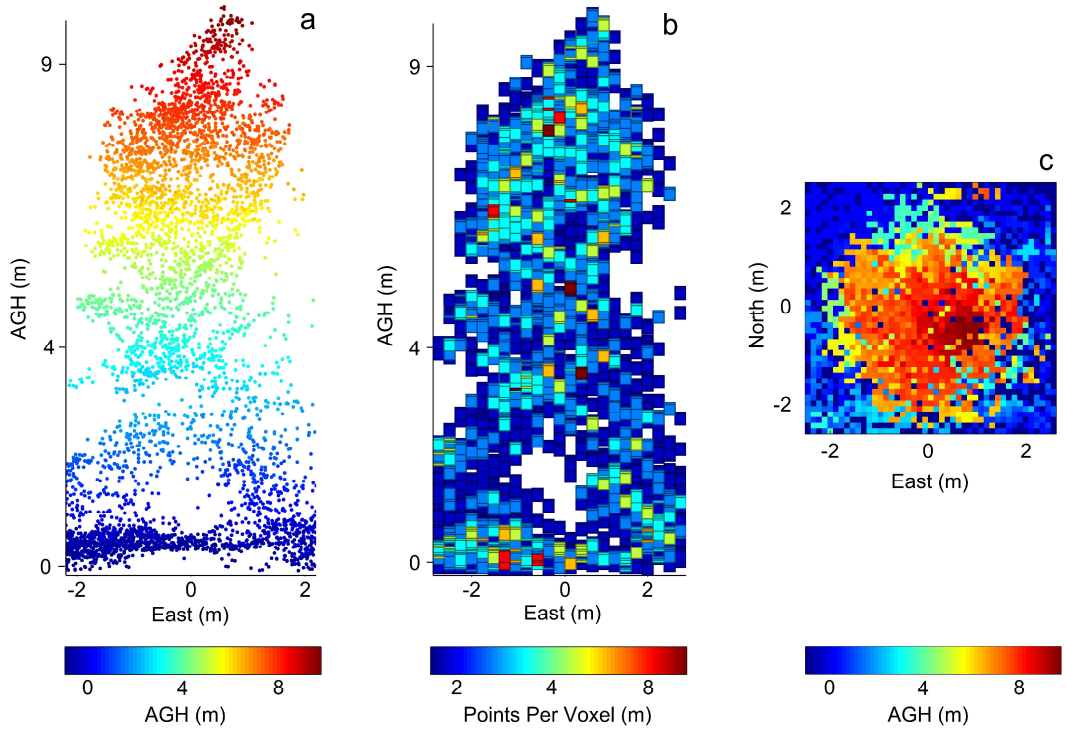

Figure 4.2: Representation of a single tree within the three feature spaces analysed in this study, a) the original point cloud, b) 0.2 m cubic voxel space and c) a 0.1 m resolution CHM.

(dt) of all points in the current tree and it satisfies criteria 1.

Once a tree has been segmented, the algorithm continues with the next highest unclassified point within the data set as a new tree. The search radius can be chosen arbitrarily, however, the threshold distance (dt) needs to be tuned to the structure of the forest being analysed. In this case, two values (1.5 and 0.9 m) were used depending if the point being examined was above or below 5 m in normalised height. In Li and Guo (2012), the process is repeated until all points have been attached to an individual tree segment. However, due to the complexity of the understory and the large number of points in this study, the search was stopped once all points 1.3 m AGL had been classified. This allows trees that have canopies extending to the ground to be almost completely delineated while stopping understory vegetation being recorded as belonging to a tree.

The algorithm presented by Li and Guo (2012) is also extended by applying a further step to merge or split a tree depending on the crown radius of a segmented tree. For segments which are deemed potentially too large based on an area to height ratio, the algorithm is repeated with relaxed distance criteria. Segments which are too small to

be a tree are merged with neighbouring segments based on Euclidean distances. Tree location is taken as the location of the highest point within a segment, and crown width is determined based on the average distance of the furthest point from the tree location and the furthest point at 90° from this location.

Voxel space detection and delineation (VDD)

The VDD Algorithm is based on the algorithm outlined in Wang et al. (2008). The point cloud data is first projected into voxel space, where each voxel is attributed with the number of points it contains. Crown objects were defined in each horizontal voxel layer based on a hierarchal morphological algorithm, in which pixels with higher densities are assumed to be the most likely location of a tree crown (Wang et al. 2008). The crown objects are traced through the voxel layers and merged if the intersection area of a segment in one vertical layer and the layer directly below is greater than 80% of both individual segment areas. In this study, a higher resolution voxel space was employed, in comparison to Wang et al. (2008), allowing the extra information in the UAV point cloud to be exploited. Tree location was defined as the centre of the maximum voxel in which the tree occurred and crown width as the mean of the horizontal projection of the tree from all merged layers.

CHM detection and delineation (CDD)

The most common form of algorithm used to detect and delineate trees from ALS data is based on detecting local maxima within the CHM. The algorithms often first apply a smoothing strategy to eliminate any spurious maxima and minor tree level fluctuations caused by branches. The degree of smoothing is often determined based on knowledge of the crown size to tree height (Reitberger et al. 2009) or by applying multiple filters and evaluating the results (Persson et al. 2002). As the study area in this paper is a plantation, it is a reasonable assumption that the trees will all be approximately the same height and width. For this reason, a Gaussian filter with a 1.5 m kernel was applied and the degree of smoothing was varied depending on the point density and cell size of the CHM. Two different CHMs, a 0.50 m resolution CHM (CDD_{50}) and a CHM with an optimised resolution to achieve an average of 2 pulses per grid cell (CDD_{opt}), were generated for each point cloud in this study.

Local maxima were then derived from the smoothed surface using a 3 x 3 kernel and any maxima greater than 2 m were considered to be the location of a tree. The delineation of tree crowns was performed using marker controlled watershed segmentation. The

crown width of a tree was considered equal to the mean distance of tree location to the boundary of the segmented area.

CHM detection and point cloud delineation (CDPD)

A hybrid algorithm presented in the literature for delineation of trees within point cloud feature space is based on seeded k-means clustering (Morsdorf et al. 2003; Gupta et al. 2010). In this approach, local maxima were first identified from a smoothed (0.2 m resolution) CHM with a similar smoothing strategy to the CDD algorithm applied. These maxima were used as seeds within the k-means clustering algorithm on a point cloud with a down scaled z-dimension by a factor of 1.5 (Gupta et al. 2010). The resulting cluster centres are used as tree locations. Crown width is then estimated based on the radii of a convex hull of the cluster.

4.3.3 Performance evaluation

The performance of each tree detection algorithm was evaluated by applying the following procedure. Segmented trees were first linked to field measured trees if the two crown areas overlapped by more than 20%. If the crown of more than one segmented tree overlapped a field measured tree, the closest tree (based on 2D Euclidean Distance) was selected as a match. The unmatched trees within the field and UAVLS datasets were assigned as false negative and false positives respectively. The detection rate (estimated tree count in proportion to number of field measured tree count), omission errors (number of false negatives in proportion to field measured tree count) and commission errors (number of false positives in proportion to field measured tree count) errors were then determined for each algorithm and grouped based on field measured height and if the tree was isolated or belonged to a group.

Stem location and crown width were used to provide an indication of the success of each algorithm in correctly delineating crown boundaries. Crown width was preferred over other metrics such as crown cross-sectional area or crown volume due to it being a more readily assessable field measurement and given the proven use of crown width in predicting inventory metrics such as DBH (Popescu 2007). The accuracy of these metrics was evaluated based on a comparison of the correctly matched trees with the collected field data. For crown width the RMSE and Bias were calculated as follows:

$$RMSE = \sqrt{\frac{\sum_{i=1}^{n}(x_{nL} - x_{nF})^2}{n}} \tag{4.1}$$

$$Bias = \frac{\sum_{i=1}^{n}(x_{nL} - x_{nF})}{n} \tag{4.2}$$

where x_{nL} and x_{nF} are the UAVLS and field measurements of each variable respectively. Only correctly matched trees were used in these calculations, therefore n is the count of correctly matched trees. RMSE and standard deviation were calculated for tree locations based on the difference between field and UAVLS measured locations.

Tuning of the input variables was carried out to ensure that each algorithm performed optimally for the forest type. The tuning procedure involved manually finding the parameters that optimised the omission and commission results of plot 5. This process was applied separately at each individual point density. As plot 5 was used in tuning the algorithms it is not included in the tree detection results.

The two values of *dt* for the PDD algorithm were found to be constant across all point densities and related to the size of the crown. Similarly the kernel size of the CDD50, CDDopt and CDPD algorithms was found to be optimal at 1.5 m. However, the degree of smoothing was found to decrease from (2.8 to 1.6) with point density. The optimal voxel width and depth used in the VDD algorithm were also found to decrease with increased point density. Voxel width was found to vary between 0.2 and 0.8 m and thickness varied from 0.5 to 2.0 m.

4.4 Results

4.4.1 Tree detection

All five of the implemented algorithms detected over 90% of the stems using full density data. For these point clouds the number of trees found by the algorithms corresponded to between 99% (VDD) and 107% (PDD) of the field measured trees. The percentage of field measured trees correctly linked to UAVLS delineated trees was between 92% (CDD_{50}) and 97 % (CDD_{opt}). In all algorithms small trees, which occurred in groups, had the highest rate of omission (Table 4.2). The small number of trees (11) of this type within the plots, therefore inflated the overall detection rate. The CDD_{opt} and the

Table 4.2: Omission errors (%) for each tree detection class within height and grouping classes from the full density data. A group is defined as two or more overlapping crowns.

Algorithm	Total (%)	**2 to 5** m		**5 to 10** m		$>$ **10** m	
		Isolated (%)	**Group** (%)	**Isolated** (%)	**Group** (%)	**Isolated** (%)	**Group** (%)
PDD	6	11	20	3	8	0	8
VDD	8	11	40	3	10	0	8
CDD_{50}	9	6	50	5	10	10	0
CDD_{OPT}	4	6	20	2	8	0	8
CDPD	5	6	40	3	5	0	0
Tree Count		20	11	117	99	12	13

PDD algorithms omitted only 20% of trees in this class, however, the PDD algorithm also omitted 11% of the small isolated trees.

At full density, commission errors for most algorithms typically involved the over-segmentation of large trees or trees that were forked or presented a large ramicorn. However, the PDD algorithms also tended to over-segment low branches into trees. Thus, the PDD algorithm had the highest rate of commission (14%), whereas the other algorithms had commission rates between 5% (CDPD) and 8% (CDD_{50}).

Commission errors typically increased for sparse stands, for example plot 6 which contained the fewest stems had above average commission errors for all algorithms. Plot 2 had an average stem count of 52 stems/ha and had the lowest omission rate of all algorithms, with only 1 tree being omitted. Plot 4 had the highest stem density and typically gave results similar to other plots for all algorithms apart from CDD_{50}, which gave a commission rate double that of any other algorithm in this plot.

Increases in point density from 5 to 50 points/m^2 allowed for improved tree detection accuracy across every algorithm apart from CDD_{50} (Figure 4.3). For this algorithm the tree detection results were best at 25 points/m^2 when 101% of trees were detected, however the commission and omission errors were lower in the full density data and 5 points/m^2 respectively. The result of decimating the point cloud for all other algorithms was an increase in the omission error. This is best demonstrated by the PDD algorithm which at 5 points/m^2 had the high omission (14%) and commission (10%) errors. At 50 points/m^2 the omission rate decreased to 5% and the commission error remained similar at 12%.

Improvement between the 50 points/m^2 point clouds and the full density point clouds was seen in the CDD_{opt} algorithm. The omission and commission rates increased

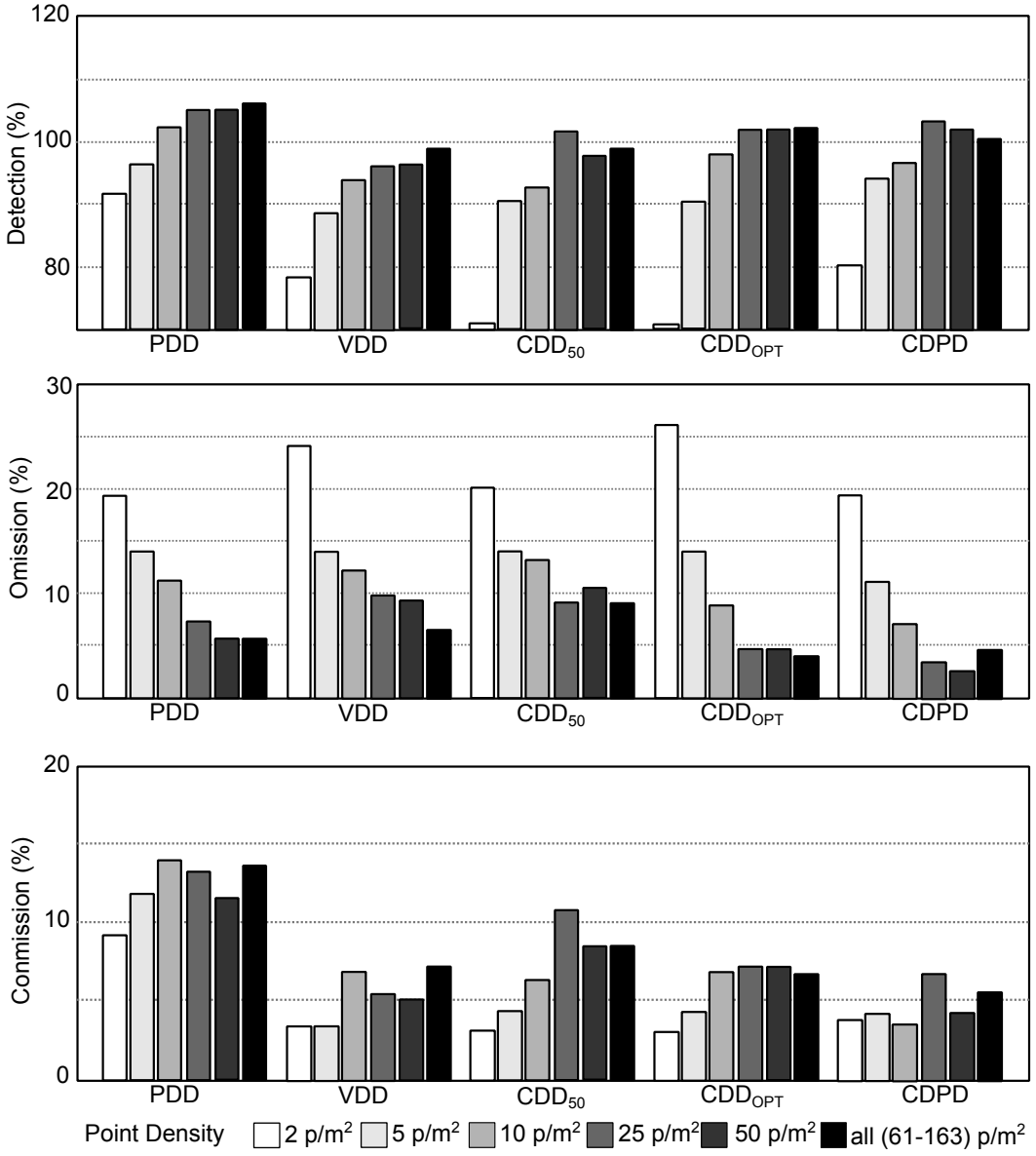

Figure 4.3: Detection, omission and commission rates for the 5 algorithms utilising the 5 different point densities. There was a total of 272 trees within 5 plots.

marginally for both the PDD and CDPD algorithms between the 50 points/m^2 and full density point clouds. Furthermore, similar detection results were found for plot 2 when using a point cloud decimated to 100 points/m^2 in these two algorithms. For instance, in the CDPD algorithm the detection rate was 106% (omission 0% and commission 6%) at 50 points/m^2, 105% (omission 0% and commission 5%) at 100 points/m^2 and 107% (omission 0% and commission 7%) at full density.

4.4.2 Tree location

For each tree matched to an equivalent field measured tree, the difference in the field and UAVLS measured locations was typically within the expected accuracy of the field data for each algorithm (Figure 4.4). This difference was similar across four of the five algorithms when using full density data as indicated by the RMSE of 0.90 m for the CDPD, 0.94 m for CDD_{opt} and 0.98 m for VDD and PDD. The CDD_{50} algorithm had the highest RMSE error at full density (1.25 m) which is a result of data resolution as tree location was taken at the centre of a 0.5 m cell. This also meant that for this algorithm, increased point density had no significant effect on the accuracy of tree locations (Figure 4.4). All other algorithms showed significant improvement with increasing point density (up to 0.28 m in the CDD_{opt} algorithm).

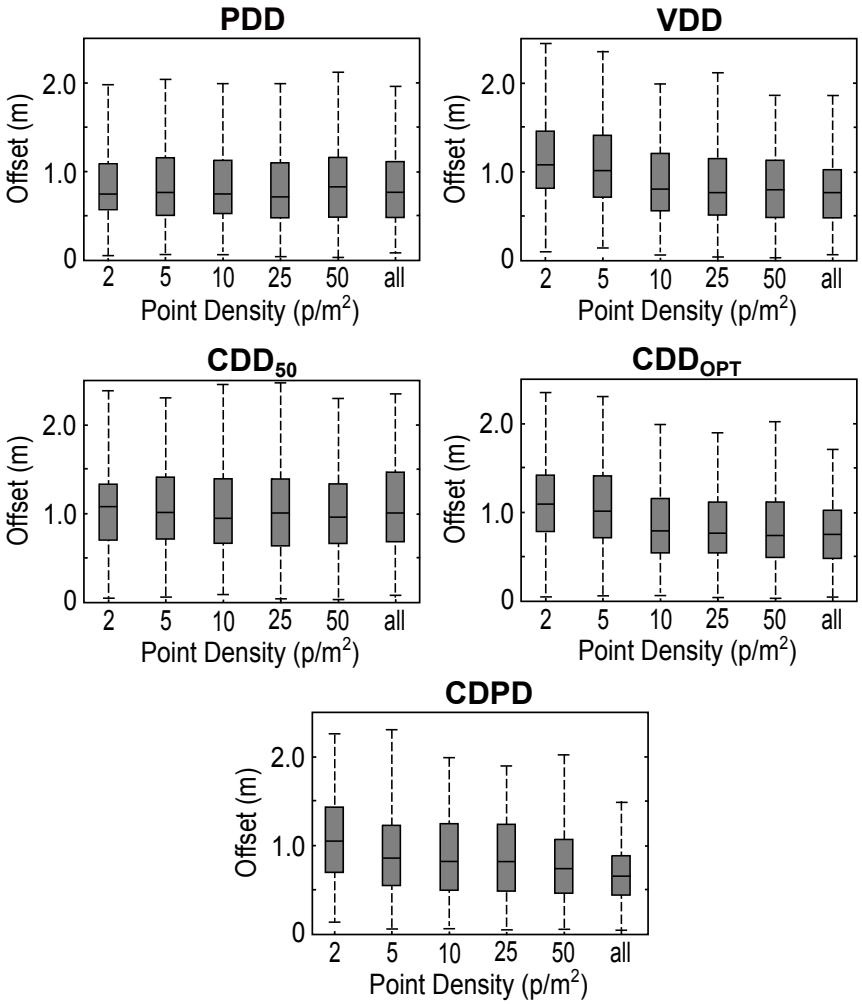

Figure 4.4: Box plot (showing the 5th, 25th, 50th, 75th and 95th quartiles) showing the absolute offsets between field and UAVLS measured tree locations for each algorithm and at each density.

Differences in the field and UAVLS measured tree location typically increased within dense stands and for stems further from the plot centre. These increased differences are a function of the increased error in the field measurements as opposed to the accuracy of the detection algorithms. Furthermore, trees in the densest plot (plot 4 with 79 stems) had the highest RMSE errors in all algorithms (for instance 1.02 m in the CDPD algorithm).

Figure 4.5 shows that for each tree, the UAVLS measured locations found in each algorithm have similar offsets (both in magnitude and direction) from the field measured location. This consistent error is due to the comparison of relatively inaccurate stem locations measured in the field with tree top locations measured from the UAVLS data in all but the CDPD algorithm, which used cluster centroids to derive stem locations. The difference in field and UAVLS measured tree location when using the lower density point clouds was more variable between the individual algorithms used. This is indicated by the higher standard deviations found in all five algorithms, for instance the VDD algorithm which had a 0.71 m standard deviation when used with the 5 points/m^2 dataset, had a 0.47 m standard deviation at full density.

4.4.3 Crown width

The choice of algorithm had a significant effect on the accuracy of crown delineation at full density (Figure 4.6). The highest accuracy algorithm was CDPD at a density of 50 points/m^2, which had an RMSE of 0.38 m and a bias of 0.0 m. The PDD and CDD_{opt} algorithms also achieved a low biases of 0.03 and -0.03 m at full density respectively, however, the PDD algorithm had a significantly higher RMSE of 0.73 m. The VDD and CDD_{50} algorithms tended to overestimate crown width at full density, indicated by the higher biases of 0.19 m and 0.11 m.

The CDPD algorithm was the only algorithm where point density had a significant effect in reducing the RMSE of crown delineation. For the CDD_{opt}, PDD and CDPD algorithms the overall biases decreased with increased point density (Figure 4.6). As these algorithms overestimate crown width at lower point densities, the decrease in bias can be correlated to the lower omission rates (i.e. from a crown being correctly split into two). In CDPD, CDD_{opt}, PDD, and VDD algorithms the bias of isolated trees tended to decrease with point density. In most algorithms this resulted in the crown width being underestimated. The CDD_{50} algorithm, which did not have a lower omission rate, showed no improvement or otherwise due to changes in point density.

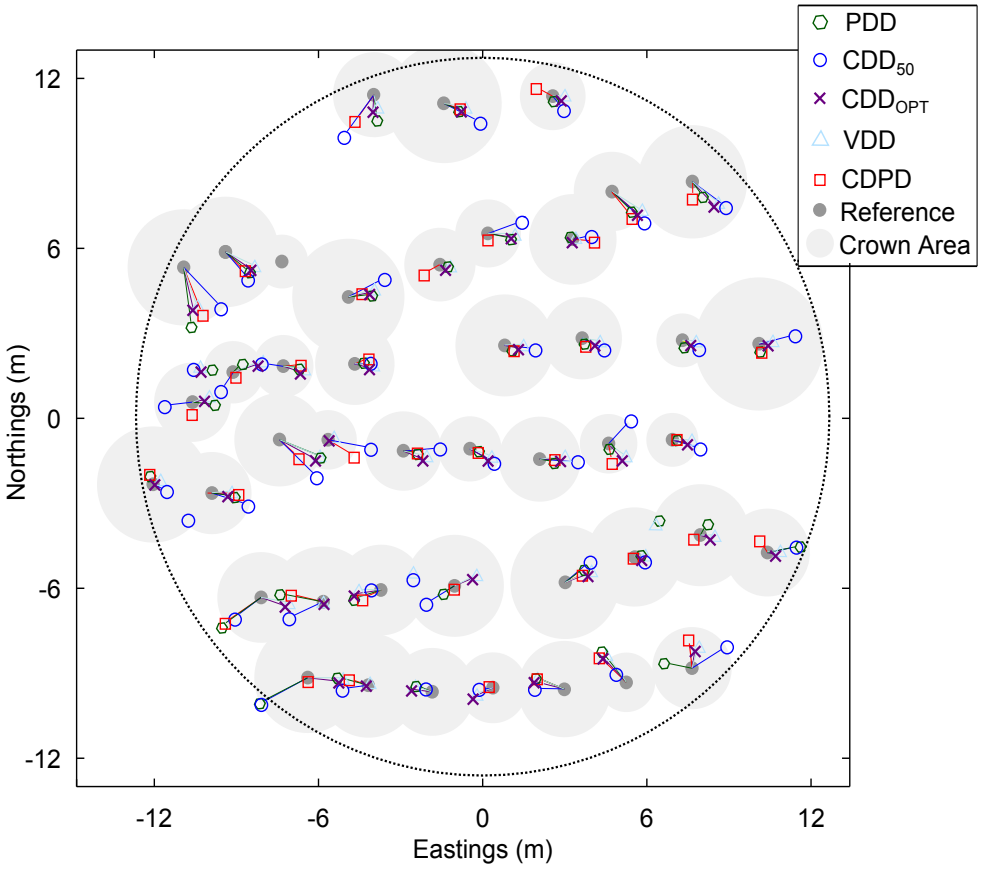

Figure 4.5: Distribution of tree location errors over plot 6, using full-scale data within the five algorithms analysed.

4.5 Discussion

The results of this study have shown that trees can be more reliably detected and delineated from UAVLS datasets when very high density data is used. Similar to the earlier ALS comparison study by Kaartinen et al. (2012), the algorithm used had a significant effect on rate of detection and accuracy of delineation when utilising low density point cloud datasets. At all point densities, the tree detection rate was higher than that found in prior studies using similar algorithms. Vauhkonen et al. (2011b) showed that the complexity of the forest had a significant influence on the detection results. Detection and delineation algorithms applied to plantation datasets have been shown to produce accurate and unbiased stem estimates (Roberts et al. 2005; Vauhkonen et al. 2011a). This is due to plantations consisting of even age forests with regular planting patterns, with typically a low number of suppressed trees. Similarly, in this study the rate of omission for all algorithms was highest for suppressed trees that were part of a group for which there was only a small number. This negates the importance

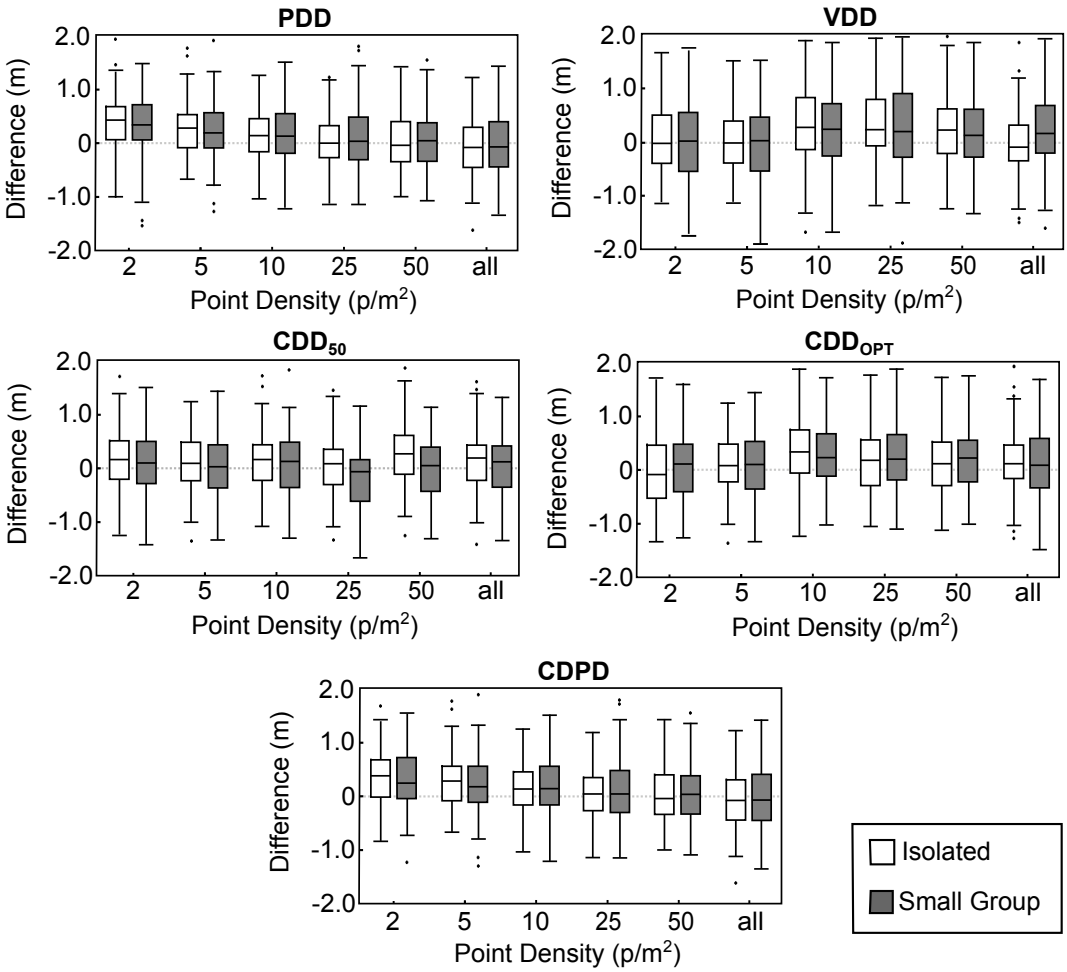

Figure 4.6: Box plot (showing the 5th, 25th, 50th, 75th and 95th quartiles) showing the difference between field and UAVLS measured crown widths of isolated trees and trees in small groups for each algorithm and at each density.

of selecting appropriate smoothing strategies in CHM based algorithms for instance.

In contrast to the study of Roberts et al. (2005), commission error tended to decrease with stem density. This again is due to the properties of the trees in the plantation. In our study, the structure of the trees was found for the most part to be poor, with 30% of the field surveyed trees having a large ramicorn or fork, which presented as false maxima for individual tree detection. This issue mainly occurred in sparse stands, where these features tended to be more prominent. Often these features were present at all point densities, therefore increases in point density had no effect on reducing the commission rate of the detection algorithms.

The primary advantage of using high point density data sets is to reduce omission rates,

which was observed with most detection algorithms. Improvement with point density was seen at all densities and was found to be more significant than the algorithm used, which is contrary to findings of Kaartinen et al. (2012) and Reitberger et al. (2009). One reason for this is that the average number of strikes per tree was comparatively low at 5 points/m^2 in a study area consisting of young trees with a mean height of 7.6 m. Therefore, a similar increase in the pulse density represents a more significant increase in strikes per tree for this type of forest. This allows maxima and ridges of smaller trees to become more evident at higher densities.

The increase in tree detection rate in high density point clouds can be attributed to the tree crowns being more accurately described. Firstly, increasing the sampling density increases the likelihood of a treetop being observed in the data. Therefore, algorithms that rely on the accurate detection of maxima such as CDD_{opt} are more likely to find trees in high density data. The VDD algorithm, on the other hand, makes use of the increased definition of the crown boundaries within the raw data. The high point density allowed the voxel layer height to be decreased meaning that small trees growing in groups were observed as distinct segments in the upper voxel layers in which they occurred. The CDPD and PDD algorithms made use of all the available extra information in the point cloud. These algorithms had the greatest improvement in the omission rates (8 and 9% respectively).

The achievable accuracy of crown delineation was not fully assessed by the algorithms used in this study as the reference data consisted of only 2 measurements of crown width. Furthermore, the 1.3 m height threshold applied in all algorithms did not allow the trees to be fully segmented as they were unpruned and had crowns which extended to ground level. Although this was the case, the technique used to determine this metric in each algorithm was similar to the algorithm used in the field. Higher resolution data also allowed UAVLS crown widths of trees in groups to more closely match field measured crown widths due to a reduction in the omission error.

Tree location accuracy was also improved by the use of full density data, as treetops had a higher likelihood of being observed within the dataset. Similar to crown width, the reference data for the comparison was not of a very high accuracy and a significant component of the error is a result of the error in the field measurements. Interestingly, the CDPD algorithm which used cluster centres to represent tree location conformed more closely to field measured locations than other algorithms. This suggests that using within cluster (or tree) information, such as with the CDPD algorithm or the algorithm in Reitberger et al. (2009), has the potential to provide a more accurate estimate of stem

location than the location of the tree top in this study area. This result is in contrast to Kaartinen et al. (2012) who found that an algorithm similar to CDPD resulted in tree locations with an RMSE of up to of 1.3 m in comparison to sub-meter RMSE values found in methods using the location of the highest point. More accurate reference information is required to fully test this theory.

It is important to note that all tree detection algorithms used in this study require prior knowledge on the potential size and distribution of crown size within the stand. For instance both the CHM and point cloud techniques require an initial estimate of crown width to achieve optimal results. In this study, one plot was used to provide optimal tuning of each algorithms. This is an appropriate approach for plantation datasets where trees can be considered to have similar properties, however, more spatially adaptive tuning would be required for more variable stands. Several studies have presented algorithms, which aim to select an optimal kernel for use with the CHM by performing the same segmentation several times and examining the properties of the segmented trees, for example in Ene et al. (2012). A similar technique for the optimal tuning of point cloud based algorithms is also required, however, extracting the extra information from high density point clouds adds extra computational burden and may preclude a similar approach. Future research is required to investigate methods that optimise tree detection algorithms based on the characteristics of the point cloud.

The results of this study have confirmed that the tree detection algorithms analysed are suitable for detecting and delineating individual trees within immature eucalyptus plantations at all densities (5 - 163 points/m^2). Exploiting the low cost nature of UAV surveys and collecting data at higher temporal frequencies will, therefore, allow plantation management decisions to be made with greater certainty. For instance, UAV data could be collected to remove subjectivity in determining the timing of pruning and thinning treatments. However, further research is required to determine if estimates of other key inventory metrics such as the rate of canopy closure, the height of the trees, and the stem quality within young eucalyptus plantations can be made with the required accuracy from the data collected with UAVs.

4.6 Conclusions

The unique characteristics of our UAVLS platform allowed us to generate point clouds at very high densities (61 - 163 points/m^2). The short flight time of UAV platforms means that for the functional deployment of UAVs as a laser scanning system, sampling

is likely to occur at the tree level and as such high accuracy of individual tree detection and delineation is essential. This study has, therefore, compared several individual tree detection and delineation algorithms for use with high density UAVLS data within a four year old *Eucalyptus globulus* plantation.

The best performing algorithm (k-means clustering/CDPD), which utilised both the original point cloud and a Canopy Height Model (CHM), was able to correctly detect 98% of the trees within the study area and delineate tree crowns with an RMSE of 0.43 m and a bias of 0.1 m. Although, detection and delineation of trees using high density data was achieved with acceptable accuracy for all algorithms, the choice of algorithm was shown to still be an important consideration. Furthermore, selecting appropriate data preparation parameters such as decreasing the CHM cell size to match the point density significantly improved tree detection and delineation outcomes.

This study has also shown that point density significantly influences successful detection of individual trees from UAVLS point clouds across a number of algorithms. The main improvement is a reduced rate of omission of up to 9% with a point density increase from 5 to 50 points/m^2. This represents a significant improvement considering the already high detection rates with low density data (i.e. 85% of trees being detected with low density data (5 points/m^2)). The improvement in tree detection also translates into a more accurate delineation of trees, with a reduction in the RMSE of tree location and crown width shown in most algorithms used.

Although this study used data collected from a UAV platform, we demonstrated that these data are similar to that of an ALS platform over our chosen forest type. The results of this study therefore suggest that as high density laser scanning data become increasingly available due to improved sensor designs on full scale platforms and more flexible platforms, such as UAVs, the utilisation of laser scanning derived individual tree inventories will become a more valuable option for the monitoring and management of eucalyptus plantations.

4.7 Thesis context

In order to effectively monitor forest attributes using UAVLS the accurate segmentation of individual trees is a key consideration. This chapter outlined the accuracy of individual tree segmentation achieved with several tree detection and delineation routines. This chapter also highlighted the advantages of the high resolution data collected by the

UAVLS system in the segmentation of individual trees. In the next chapter we make use of a method based on normalised cut segmentation. Although this method is not assessed in this chapter, it was chosen due to the ability to detect 3D space between crowns. The results presented in the next chapter highlight the accuracy of this method.

5 | An assessment of the repeatability of automatic forest inventory metrics derived from UAV-borne laser scanning data

Chapter 5 focuses on the assessing the repeatability of Individual Tree level metrics extracted from UAVLS generated point clouds and is in press in *IEEE Transactions on Geoscience and Remote Sensing* (Wallace et al. Accepted for publication[a]).

Abstract

We assessed the reproducibility of forest inventory metrics derived from an Unmanned Aerial Vehicle (UAV) laser scanning (UAVLS) system. A total of 82 merged point clouds were captured over six 500 m^2 plots within a *Eucalyptus globulus* plantation forest in Tasmania, Australia. Terrain and understory height, together with plot- and tree-level metrics were extracted from the UAVLS point clouds using automated methods and compared across the multiple point clouds. The results show that measurements of terrain and understory height, and plot-level metrics can be reproduced with adequate repeatability for change detection purposes. At the tree level, the high density data collected by the UAV provided estimates of tree location (mean deviation (md) of less than 0.48 m) and tree height (md of 0.35 m) with high precision. This precision is comparable to that of ground based field measurement techniques. The estimates of crown area and crown volume were found to be dependent on the segmentation routine and as such were measured with a lower repeatability. The precision of the metrics found within this study demonstrates the applicability of UAVs as a platform for performing sample based forest inventories.

5.1 Introduction

The timing of silvicultural activities within a plantation forest is of critical importance for optimal management. Mistimed treatments, including pruning and thinning, can affect the growth of the trees and the quality and value of the produced timber (Pinkard et al. 2004; Muñoz et al. 2008). In order to ensure that these decisions are informed with accurate and timely information, forest inventories are collected at key stages of the

plantation growth cycle. These inventories involve the measurement of several properties that describe the geometry and spatial distribution of trees including stem count, tree height and diameter at breast height (DBH), and the visual and subjective assessment of canopy closure and stem form.

Forest inventory metrics have historically been acquired from sampling plots distributed within a stand or stands using ground-based field measurement techniques. Statistical inference methods are then applied to these sample plot observations to achieve estimates of the stand-level conditions (Mandallaz 2007). Amongst many factors, the quality of these inferences relies on the variability in the stand being accurately captured within the set of observations (Lovell et al. 2005). This is a function of the number of observations in relation to the variance of the whole population. As a consequence, meeting precision requirements with traditional inventory methods can be both a costly and time consuming exercise (Hopkinson et al. 2004). Therefore, new approaches to obtaining these metrics have been continually developed with the goal of increasing measurement accuracy as well as reducing the cost of inventory collection.

The use of remote sensing data for the collection of forest inventory metrics has been widely researched and these data are now commonly used within the forestry industry. Air- and space-borne sensors allow spatially explicit data to be collected over large areas in a timely and economic fashion (Wulder et al. 2008; Boudreau and Nelson 2008; Li et al. 2013). However, as spatial extent and resolution are inversely related, the precision and accuracy are often sub-optimal for many applications (Xie et al. 2008; Wulder et al. 2012). Airborne Laser Scanning (ALS) data captured at heights between 500 and 5000 m provide observations of 3D canopy structure and are often successfully used within model and design-based inference approaches to provide estimates of forest properties such as biomass and Leaf Area Index (LAI) at the stand level (Nelson et al. 2003; Andersen et al. 2011; Ståhl et al. 2011). The detection of individual trees from this information has proved to be more difficult with reported detection rates varying significantly (between 40 and 96%)(Reitberger et al. 2009; Holopainen et al. 2010; Kaartinen et al. 2012). Although, Reitberger et al. (2009), Ferraz et al. (2012) and Yao et al. (2012) demonstrated that 3D segmentation techniques improve the accuracy of the information derived from tree level analysis, the required accuracy of tree segmentation is still not sufiňĄcient to estimate a number of forest metrics. For example, Vastaranta et al. (2011) showed that, bias towards large dominant trees can cause significant overestimation of final inventory values such as timber yield. As a consequence, extensive networks of ground plots are required to link statistical properties of the point cloud with properties of the forest to derive stand level metrics and allow ALS to be used as

an operational inventory tool (Wulder et al. 2012).

Terrestrial remote sensing techniques have also been deployed to provide estimates of inventory metrics (Macfarlane et al. 2007; Maas et al. 2008). In contrast to the data collected by air- and space-borne sensors, the woody components of the canopy are often visible within the data collected by terrestrial sensors, allowing for the objective and reproducible measurement of a number of key tree-level inventory metrics such as DBH, stem ovality and crown length that may improve estimation of timber quality at harvest (Maas et al. 2008). The precision of these data also allows direct observation of change to be made (Liang et al. 2012). However, terrestrial techniques can only be used to measure small areas, as the data collected with Terrestrial Laser Scanning (TLS) instruments are highly affected by occlusions and multiple viewing points are required within each plot to avoid downward bias in stem detection. Mobile Laser Scanning (MLS) systems overcome the small area restriction of TLS by deploying the laser scanner onboard a moving vehicle (Lin et al. 2012) or using hand-held instrumentation. These systems have shown potential in deriving individual tree level parameters (Lin et al. 2012), however, their use in forest inventories requires further investigation.

Recently, Unmanned Aerial Vehicle-Laser Scanning (UAVLS) systems have been proposed as a tool for mapping and measuring tree metrics (Jaakkola et al. 2010; Wallace et al. 2012b). These systems offer comparatively low-cost collection and generate data with point densities up to 1000 points per m^2 (Jaakkola et al. 2010). UAVLS systems are a relatively new technology and to date their deployment within a forest inventory context has focussed on system development and potential, with limited observation of tree parameters. Jaakkola et al. (2010) presented a pilot study showing that the underestimation of tree height present in both ALS and TLS due to the tree tops not being observed was significantly reduced within UAVLS data. Jaakkola et al. (2010) suggested this was due to the increased point density of the collected point clouds in comparison to ALS. However, their study relied upon measurements from only 26 trees. Similar results for tree height observations were found by Wallace et al. (2012b) from repeat measurements of six isolated trees. Within this latter study it was also shown that measurements of the crown width of these trees are repeatable to within a standard deviation of 0.6 m.

In comparison to ALS systems, the scanner and the sensors used for direct georeferencing the point cloud on-board UAVLS platforms typically have higher errors and different sources of error. Although data capture from these platforms enables some desirable properties, the effects of the sensor characteristics on estimates of forest metrics are

unknown. The aim of this study is, therefore, to validate and verify the precision of forest metrics from data collected with a UAVLS system in a Eucalypt plantation forest. The paper describes a workflow for the automatic extraction of inventory metrics at the individual tree level. This workflow includes a determination of the effect of scan geometry on the output. The repeatability of all stages of this workflow and metrics derived at both the plot and tree level are assessed utilising multiple datasets collected over 6 plots.

5.2 Study Area and Field Data

The study area is a four year old Blue gum (*Eucalyptus globulus*) stand in south eastern Tasmania (Figure 5.1). Six field plots with fixed radii of 12.62 m (500 m^2) were selected within the study area. These plots were visually selected based on a prior site visit to ensure suitability for UAV data capture and that variations in tree density across the stand were represented within the collected data. A field survey of the 308 individual trees within these plots was conducted in May 2012. Crop tree stem position, crown radius and total height were measured within each plot. Only tree location was recorded for non-crop species (2 % of stems). Plot centres were surveyed using a differential GPS receiver ($\pm$0.05 m) and stem locations were measured at 1.3 m using a Forestor Vertex hypsometer and compass bearing to the plot centre. Due to occlusions in measuring a bearing to trees at the edge of a plot, the error in tree location is estimated to be between 0.5 and 1 m. Tree height was also measured to within an estimated error of 1 m using the Hypsometer. Crown radius was defined as the mean of the length of longest branch from the stem (derived through ocular estimates) and the length of a branch at 90° to this initial measurement. The distributions of tree density and tree height varied significantly between each plot (Table 5.1). Plot mean tree height ranged from 5.7 to 8.9 m and tree density (mean of 1020 stems/ha) reached as low as 680 stems/ha in plot 2 and as high as 1560 stems/ha in plot 4.

5.3 Methods

5.3.1 UAVLS data and processing

Discrete return small footprint UAVLS data were captured in transects with a multi-rotor UAV system (OktoKopter), equipped with an Ibeo LUX laser scanner (Wallace

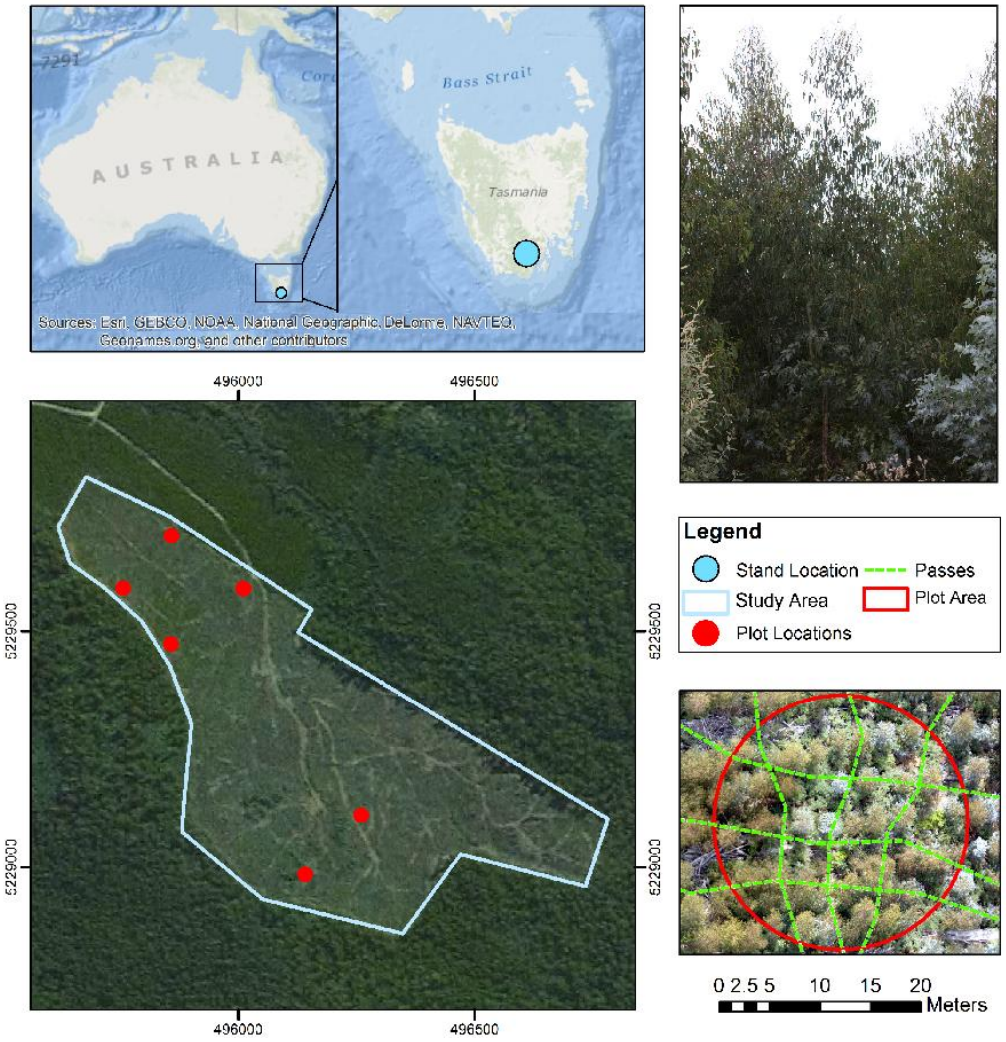

Figure 5.1: Study area. Top Left: Location of the study area in Tasmania, Australia. Bottom left: The stand used for the study area showing the location of the six plots (GDA94 MGA zone 55). Upper right: image of the *Eucalyptus globulus* within one of the chosen plots. Lower right: Example of selected UAV flight lines over a single plot.

Table 5.1: The properties of the six measured plots within the *Eucalyptus globulus* plantation. Showing mean and standard deviation (σ) tree height, DBH and crown radius.

	stem	Tree Height (m)		DBH (m)		Crown Radius (m)	
Plot	count	mean	σ	mean	σ	mean	σ
1	49	5.71	0.99	0.07	0.01	1.51	0.35
2	34	6.47	1.42	0.09	0.01	1.90	0.46
3	59	8.93	1.31	0.09	0.02	1.80	1.03
4	78	7.05	1.59	0.08	0.02	1.58	0.34
5	46	8.80	1.45	0.09	0.01	1.53	0.52
6	42	8.86	1.50	0.11	0.03	1.52	0.47

et al. 2012b). The laser scanner, which operates at a wavelength of 905 nm, employs four parallel scan lines in the along-track direction capable of recording up to 3 returns per pulse and has a beam divergence of 0.8° along-track and 0.08° across-track. Direct georeferencing of laser returns was achieved through the use of a dual frequency GPS receiver, a Micro-Electro-Mechanical (MEMS) based Inertial Measurement Unit and a HD Video camera. Observations of orientation based on frames taken from the video camera are used to constrain the error characteristics of the IMU and achieve a more reliable estimate of orientation. This allows the root mean square error (RMSE) of the directly georeferenced returns to be 0.30 m horizontally and 0.15 m vertically. See Wallace et al. (2012b) for a detailed description of the UAVLS system, including an assessment of the error budget.

Each transect was flown with a nominal velocity of 2.8 m/s and a flying height of 40 m Above Ground Level (AGL). Based on the analysis in Wallace et al. (2012a) the use of large scan angles causes significant occlusion within the final point cloud.The scan angle range was, therefore, restricted to ±30°from nadir. Under these conditions a point cloud with greater than 50 pulses per square meter (p/m^2) is produced with an on ground swath width of 46 m and footprint ranges of 0.55 to 0.64 m and 0.05 to 0.06 m across and along track respectively. All of the following data processing steps were carried out using in-house MATLAB code.

Ten individual transects were flown over each of the 6 plots. Transects over plots 1, 2 and 3 were flown in May 2012 and transects over plots 4, 5 and 6 were flown in July 2012. As data were acquired in winter there were no significant seasonal differences in the vegetation between these periods. Two different merging strategies were trialled for this study. In both strategies data collected in two different transects were merged based on the georeferenced location of the laser returns without adjustment. In the first strategy (Fig. 5.2), two parallel transects approximately 10 m apart on either side of the plot centre were merged. This produced a merged point cloud in which the entire plot was observed with a minimal scan angle, but the point density in the middle of the plot was significantly greater than the point density towards the plot boundary. In the second strategy (Fig. 5.2), two perpendicular flight lines were merged. This created a merged point cloud in which the scan angles of individual points varied widely but the point density was more evenly distributed across the plot. Variations in flight parameters resulted in inconsistencies in the area captured within each transect. Only merged point clouds with complete coverage of the plot area plus a 2 m buffer were included in any further analysis. As a result, for each plot the final number of merged point clouds was as low as 10 and as high as 19.

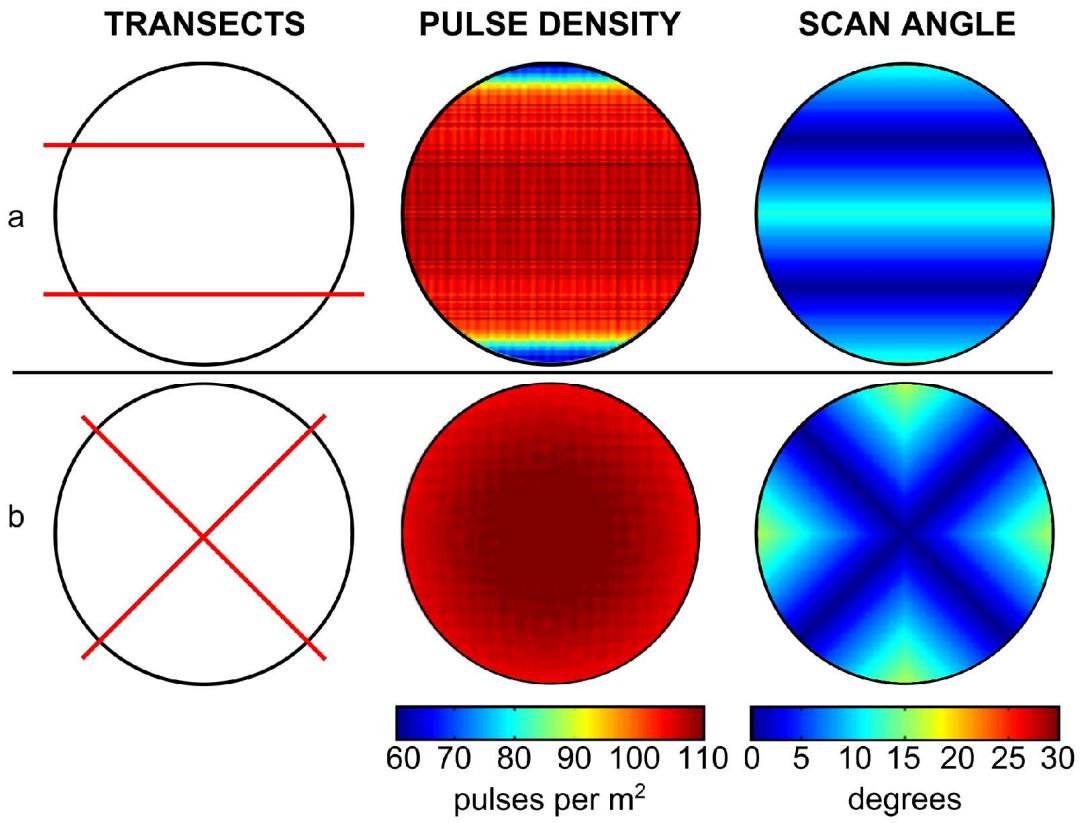

Figure 5.2: Simulated distribution of scan angle and point density at the top of the canopy of a 12.62 m radius plot based on the a) parallel transect and b) crossed transect merging strategies applied in this study. Simulation assumes a flying height of 30 m above the canopy height and a speed of 2.8 m/s. Flying height above canopy was used to ensure that the maximum scan angle used to observe the data is included in the simulated output.

For each merged point cloud, single and last returns were classified into ground and non-ground using the filtering algorithm outlined in Axelsson (1999). All first of many and intermediate returns were considered as non-ground, as these returns were unlikely to be from ground sources and found in initial investigations to be often erroneously classified by the filtering algorithm. Once the ground points were identified, natural neighbour interpolation was used to generate 0.25 m resolution Digital Elevation Models (DEMs). Subsequently, all non-ground points were normalised to vegetation height by subtracting the DEM elevation at the planimetric location using linear interpolation.

Due to the high spatial density of the data and an understory cover which varied significantly in height and coverage across each plot, a second filter was then applied to separate understory and tree returns. An understory filter was implemented in which all points below 2.5 m with no higher points ($>$ 2.5 m) within a 0.7 m radius were classified as understory. The 2.5 m height threshold was chosen as it is significantly higher than the expected maximum height of understory in this area. A 0.7 m radius threshold

allowed sufficient space to ensure low branches were not included as understory. This initial set of understory points was used to create an initial Triangular Irregular Network (TIN). All points above this TIN are consider as canopy returns and the lowest point below each facet of the TIN were added to the set of understory points from which a new TIN is created. This process was continued until there were no non-ground points below the TIN. Iterating in this manner ensured the lower parts of the crowns were included as tree vegetation and the majority of the understory removed by the filter. This approach was taken instead of a simple height threshold as the trees within the study were yet to be pruned and the field data indicated that the crown base height ranged from ground level to 1.2 m.

5.3.2 Plot Level Metrics

A set of descriptive statistics representing key canopy attributes (Goodwin et al. 2006) were calculated from the canopy points. These statistics comprising Above Ground Height (AGH) percentiles (AGH10, AGH20, ..., AGH99), mean AGH, AGH standard deviation, AGH skewness and AGH Kurtosis, were calculated for all returns, first returns only, and last returns.

Two canopy cover metrics were also calculated from the canopy points. The First Cover Index (FCI) measures canopy cover as the ratio of canopy first returns to all first returns (Morsdorf et al. 2006). In the α-shapes Cover Index (ACI) method, canopy cover was estimated as the percentage of the total plot area covered by canopy. The canopy area was estimated based on α-shapes of the horizontal 2D projection of the point cloud. α-shapes allow the reconstruction of an object's shape from a set of unorganized points (Edelsbrunner and Mücke 1994). The parameter α is used to tune the 'tightness' of the shape around the points. For a very large value of α (e.g. approaching ∞) the shape is equivalent to the convex hull. For a very small value of α, the α-shape forms holes and pockets with the shape clustering around the original points. α-shapes have previously used been used to estimate forest attributes from laser scanning data by Holmgren et al. (2008), Vauhkonen (2010b), and Rutzinger et al. (2011). These studies have shown that if an appropriate α is selected, the forest structure represented in the point cloud can be more accurately modelled with this algorithm in comparison to other similar methods.

To accurately capture the variations within the crown and eliminate any unnecessary noise, α was chosen as a function of the plot level point density. The relationship between point density (d) and α was determined by using several decimated versions

of one merged point cloud from each plot and finding the value for which the estimate of cover was equal to FCI of the full density merged point cloud giving the function (Wallace 2013):

$$\alpha = 0.14 + \frac{1.74}{d} \tag{5.1}$$

5.3.3 Individual tree extraction

We undertook a segmentation of individual trees using an adaptation of the method outlined by Reitberger et al. (2009). First, stem location was derived from the CHM with the grid size optimised to achieve an average of 2 first return points per grid cell. This CHM was then smoothed using Gaussian smoothing with a square 1.5 m kernel and a sigma value of 1.8. The CHM was smoothed in an attempt to negate any within crown variation caused by the properties of the trees (Koch et al. 2006). The kernel size was set to be equal to the average crown radius and sigma was chosen based on an initial tuning with one merged point cloud from within one plot. The tuning involved finding the value sigma for which the number of maxima matched the number of field measured stems. Second, local maxima within a 3×3 window were then detected from within this smoothed CHM and considered analogous to stem location. These locations were then used within a marker controlled watershed segmentation to provide an initial estimate of the crown area (Hyyppä and Inkinen 1999). An initial investigation of the 3D clusters suggested that the delineation in the lower parts of the canopy was not repeatable. The method was therefore adjusted such that only the points above the 65^{th} AGH percentile were used to provide an initial determination of stem location.

To segment points below the 65^{th} AGH percentile, normalised cut segmentation was applied directly to the point cloud. Normalised cut segmentation involves finding the two disjoint segments A and B of a graph (consisting of the individual points) by maximising the similarity of the members in each segment and minimising the similarity between the two segments found as the minimum solution to the cost function (Reitberger et al. 2009):

$$NCut(A,B) = \frac{CUT(A,B)}{ASSOC(A,V)} + \frac{CUT(A,B)}{ASSOC(B,V)} \tag{5.2}$$

Where $Cut(A,B) = \sum_{i \epsilon A, i \epsilon B} w_{ij}$ is the sum of the weights between segments A and B

and $Assoc(A, V) = \sum_{i \epsilon A, j \epsilon V} w_{ij}$ is the sum of the weights of all edges ending in segment A. The minimisation of $NCut(A, B)$ to form the two disjoint segments was solved using the corresponding eigenvalue problem (Reitberger et al. 2009). The similarity between any two points, i and j is defined by weights, w_{ij}, given as follows:

$$w_{ij} = e^{-3 \times X_{i,j}} \times e^{-Z_{i,j}} \times e^{-S_{i,j}} \tag{5.3}$$

Where X_{ij} is the weighted horizontal Euclidean distance between points i and j, Z_{ij} is the vertical distance and S_{ij} is the weighted maximum distance of the two comparison points to the nearest point in a tree segment derived from the watershed segmentation. A weight of 3 was applied to the Euclidean distance in X_{ij} to enhance the horizontal space between trees within the segmentation. Normalised cut segmentation was performed on the initial point cloud and subsequent segments until the value of $NCut(A, B)$ was less than 0.16 or the segment contained fewer than 100 points. Finally, crown delineation was achieved by merging the segments produced using normalised cut segmentation with those produced using watershed segmentation based on horizontal overlap. The z-exaggeration factor and minimum point threshold were determined based on a sensitivity analysis using a single merged point cloud and varying these thresholds. Assessment of the result of each threshold combination was made by visually examining the 3D delineation of crowns where clear differentiation between neighbouring crowns was observed.

For each plot, the tree list resulting from the segmentation of a dataset with a stem count closest to the mean stem count was considered as the initial tree list for each plot. Segments extracted from the remaining datasets were then linked to trees in the list sequentially from the tree with the largest crown area to the tree with the smallest using the following criteria:

1. If the area of overlap between the reference segment and the segment being added is over 80 % of the area of both segments, the segment is considered a matching tree.

2. If only one segment matched the above criteria, neighbouring trees in the list which matched the criteria were checked for crown overlap. If another segment with a large overlap (> 80 %) was found only the segment with the highest above ground point was considered to be a match.

A new tree was added to the list when no match was found within the existing list of trees for each plot. Once the tree list had been built the UAVLS measured trees were again matched to the field measured trees based on crown overlap. UAVLS trees not matched to field measured trees were considered commission errors and field trees with no matching UAVLS tree were considered omission errors.

5.3.4 Tree-level metrics

Only tree level metrics which could be directly observed from the tree segments were considered, namely tree location, tree height, crown area and crown volume. Observations of tree height were calculated as the height difference between the highest point of a tree segment and the ground represented by the DEM. As tree height can be underestimated from ALS data, two observations were recorded, the height above the DEM and the absolute height (or height above mean sea level) of the highest point. Differences in the variability of these two measurements were used to provide insight into the cause of tree height measurement variation. Stem location was defined as the location of the highest point. Observations of tree height and tree location are demonstrated in Fig. 5.3.

The other directly observable properties of a tree from the UAVLS data are related to the crown. As the crown base height of the majority of trees (98 %) was below 1 m, only crown area and crown volume were measured in this study. To derive these measurements, α-shapes were again used and appropriate values for α calculated based on a trial plot. Crown area was calculated by applying the α shape algorithm to the 2D projection of the points within the tree segment. α values were chosen based on the density of the points (d_c) within a 0.5 m^2 radius around the stem location. Alpha was determined as:

$$\alpha(n) = \begin{cases} \frac{12}{d_c}, & \text{if } d_c <= 120 \; points \; per \; m^2 \\ 0.1, & \text{if } d_c > 120 \; points \; per \; m^2 \end{cases} \tag{5.4}$$

Using equation 5.4 ensured that α was always chosen to be slightly larger than the point spacing within the crown allowing crown detail to be captured, without introducing holes within the crown itself. If the α-shape algorithm creates multiple segments the area of a crown is considered the area of the largest shape.

Crown volume was also determined using α-shapes. In this case the α-shapes algorithm

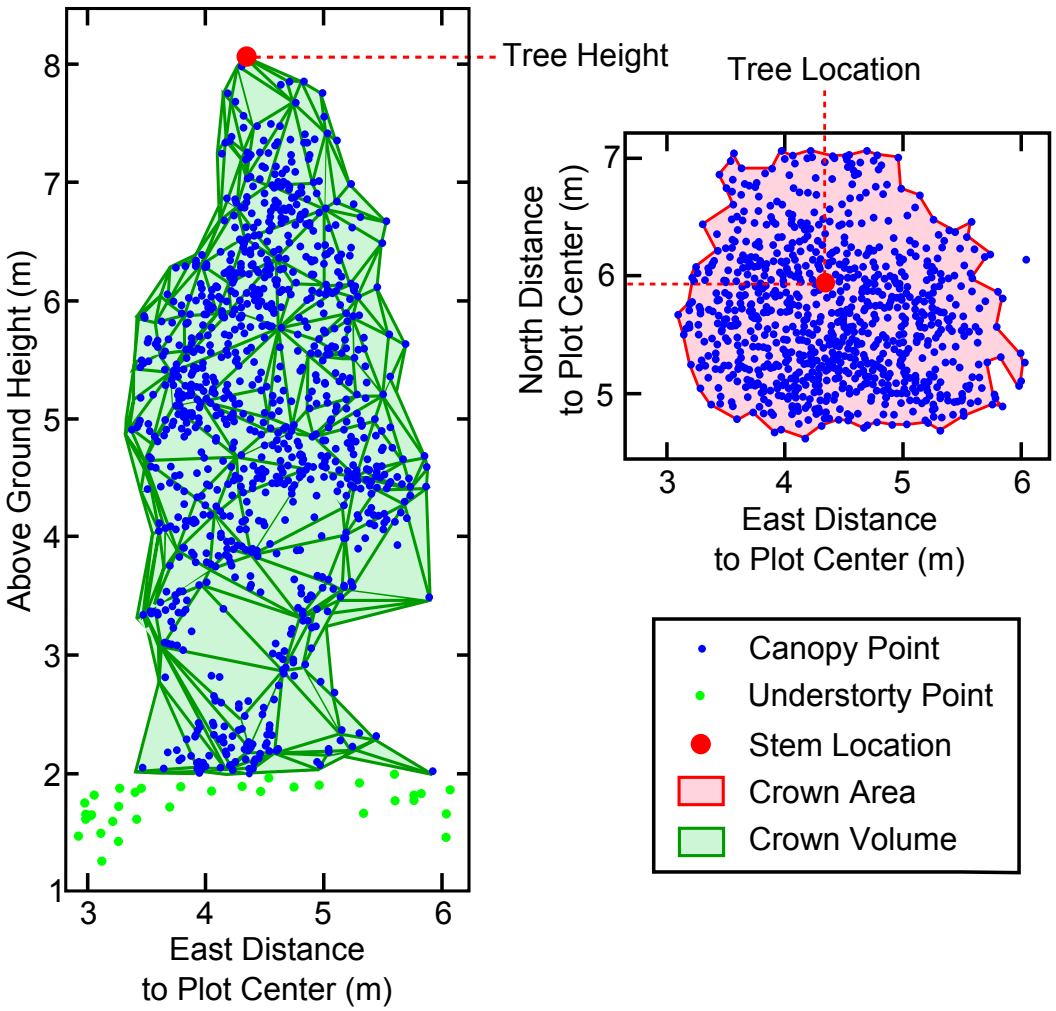

Figure 5.3: An example 2D representation of an individual tree segmented from a UAVLS showing the measurement of crown area and crown volume via α-shapes, together with observations of stem height and stem location.

was applied to the 3D point cloud with a standard value of α. A single value of α was used as returns typically occurred on the outside of the crowns and using smaller α values resulted in a hollow α-shape and an underestimation of crown volume. A 2.0 m α value was chosen to adequately capture the variability within the crown for the range of tree level point densities used in this study.

5.3.5 Assessment of Results

The variability in the metrics was assessed based on the mean absolute deviation from the mean (MD). We employed MD in this case as it is more robust to residual non-normality than standard deviation since we postulate that the segmentation routine is likely to cause outliers in the measurements of crown metrics. In the cases where

comparable field measures exist (i.e. for tree height, stem count, and stem location) RMSE and bias are also calculated:

$$RMSE = \sqrt{\sum_{i=1}^{n} \frac{(x_{iL} - x_{iF})^2}{n}} \tag{5.5}$$

$$Bias = \sqrt{\sum_{i=1}^{n} \frac{(x_{iL} - x_{iF})}{n}} \tag{5.6}$$

Where, n is the number of observations and x_{iL} and x_{iF} are the UAVLS and field measurements of each variable respectively. In the case of stem location, an assumption is made that stems are straight and field measured stem location at breast height and UAVLS measured stem location at the top of the crown are equivalent.

Analysis of variance (ANOVA) with repeated measures was employed to determine the repeatability of terrain and understory height observations at the cell level. However, ANOVA was not employed for tree-level metrics as consistency in each test was highly dependent on the results of the segmentation routine and therefore not consistent between the datasets.

5.4 Results

5.4.1 Repeatability of the flight parameters

Although the same flight parameters were used for each flight, variations in the UAVâĂŹs velocity, trajectory, and flying height caused variability in transect coverage. This resulted in 10 to 19 merged point clouds with full plot coverage being generated for each plot. These variations, particularly in velocity and flying height also caused the number of returns to differ between each transect and consequently each dataset. The average number of returns for a single dataset across all plots was 43,951 reaching as low as 27,532 and as high as 78,952 (see Table 5.2). Despite the variation in the number of returns, the proportion of first, second, and third returns were similar within each individual plot. Across all plots the largest minimum scan angle used to observe any one CHM grid cell was 27°. This occurred in a dataset with two merged perpendicular transects. For datasets with parallel transects this scan angle did not exceed 21°.

Table 5.2: Point cloud characteristics for each of the six plots.

Plot Number	**1**	**2**	**3**	**4**	**5**	**6**
No. of merged point clouds	10	18	11	19	14	10
Mean no. returns	349085	353192	416693	444713	671618	401804
MD no. returns	76341	50735	9593	61895	196136	73467
Mean % 1^{st} returns	84.2	78.0	69.0	70.0	73.9	77.8
MD % 1^{st} returns	1.2	1.7	0.6	0.9	1.5	1.5
Mean % 2^{nd} returns	14.2	19.3	26.1	24.6	21.9	19.0
MD % 2^{nd} returns	1.1	1.3	0.6	0.6	1.4	0.8
Mean % 3^{rd} returns	1.6	2.7	4.8	5.3	4.3	3.2
MD % 3^{rd} returns	0.1	0.3	0.1	0.3	0.3	0.3

Table 5.3: Differences observed in estimates of terrain and understory (US) height.

Plot Number	**1**	**2**	**3**	**4**	**5**	**6**
Plot-level mean DEM Height MD (m)	0.01	0.02	0.02	0.01	0.03	0.03
Max cell level DEM MD (m)	0.34	0.39	0.18	0.20	0.30	0.27
Mean cell level DEM MD (m)	0.05	0.07	0.05	0.03	0.04	0.07
Plot-level mean US Height MD (m)	0.02	0.07	0.05	0.01	0.05	0.02
Max cell level US MD (m)	0.52	0.50	0.64	0.45	0.58	0.52
Mean cell level US MD (m)	0.13	0.18	0.14	0.15	0.19	0.13

5.4.2 Terrain and Understory Heights

Correct observations of terrain height are of great importance as any errors directly propagate into errors in the observation of canopy and tree level metrics (Hyyppä et al. 2008). No large differences in the mean height of the DEM were observed between datasets (Table 5.3). The largest MD within any one cell was 0.39 m observed in plot 2. Analysis of the spatial distribution of the within cell MDs shows that cells with large differences (MD $>$ 0.15 m) occurred towards the edges of the plots typically in areas obscured from the sensor behind tall trees or high understory vegetation cover (an example is given in Fig. 5.4). The main cause of DEM error can be attributed to the angle of incidence between the laser and the canopy that reduces the likelihood of the laser pulse penetrating to ground level. This meant that the observation of terrain height differences were occasionally weakly significant between datasets with opposing transect merging methods (ANOVA p-values between 0.03 and 0.27). This difference was not observed when comparing two datasets using the same merging routine (p-values between 0.17 and 0.6).

Visual inspection of the understory layer suggested that the filtering process was successful (see for example Fig. 5.5). However, large MDs (maximum 0.65 m) occurred at the edge of tree crowns as the result of large branches that were classified as a mixture

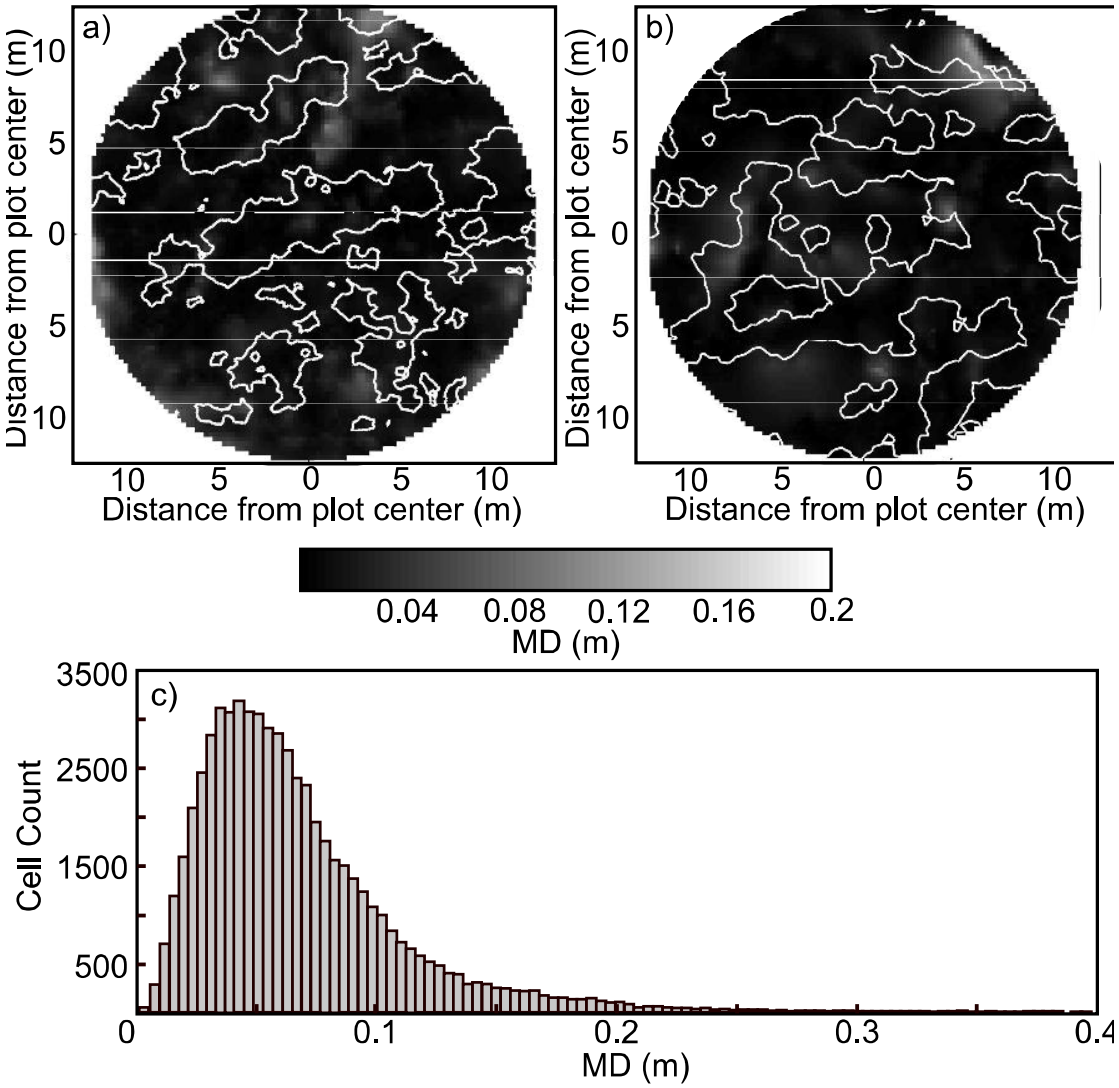

Figure 5.4: a) and b) cell wise deviation in plots 3 and 4 with the canopy highlighted by the solid white line;c) Distribution of deviations within all plots with a mean variance of 0.03 m and a standard deviation of 0.01 m.

of understory and canopy within the repeated datasets. For mean understory height the differences were found to be significant between all datasets (p-values between 0.01 and 0.07).

5.4.3 Plot level metrics

Only small differences were found in the vertical distribution of points between flights (Fig. 5.6) and all first return height statistics, including maximum height, were found to be robust. The MD for mean height, height standard deviation, skewness and kurtosis

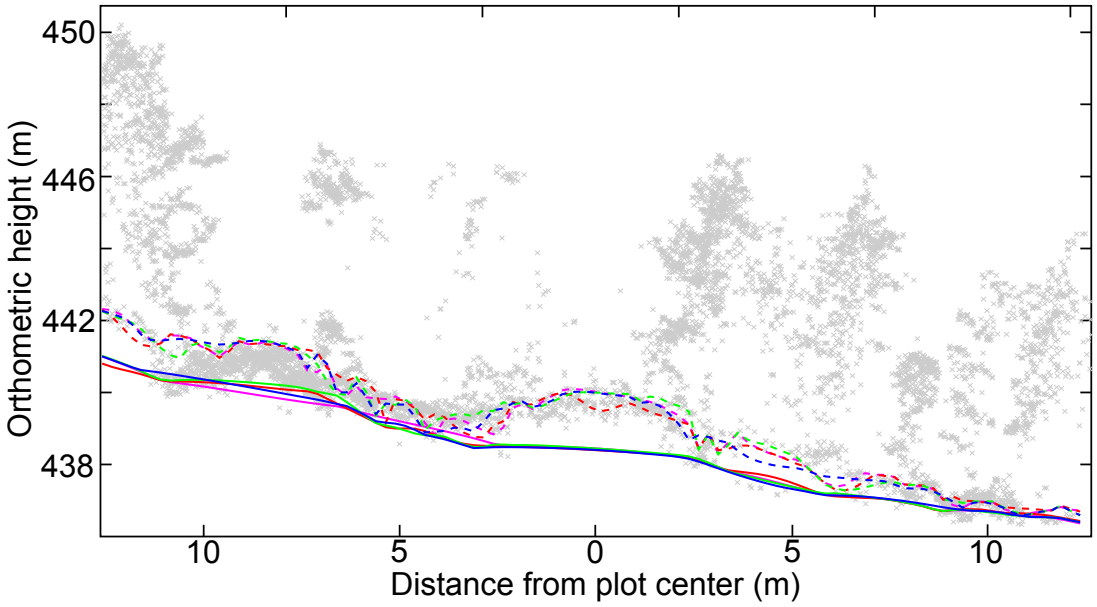

Figure 5.5: Transects of terrain (solid line) and mean understory height (dashed line) as measured from four datasets of plot 3 (Height datum AHD98)

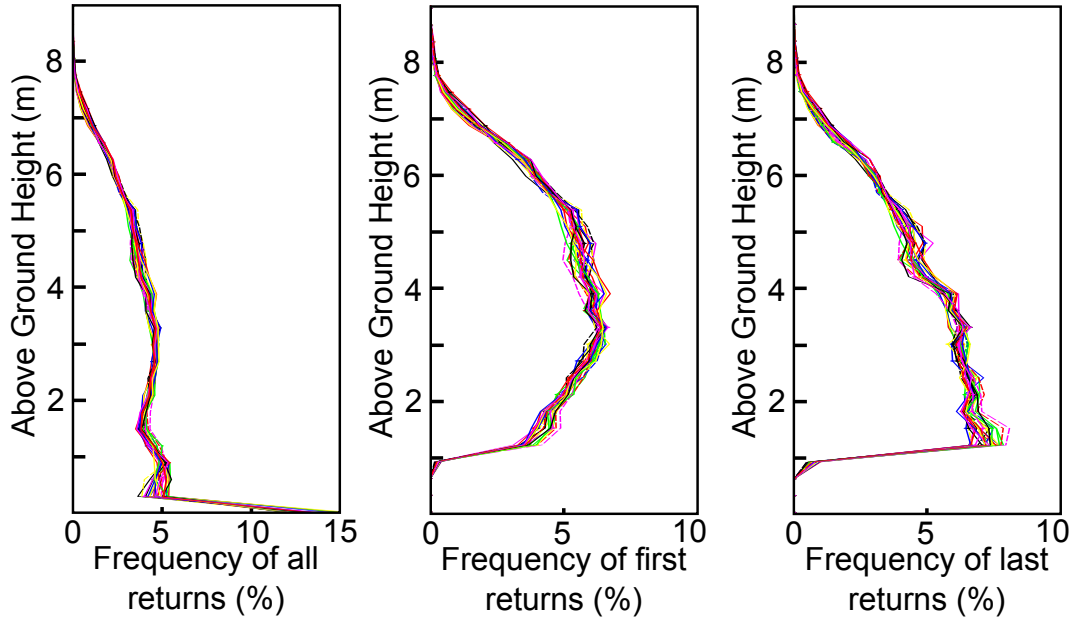

Figure 5.6: Aggregated vertical distributions of all returns, first returns from the canopy only, and last returns from the canopy for the 11 datasets captured over plot 3.

were all less than 0.05 m. The largest differences occurred in the lower height percentiles (AGH20, AGH30, AGH40), however, these differences were still only at the decimetre level (MD less than 0.09 m). No significant differences in AGH statistics between parallel or crossed transects was found, suggesting that the vertical distribution of point clouds collected from the UAV was robust to the transect merging strategy.

Table 5.4: Canopy cover estimates and the mean deviation within each of the three methods trialled.

Plot Number	1	2	3	4	5	6
Mean FCI (%)	60.58	65.52	78.11	91.80	60.27	69.25
Mean FCI MD (%)	1.59	1.54	1.18	0.42	1.24	1.73
Mean ACI (%)	53.98	60.74	57.19	90.67	46.62	62.87
Mean ACI MD (%)	1.54	1.62	2.15	2.31	1.86	1.97
Mean TCI (%)	55.65	62.92	61.22	92.78	49.31	64.52
Mean TCI MD (%)	1.55	0.85	0.78	1.92	1.23	1.42

Table 5.5: Result of tree segmentation showing the mean and MD for each variable.

Plot Number	1	2	3	4	5	6
Field Stem Count	45	29	51	69	44	32
Mean UAVLS Stem Count	43.25	30.27	50.83	71.26	44.14	33.80
MD UAVLS Stem Count	1.38	1.25	1.33	1.15	1.46	0.44
Mean Stem Omissions	3.50	0.84	2.51	1.47	1.71	0.40
MD Stem Omissions	1.06	0.67	1.05	0.84	0.82	0.54
Mean Stem Commissions	1.75	2.07	2.33	3.73	1.85	2.20
MD Stem Commissions	0.71	1.02	0.82	0.45	0.95	0.89
Mean Matched Stems	38.00	27.34	46.16	66.05	40.57	29.8
MD Matched Stems	2.13	1.35	2.09	1.68	1.65	0.44

Differences in the FCI metric for canopy cover (MD 0.42 to 1.73 %) were typically smaller than differences found in the ACI method (Table 5.4). Although the mean plot pulse density had no clear correlation with the differences found in the ACI method, it was found that within plot variations of pulse density affected the canopy cover map. This was particularly evident in datasets with overall higher point densities and higher rates of canopy cover. For instance, the maximum MD of 2.31 % for ACI was found in plot 4 which exhibited the highest level of canopy cover and the datasets with the highest point densities (up to 300 points per m^2). The FCI method performed better in this plot (MD 0.42 %).

5.4.4 Stem Detection

Typically, stems within each plot were over-segmented (Table 5.5). The mean stem detection rate from the UAVLS data was 102 % (MD of 4 %). Errors in the segmentation could be attributed to four sources: the over-segmentation of a crown (1.32 stems per plot), the under-segmentation of multiple crowns (2.36 stems per plot), trees at, or near the edge of the plot being included (0.1 stems per plot), and trees missed (0.3 stems per plot) from the stem count.

Although the same four segmentation error types occurred within most datasets, the stem count varied by between 0 and 6 stems (MD of 1.16 stems). This was a result of the under-segmentation of suppressed trees and the over-segmentation of large stems due to forks or ramicorns causing variations within the number of stems correctly matched to field measurements (MD of 1.55 stems). Nevertheless, 91 % of field measured trees were correctly matched to a UAVLS segmented tree across all datasets.

5.4.5 Tree level metrics

The 248 trees that were represented in three or more of the repeated datasets were used in determining the repeatability of tree level metrics. MD for stem location ranged from 0.02 to 0.48 m in 2D space (Fig. 5.7). No relationship between the location of a plot and the magnitude of the MD was observed. In comparison to field measured tree locations, the UAVLS stem locations had a mean RMSE of 0.62 m. Stems with large RMSE (e.g. > 0.5 m) were located near the edge of the plot where the error in the field measurements is likely to have been greater due to multiplicative error associated with compass bearings.

The distribution of the differences between the estimates of tree height and absolute tree height were similar. For 95 % of trees the MD between any two measurements of tree height was less than 0.35 m (Fig. 5.7) and less than 0.34 m for absolute tree height (Fig. 5.7). These results show that differences in terrain height play only a minimal role in the variability of UAVLS measured tree height. The maximum difference between any two repeat measurements of height was 1.4 m. This was a result of a segmentation error in which the branch of a dominant crown had been attributed to a suppressed neighbouring tree.

In comparison to the field measurements of tree height, the mean RMSE of all measurements was 0.52 m (Fig. 5.8). Within-plot biases were predominantly negative and tree heights were underestimated by 0.11 m when all observations were considered. Plot 4 was the only plot in which the bias was positive. This plot had the highest stem density and percent canopy cover, suggesting that the terrain height may have been underestimated. If only the maximum observation of tree height for each tree is considered, the RMSE of all measurements was 0.54 m and the overall bias was marginally positive (0.04 m).

Ninety percent of differences in the estimation of mean crown area and crown volume

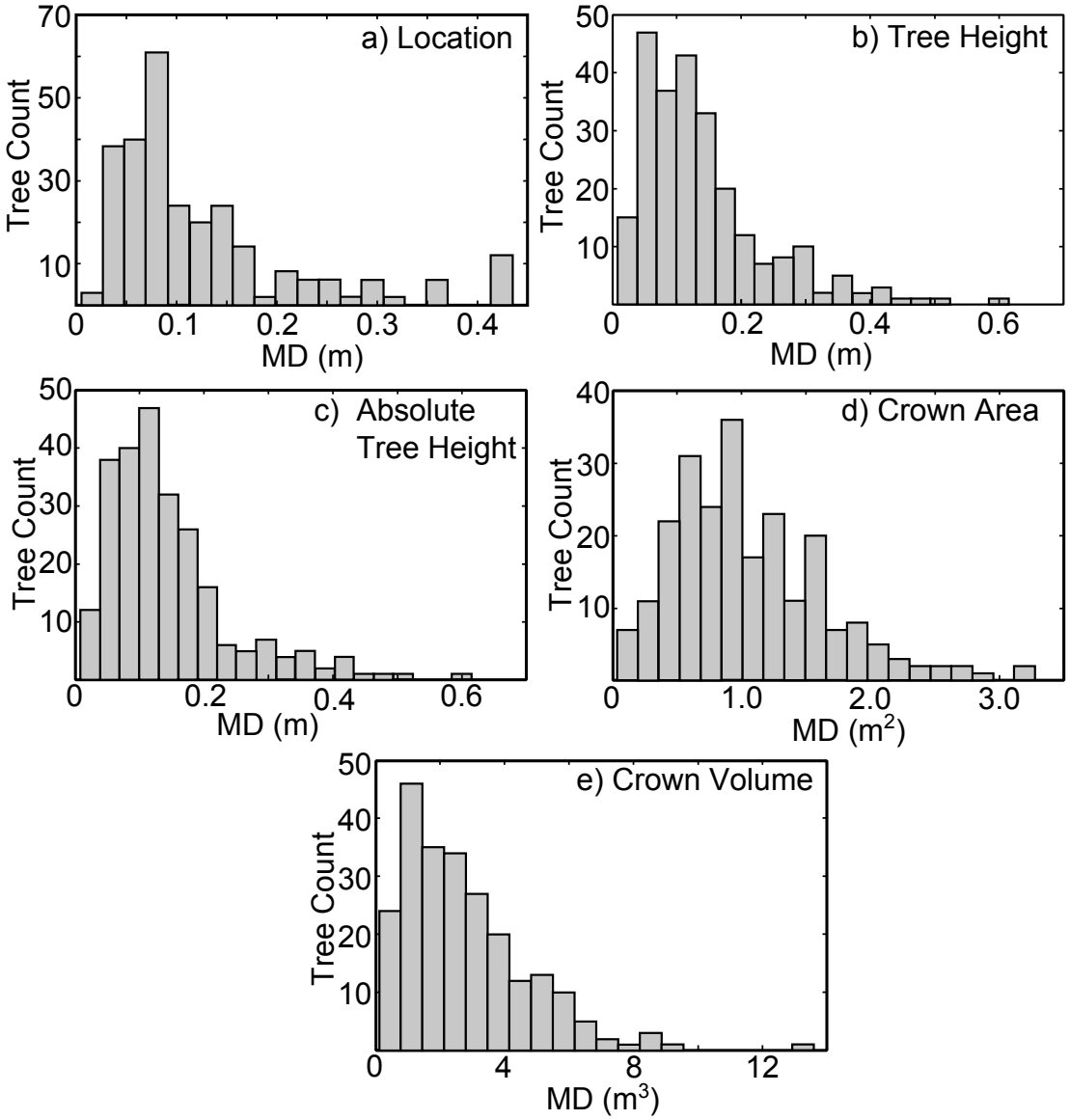

Figure 5.7: Histograms of MD errors of a) stem location (mean distance from mean location), b) tree height, c) absolute tree height, d) crown area, and e) crown volume for each of the 248 stems that were delineated from 3 or more datasets.

were between 5 and 37 %, and between 3 and 35 % respectively. These differences were dependent upon the repeatability of the segmentation method. Large differences of up to 3.3 m^2 for area and 14.4 m^3 for volume were observed for trees that were clustered within groups where over- or under-segmentation occurred. The crowns of isolated trees were measured with significantly less variation (crown area differences between 0.2 and 1.1 m^2 and crown volume differences between 0.3 and 4.2 m^3). At the plot level, differences in crown area represented between 0.78 and 1.92 % (MD) of the total plot area.

Comparing UAVLS crown area to the field measurements (mean crown radius^2 $\times$ π)

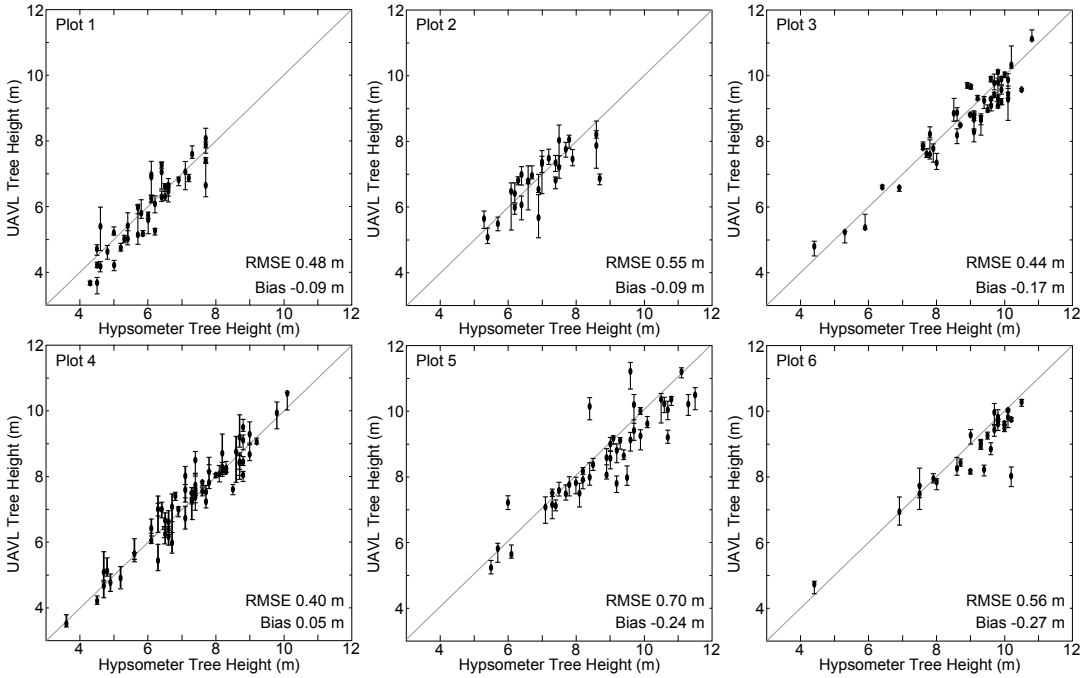

Figure 5.8: Tree heights as measured with UAVLS plotted against field measured tree heights. The solid circle shows the mean UAVLS measured height and the bars represent maximum and minimum observations.

suggested that UAVLS crown area was typically underestimated (RMSE 4.61 m^2 and bias -1.92 m^2). This can be attributed to interlocking canopy areas not being considered within the segmentation routine. This bias reduced to -0.27 m^2 when considering crowns with limited overlap (Fig. 5.9). This suggests that crown volume is also likely to be underestimated for trees with significant crown overlap, however, no field measurements were available to confirm this.

5.5 Discussion and Conclusions

The results from this study highlight the potential of UAVLS for measuring forest inventory metrics. Although UAVLS data was captured with different flight parameters and scan geometries compared to ALS data, comparable plot level repeatability was found in this study to those shown in studies analysing similar metrics derived from ALS data (Musk and Osborn 2007; Bater and Wulder 2011). Variations in the above-ground height distribution of point clouds acquired using UAVLS have been shown to be caused by large scan angles ($> 15°$) and variations in flying height (from 30 m AGH to 70m AGH) (Wallace et al. 2012a). The optimisation of the flight configuration using the two transect merging strategies adopted in this study allowed scan angle to be minimised

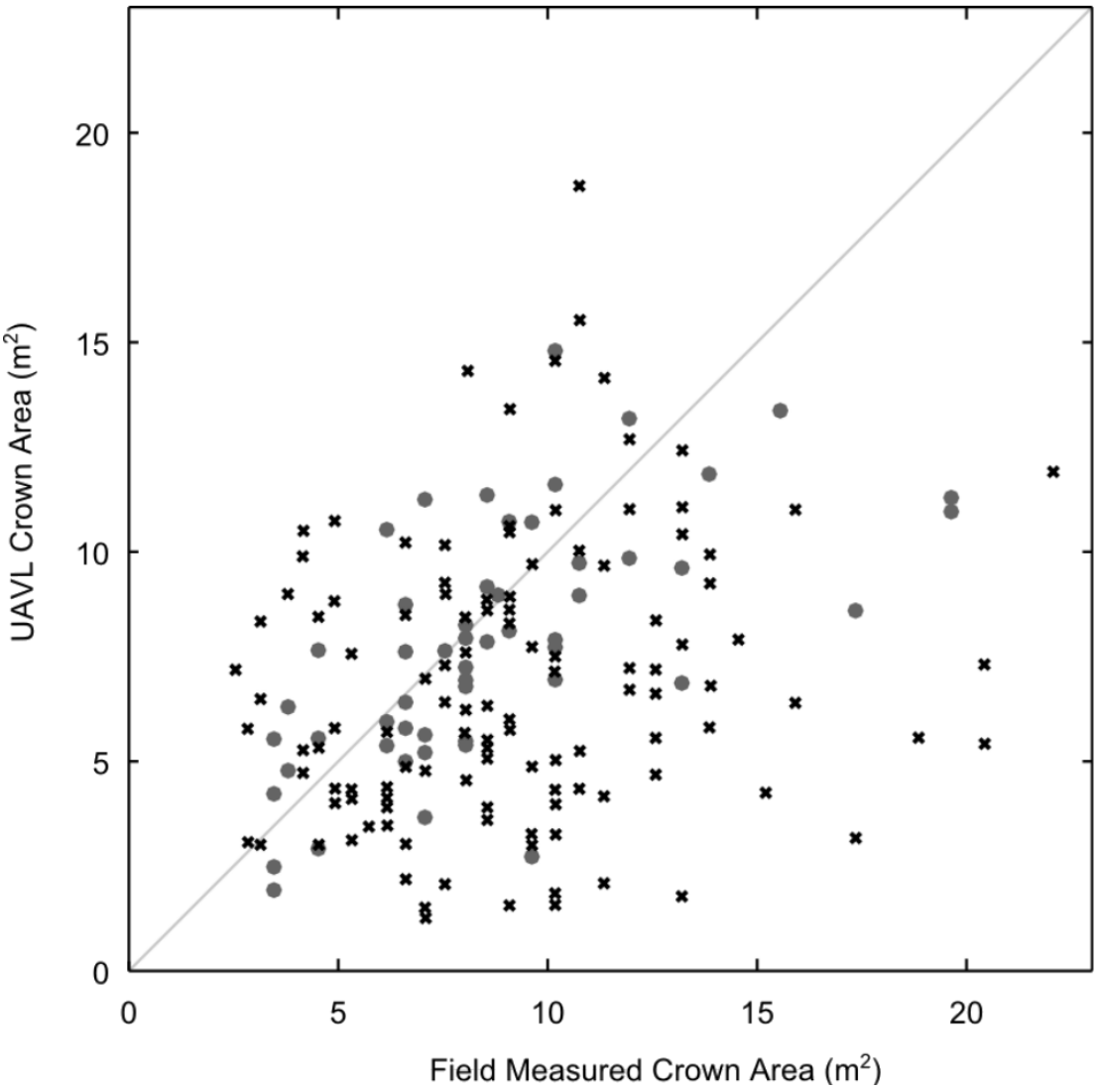

Figure 5.9: Mean UAVLS Crown Area against field crown area (dots = isolated crowns, crosses = crowns in groups).

while still capturing a substantial area of interest.

The precision in the observation of terrain demonstrates the positional precision of the UAVLS system as no adjustment was required in collocating transects or repeat datasets. Differences in the observation of terrain and understory height were only found to be significant when comparing two datasets created using the two different transect merging methodologies. Large differences (up to 0.39 m in terrain height) were primarily observed in cells towards plot boundaries in situations where large discrepancies in the scan geometry occurred. In these cases merged point clouds which required the use of large scan angles to capture the plot area typically overestimated terrain height.

As variability in the observation of terrain height directly underneath crown objects was minimal, any large differences in terrain height typically did not contribute to variability in inventory metrics such as tree height. Stem location and tree height were measured with a precision comparable to that observed in commonly used field techniques. For instance, Kitahara et al. (2010) demonstrated that a standard deviation of 0.8 m can be achieved for tree height measurements with a Vertex Hypsometer. In comparison, a MD of 0.35 m for this metric was achieved in this study. Ferraz et al. (2012) showed that ALS data can be used to measure tree height with an RMSE of 0.86 m in forest dominated by *Eucalyptus globulus*. An RMSE value of 0.52 m suggests that UAVLS data offered slight improvements in comparison to ALS data in the measurement of tree height. Similar improvements in the measurement of tree location (RMSE of 0.62 m) were found in comparison to ALS studies which often achieve accuracies of around 1 m Kaartinen et al. (2012).

The comparison of field data and UAVLS-derived height suggested that the bias commonly observed in ALS data was reduced in the UAVLS datasets (bias < 0.27 m). This reduction in bias can be attributed to the increased pulse densities achieved from the UAVLS sensor. Any remaining bias is likely due to a combination of the accuracy of the low cost sensor and an overestimation of terrain height due to the high levels of understory cover in the study area.

Large differences in crown area (MD of up to 47 %) and crown volume (MD of up to 57 %) were observed in the repeat measurements performed in this study. The segmentation of individual crowns from clustered trees with significant overlap was found not to be repeatable using the normalised cut segmentation methodology. These differences arise as a consequence of the application of the point cloud segmentation routine and do not indicate or preclude a lack of information within the point cloud. The repeatability in the information contained in the point cloud is highlighted by the small differences seen in plot level crown area (MD between 0.78 and 1.55 %). Further refinement in the segmentation algorithm is therefore required in order to assess crown properties with improved precision.

The results of the percent canopy cover analysis suggest that UAVLS data can provide this information with the required precision in a fast, low-cost, and non-subjective manner, potentially replacing current techniques based upon subjective visual assessment. Morsdorf et al. (2006) showed that FCI can be correlated with Leaf Area Index (LAI), however, this correlation is likely to depend on the properties of the sensor (such as beam divergence and the triggering mechanism) being used. ACI and TCI make use of

the full 3D geometry of the point cloud and are therefore less likely to be affected by variations in the properties of the sensor.

Precision in the directly measurable metrics examined here are of further importance as they can be used to provide an estimate of metrics that cannot be directly derived from the point cloud and thus provide additional information on forest structure. For instance, Bi et al. (2012) showed that the inversion of tree height-diameter functions can produce DBH estimates from ALS-derived tree height estimates with the prediction accuracy required for many forest inventory purposes. The precision and reduction in bias obtained using UAVLS-derived tree height metrics in this study suggest that the derivation of metrics such as DBH is feasible using the data collected with this platform.

The value in the derivation of forest inventory metrics from UAVLS data comes from the two primary advantages of UAVs as a remote sensing platform over manned aircraft. These are the high temporal and spatial resolution that can be achieved and relatively low deployment costs. Although the UAV is required to be operated in-situ, the use of pre-programmed GPS waypoints means that the operator only needs to find a small clearing near the plot to operate the platform. This stands in contrast to the difficulties that can be encountered in locating the plot when operating TLS systems. The current limitation of the UAV platform used in this study is the short time of flight achievable on one 5000 mAh battery pack (5 minutes). As battery technology improves and laser scanners become lighter there is potential for the surveys of all plots within a stand to be completed from one take-off point or in a single flight.

The collection of data (including set-up, pre-processing, and pack up) for plots and larger areas can be performed within 30 minutes and provides accurate representation of key 3D attributes of trees with a high degree of repeatability. In comparison, the field data collected for this study took between 2 and 4 hours per plot for a two man team. Furthermore, the use of automated techniques together with the georeferencing methodology outlined in Wallace et al. (2012b), meant that the processes to extract the final metrics from the data could be run with minimal user interaction.

For the UAV platforms to become an operational tool for use in forestry or ecological monitoring, further attention needs to be paid to the sampling strategy. Current technology limitations and the need to avoid large scan angles suggest that individual transects collected by ALS (in Wulder et al. (2012) for example) are not feasible with UAV systems. Although, this study has focused on a plot-scale area, multiple passes over a plot were achievable within a single five minute flight. This suggests that larger,

more comprehensive, plots could be designed for use with UAVLS.

5.6 Thesis context

This chapter outlines the repeatability of key forest metrics derived from UAVLS data. Given the importance of repeatability for determining change detection, the stability of the metrics found in this chapter highlight the applicability of UAVLS for this task. The next chapter builds on this foundation by using UAVLS to perform change detection.

6 | Detecting pruning of individual stems using Airborne Laser Scanning data captured from an Unmanned Aerial Vehicle

Chapter 6focuses on the detection of change due to silvicultural treatments at the Individual Tree Level and is published in the *International Journal of Applied Earth Observation and Geoinformation* as Wallace et al. 2014.

Abstract

Modern forest management involves implementing optimal pruning regimes. These regimes aim to achieve the highest quality timber in the shortest possible rotation period. Although a valuable addition to forest management activities, tracking the application of these treatments in the field to ensure best practice management is not economically viable. This paper describes the use of Airborne Laser Scanner (ALS) data to track the rate of pruning in a *Eucalyptus globulus* stand. Data is obtained from an Unmanned Aerial Vehicle (UAV) and we describe automated processing routines that provide a cost-effective alternative to field sampling. We manually prune a 500 m^2 plot to 2.5 m above the ground at rates of between 160 and 660 stems/ha. Utilising the high density ALS data, we first derived Crown Base Height (CBH) with an RMSE of 0.60 m at each stage of pruning. Variability in the measurement of CBH resulted in both false positive (mean rate of 11 %) and false negative detection (3.5 %), however, detected rates of pruning of between 96 and 125 % of the actual rate of pruning were achieved. The successful automated detection of pruning within this study highlights the suitability of UAV laser scanning as a cost-effective tool for monitoring forest management activities.

6.1 Introduction

The application of treatments such as thinning, to increase volume, and pruning, to ensure timber quality have become essential activities in modern forest management. The optimal timing and level of treatment for many plantation species have been widely studied resulting in the design of best practice treatment regimes (Pinkard 2002; Montagu et al. 2003; Wills et al. 2004; Alcorn et al. 2008). In *Eucalyptus* plantations for

instance, the rate (stems/ha) of pruning needs to be targeted to match the desired harvest rate and the timing of pruning needs to coincide with canopy closure (Pinkard 2002). The height of pruning is also critical in order to prevent a significant reduction in growth (Pinkard 2002). In the forest industry, the application of these treatments is often performed by contractors, with very little if any checking to ensure that the treatment has been applied correctly. One reason for limited quality assurance is that post treatment inventories are currently not economically viable. Detailed tree-level inventory data, however, would be valuable for optimal decision-making on pruning.

Airborne Laser Scanning (ALS) has become a key tool for gathering information on the 3D structure of forested environments (Wulder et al. 2012). The information derived from ALS point clouds allows detailed estimates of the characteristics of the forest to be collected over wide areas at relatively low cost (Hilker et al. 2013). Recently, the high geometric accuracy and precision of the data collected by modern ALS sensors has led to individual tree crowns being increasingly used as the object of analysis (Yao et al. 2012; Ørka et al. 2012; Maltamo et al. 2012; Korhonen et al. 2013). Key metrics such as tree count, species, location, height, and crown properties can be accurately measured with high resolution ALS data (Maltamo et al. 2012).

In order to monitor silvicultural activities with this technology, the ability to accurately track individual tree-level changes on demand is essential. Although ALS data can be used to monitor forest change at the plot-level, with for example forest growth (Næsset and Gobakken 2005; Hopkinson 2008), changes in canopy closure (Vepakomma et al. 2008), defoliation and damage (Solberg et al. 2006a; Vastaranta et al. 2013; Nyström et al. 2013) and variation in biomass (Bollandsas 2013; Næsset et al. 2013) all shown to be quantifiable, individual tree-level change has been less comprehensively studied. The precision of individual tree-level metrics demonstrated in several studies, such as Holmgren and Persson (2004) and Vastaranta et al. (2011), imply there is potential for repeat acquisition ALS data to be used to monitor and detect change. Yu et al. (2008), for instance, demonstrated that it is possible to track growth at the individual tree-level.

Although previous research shows potential for monitoring growth and dramatic change such as thinning, little emphasis has been placed on the detection of change occurring in the lower part of the crown, where pruning occurs. Several properties of individual tree crowns have, however, been shown to be measurable from ALS data. Pyysalo and Hyyppa (2002), for instance, developed polygon models for extracting these attributes from ALS data with a point density of 10 points/m^2. Although this method readily described the upper parts of the crown, there were greater errors in the estimation of

the properties of lower parts of the crown. Holmgren and Persson (2004), Solberg et al. (2006b), Popescu and Zhao (2008), and Maltamo et al. (2010) all used techniques based on vertical binning of the ALS returns to estimate Crown Base Height (CBH). The errors in these estimates were, however, typically greater than 1 m. In order to track changes in the lower part of canopy, CBH (or a similar variable) would be required to be made with greater precision. To achieve this Vauhkonen (2010b) suggested that collecting data at increased point densities may allow a more accurate representation of the actual discontinuities in the crown.

The collection of higher density ALS data requires a slower moving platform flying at lower altitudes. The low-cost (per unit area) nature of ALS surveys is made possible by the wide area data capture. As such, restricting the speed and flying height of the platform to achieve greater point densities, typically makes manned surveys prohibitively expensive. Unmanned Aerial Vehicles (UAVs) are being increasingly used as an alternative remote sensing platform. Laser Scanning data collected from UAVs (UAVLS) can be captured with significantly higher point densities and with more regular repeat visit times, due to the relatively low survey deployment costs. The ability to measure tree properties has been demonstrated by Wallace et al. (2012b) and Jaakkola et al. (2010). Jaakkola et al. (2010), for instance, demonstrated the applicability of UAVs for the detection of within canopy change by manual defoliating a single tree at several stages. The change in the number of canopy returns was found to be highly correlated to the removed biomass at each stage of defoliation.

The objectives of this paper are to determine the potential for UAVLS data to be used in the assessment of change due to pruning of a *Eucalyptus* stand. This paper is motivated by the development of UAV systems as a remote sensing platform, which can be used to collect high spatial resolution data at a relatively low deployment cost. These attributes will allow UAVLS surveys to be utilised to collect highly detailed information on-demand, allowing silvicultural treatments and other forest management activities to be monitored with greater precision.

6.2 Methods

6.2.1 Study Area and Field Data

The study area was a 500 m^2 circular plot in a 4-year old *Eucalyptus globulus* stand located in southeast Tasmania, Australia (Figure 6.1). The terrain had a moderate east

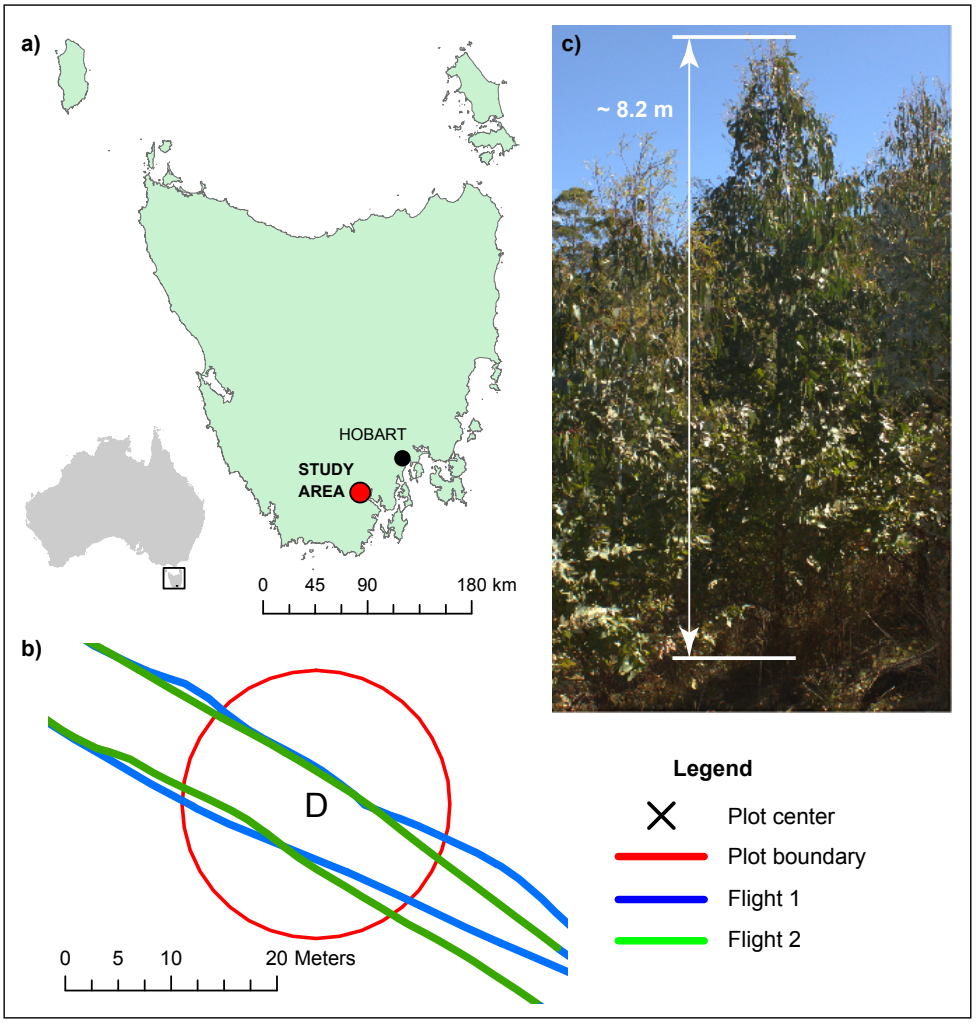

Figure 6.1: Study area. Top left: Location of the study area in Tasmania, Australia. Upper right: Image of a *Eucalyptus globulus* tree within the plot. Lower left: Example of the repeatibility of UAV flight lines over the plot.

facing slope of between 6 and 10°. There was moderate understory cover up to 1.2 m. Trees within the site were planted with within- and between-row spacings of 2.25 and 4.0 m, respectively, resulting in a planting density of approximately 1100 stems/ha. The 47 trees within the plot were measured *in-situ* for height, location, crown width and Diameter at Breast Height (DBH). The plot had a mean height and DBH of 9.4 cm and 8.7 m respectively.

The stand was approaching canopy closure meaning that the first lift of pruning was to be undertaken in order to ensure increased timber quality (Gerrand et al. 1997). For the purposes of this study, manual pruning within the plot was performed in five stages. Each stage represented a pruning treatment at rates of 160 to 660 stems/ha (i.e. 8 to 28 stems), in steps of 100 stems/ha (i.e. 5 stems). Stems were randomly selected for

Table 6.1: Properties of the two datasets captured before pruning (Ba/b) and the two datasets captured at each stage of pruning (P1a/b to P5a/b). Metrics include point density and the proportion of the number of first, second and third returns.

Data	Prune Rate [stems/ha]	Point Density [pulses/m^2]	% 1st returns	% 2nd returns	% 3rd returns
Ba (b)	0	167 (145)	60 (60)	31 (30)	9 (10)
P1a (b)	260	210 (168)	59 (60)	33 (32)	8 (8)
P2a (b)	360	196 (184)	60 (59)	31 (32)	9 (8)
P3a (b)	460	190 (188)	59 (60)	32 (32)	9 (8)
P4a (b)	560	207 (152)	59 (60)	33 (31)	8 (9)
P5a (b)	660	220 (155)	59 (58)	32 (33)	9 (9)

pruning. The height of pruning followed the prescribed guidelines for first lift pruning within a *Eucalypt* stand with all green branches up to 2.5 m being removed resulting in final CBH of between 2.5 and 3 m . CBH was recorded at the location of the stem using a measuring tape before and after pruning.

6.2.2 ALS Surveys

ALS surveys were flown with a multi-rotor UAV Laser Scanning system (UAVLS) before pruning (B) and after each stage of pruning (P1 to P5). The UAVLS, fully described in Wallace et al. (2012b), consists of an Ibeo LUX laser scanner and direct georeferencing sensors mounted on an OktoKopter multi-rotor UAV. The Ibeo LUX laser scanner utilises four parallel scanning layers each with a scan frequency of 12 Hz, and is capable of recording up to 3 returns per pulse with a transversal beam divergence of 0.8°. The direct georeferencing sensors consist of a Micro-Electro-Mechanical Inertial Measurement Unit, a high definition video camera and a dual frequency GPS receiver. All sensor observations are recorded on-board and post-processed with the use of a short baseline GPS ground station and a novel post processing algorithm (described in Wallace et al. (2012b)) enabling horizontal and vertical accuracies of 0.34 m and 0.14 m (RMSE) respectively to be achieved.

Two flights, capturing two independent point clouds, were flown before pruning (B) and after each stage of pruning (P1 to P5). Each flight was flown at a approximate height 40 m Above Ground Level (AGL) at a nominal velocity of 2.8 m/s with a restricted scan angle of ± 30 °. This flight configuration results in a on-ground swath width of 46 m. Forward and reverse swaths, offset by 12 m either side of the plot center, were captured in an individual flight and merged to produce a single point cloud with a point density of between 145 and 220 pulses/m^2(Table 6.1).

6.2.3 Point Cloud Preprocessing

The point clouds were preprocessed to produce individual tree segments following the workflow summarised in Figure 6.2. This workflow involves first clipping the georeferenced and merged point clouds to an area with a 5 m buffer surrounding the field measured plot. Ground and non-ground returns were then separated using the filtering algorithm outlined in Axelsson (1999). A 0.25 m Digital Elevation Model (DEM) was then generated based on the ground returns using natural neighbour interpolation. The Above Ground Height (AGH) of all non-ground returns were then determined based on this DEM.

To separate understory returns from canopy returns, a second filter was then applied. This filter involved initially classifying all returns with a normalised height below a 2.5 m threshold and with no returns above this threshold within a 0.7 m radius as understory. The threshold value and radius were chosen based on the properties of the vegetation in the study area. This initial set of understory returns was used to create a Triangular Irregular Network (TIN). All returns above this TIN were considered to have originated from the canopy. The lowest non-ground return below each TIN facet was then classified as originating from the understory, with all other points remaining unclassified. A new TIN was then created and the process continued until all points were classified as originating from the understory or the canopy.

Individual tree crowns were automatically segmented from the data using an adaptation of the normalised cut segmentation procedure outlined in Reitberger et al. (2009). Initially, individual trees were identified from a smoothed Canopy Height Model (CHM) as local maxima within a 3 x 3 window pixel. The CHM was created, with a resolution of 0.1 m by attributing each cell with the height of the highest normalised canopy return it contained. Cells containing no returns or considered as pits were filled based on the algorithm outlined in Ben-Arie et al. (2009). The CHM was smoothed using Gaussian smoothing with a square 1.5 m kernel and a sigma value of 1.8. Local maxima within a 3 x 3 pixel kernel were then found and used within a marker controlled watershed segmentation of the CHM (following Maltamo et al. (2009)). All returns above the 65^{th} AGH percentile were then attributed to a watershed defined segment to provide an initial estimate of the crown location and upper boundaries.

Points below the 65^{th} AGH percentile were attributed to the initial crown clusters based on normalised cut segmentation. Normalised cut segmentation involves finding the two disjoint segments A and B of a graph (consisting of the individual points) by maximising

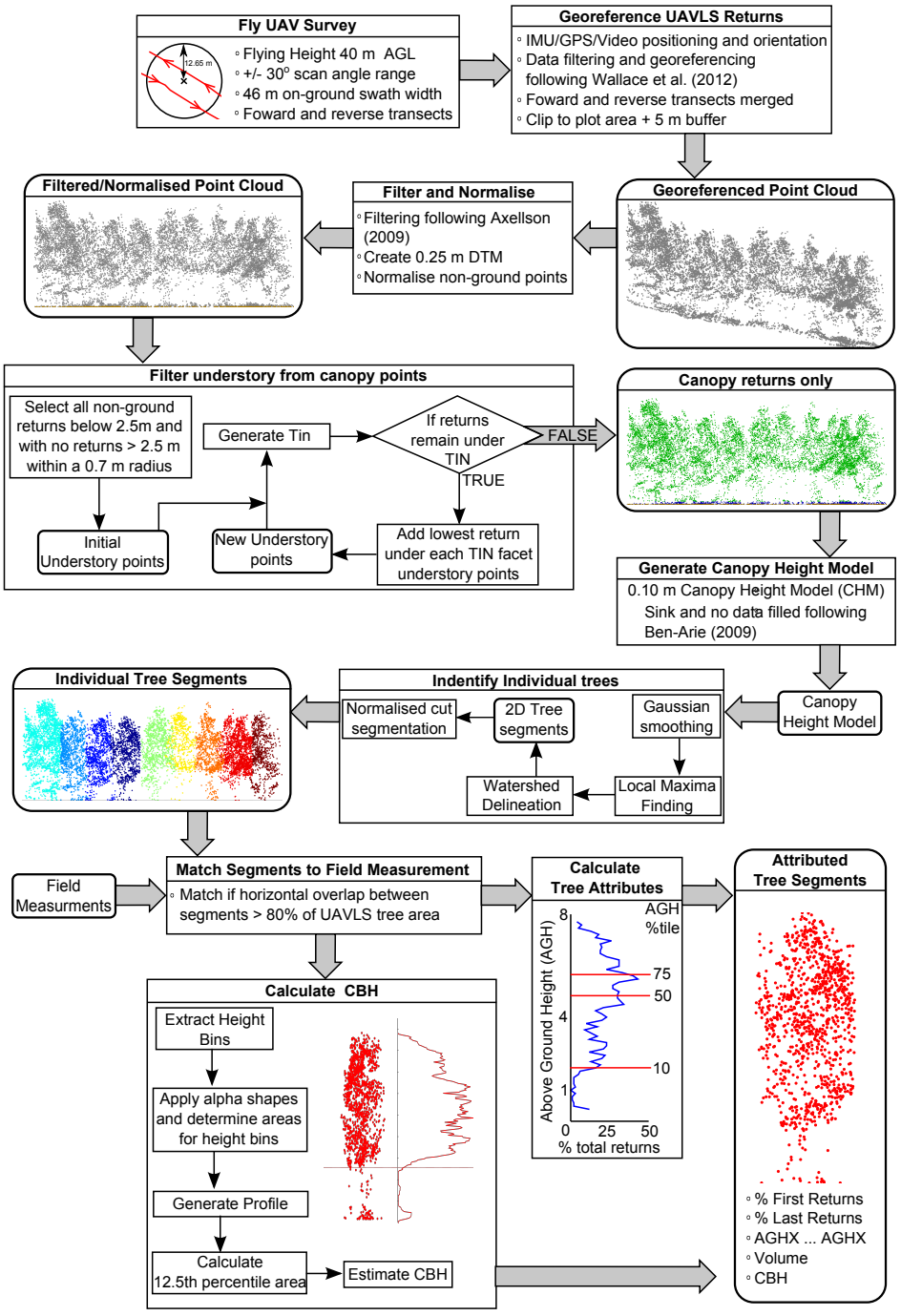

Figure 6.2: The workflow used to derive individual tree segments and associated attributes from point clouds captured using the UAVLS system.

the similarity of the members in each segment and minimising the similarity between the two segments and was implemented as outlined in Reitberger et al. (2009). Similarity within the normalised cut segmentation, as applied in this paper, was based on the horizontal and vertical euclidean distance between pairs of points within the feature space. A weight of 3 was applied to the horizontal euclidean distance in order to enhance

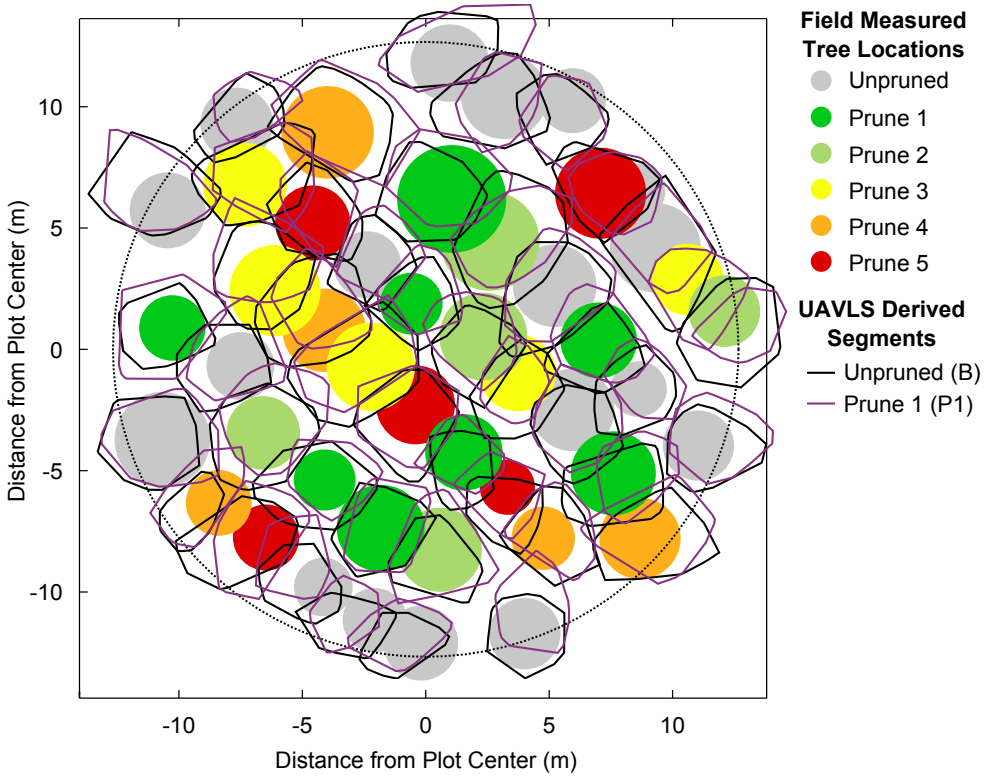

Figure 6.3: Crown map showing convex hull of ALS derived segments from the baseline and prune 1 datasets as well as field measured tree locations (shaded circles) showing the stage of pruning.

the space between the trees. A weight of 3 was chosen for this purpose based on the height to width ratio of trees within the study area.

For each stage of pruning the 3D tree segments were matched to a field measured tree if the horizontal overlap of the 2D projection was greater than 80% of the convex hull of the UAVLS segment. The homogeneity of the plot and the high point density of the dataset allowed 45 to 48 (of the available 47) trees to be segmented from each point cloud using this method. In all datasets, 45 of the 47 field measured trees were correctly matched to an ALS derived segment across all datasets. In a limited number of datasets, one pruned and one unpruned stem were not matched to UAVLS segments due to errors in the segmentation routine. Further analysis was restricted to the 45 correctly segmented trees (Figure 6.3).

6.2.4 Extraction of Tree Level Features

A set of descriptive statistics representing canopy attributes were calculated from the canopy points of each tree-level segment, for each dataset. The descriptive parameters comprised AGH percentiles (AGH5, AGH10, AGH20, ... AGH90, AGH99), mean AGH, AGH standard deviation (AGH_σ), AGH skewness, AGH kurtosis and the proportion of 1^{st} and last returns in the segment, as well as the proportion of canopy returns to other returns.

The effect of pruning on the representation of a stem, as demonstrated in Figure 6.4, is analogous to a reduction in the overall crown volume or an increase in the CBH. As such in this study, both crown volume and CBH were also modelled using the geometry of the point cloud. The CBH of the individual tree segments within the point cloud was determined based on the approach implemented by Holmgren and Persson (2004), which uses the relative area of the crown in several height layers to determine CBH. Initially the point cloud representation of a tree is divided into 0.10 m bins overlapping by 0.05 m. Within each layer, the area of the crown is calculated using α-shapes. The α-shapes algorithm allows the shape of a set of unorganized points to be described (Edelsbrunner and Mücke 1994). The shape described by this algorithm is determined by the set of points and the value of α, which controls the level of detail reflected in the final shape. In this case, α was set to 0.4 m . This allowed adequate detail in the outer shape of the crown without introducing a large number of within crown voids.

The areas calculated within each layer were then normalised based on the maximum area in any one single layer. The crown was then traversed from bottom to top and the crown base height defined as the height above the ground of the first layer for which the next 20 consecutive layers (totaling 1 m) were greater than 12.5^{th} percentile of all crown areas. To assess the accuracy of this routine in determining CBH, RMSE and bias were calculated in comparison to the field measurements.

To calculate the crown volume α shapes were applied to the 3D point cloud. In order to preserve the true spatial relationship between the ALS points, the ellipsoidal heights were used in the calculation of crown area. An α equal to 2 m was chosen to adequately capture the variability within the crown for the range of tree-level point densities used in this study. Crown volume was then taken as the volume of the largest distinct α-shape only.

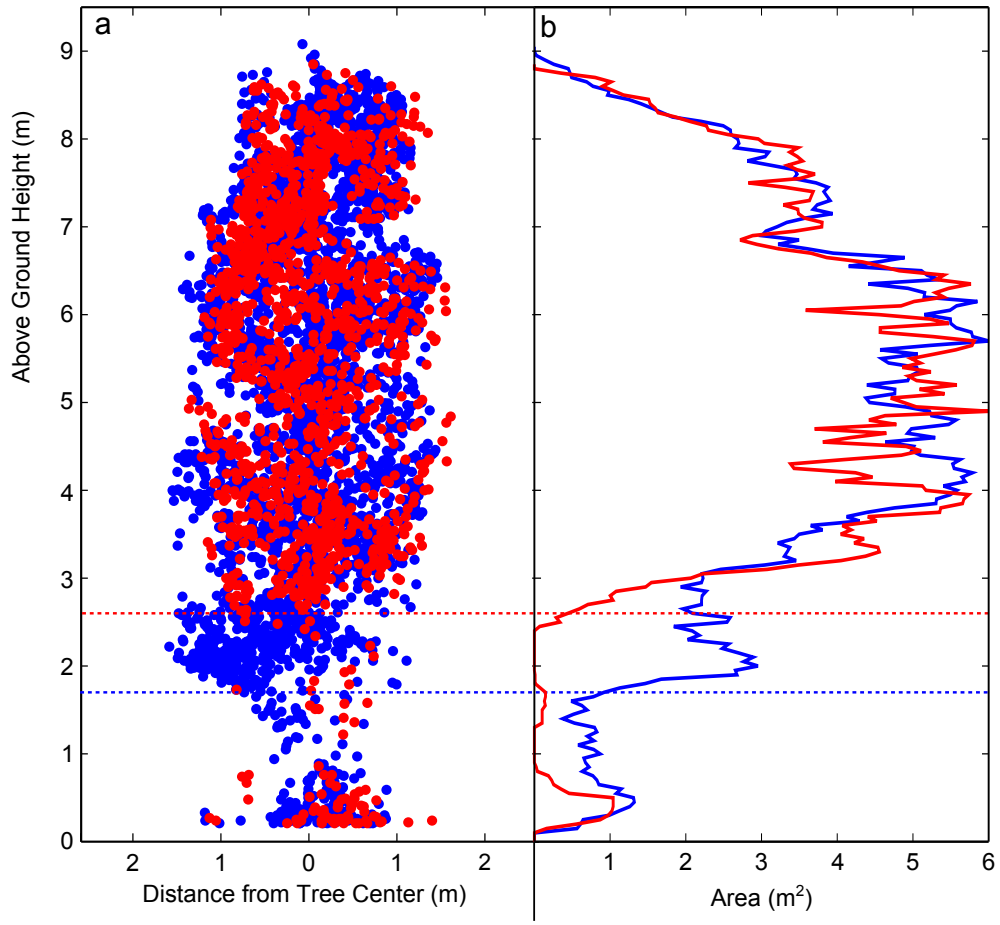

Figure 6.4: a) A single tree as represented in UAVLS point clouds before (blue) and after prunning (red). b) Area profile generated based on alpha shape and the determined CBH (dashed line) for point clouds depicted in a

6.2.5 Repeatability

The instability of the flying parameters of the UAV, the characteristics of the low-cost sensor, and the algorithms used to derive tree segments, are all sources of variation in the properties of the collected point clouds between flights (Wallace et al. 2012a). For example, it was shown in Wallace et al. (2012a) that a 20 m increase in flying height can cause a significant reduction in the proportion of returns originating from the mid and upper canopy. In order to determine the repeatability, we compared each specific feature per tree segment from unique datasets in which no change had occurred to the segment. Two to twelve independent segments of any individual tree were measured from the two datasets captured at each stage of pruning. The repeatability in each statistic was then determined based on the standard deviation (σ) from trees for which three or more repeat measurements had been made without change.

6.2.6 Change detection

Change detection was performed using the datasets from the baseline flights and each stage of pruning. In order to determine if pruning was likely to cause significant deviation in the measured statistic, we first compared the 27 pruned segments in the final stage of pruning with the baseline segments of these trees using Wilcoxon rank sum test. The null hypothesis, stating that the two sets of samples are drawn from the same distribution, was rejected at $p < 0.01$, confirming that change is detectable at the plot-level in a metric following the final stage of pruning. As multiple attributes were being compared, we applied boneferroni adjustment to avoid false rejections of the null hypothesis due to a multiple testing problem (Hastie et al. 2009).

Change detection at the tree-level was then performed by comparing the magnitude of the differences in the statistics deemed to show significant change using the Wilcoxon rank sum test. Change was considered to have occurred on a stem when the difference in the statistics was greater than 2σ (95 % confidence interval) of that statistic. We performed this change detection procedure for each dataset in sequence, as well as comparing each stage of pruning against the baseline dataset.

The results were analysed by comparing the known state of pruning (i.e. pruned or unpruned) of each tree with the detection result using the UAVLS segments. Trees were identified as correctly detected as pruned, correctly unpruned or an incorrectly detected as pruned (false positive) or not detected as pruned (false negative). The rate of detection was determined as the number of UAVLS-derived stems divided by the correct number of stems.

6.3 Results

6.3.1 Crown Property Determination

UAVLS-derived CBH and field measured CBH were moderately correlated ($r^2 = 0.686$) (Figure 6.5). The measurement of UAVLS CBH had a bias of -0.03 m and an RMSE of 0.47 m in comparison to the field measurements. The RMSE and bias were slightly lower for pruned stems (bias of -0.05 m, RMSE of 0.33 m) than unpruned stems (bias of -0.02 m, RMSE of 0.52 m).

The standard deviation between repeat measurements of CBH in the unpruned segments

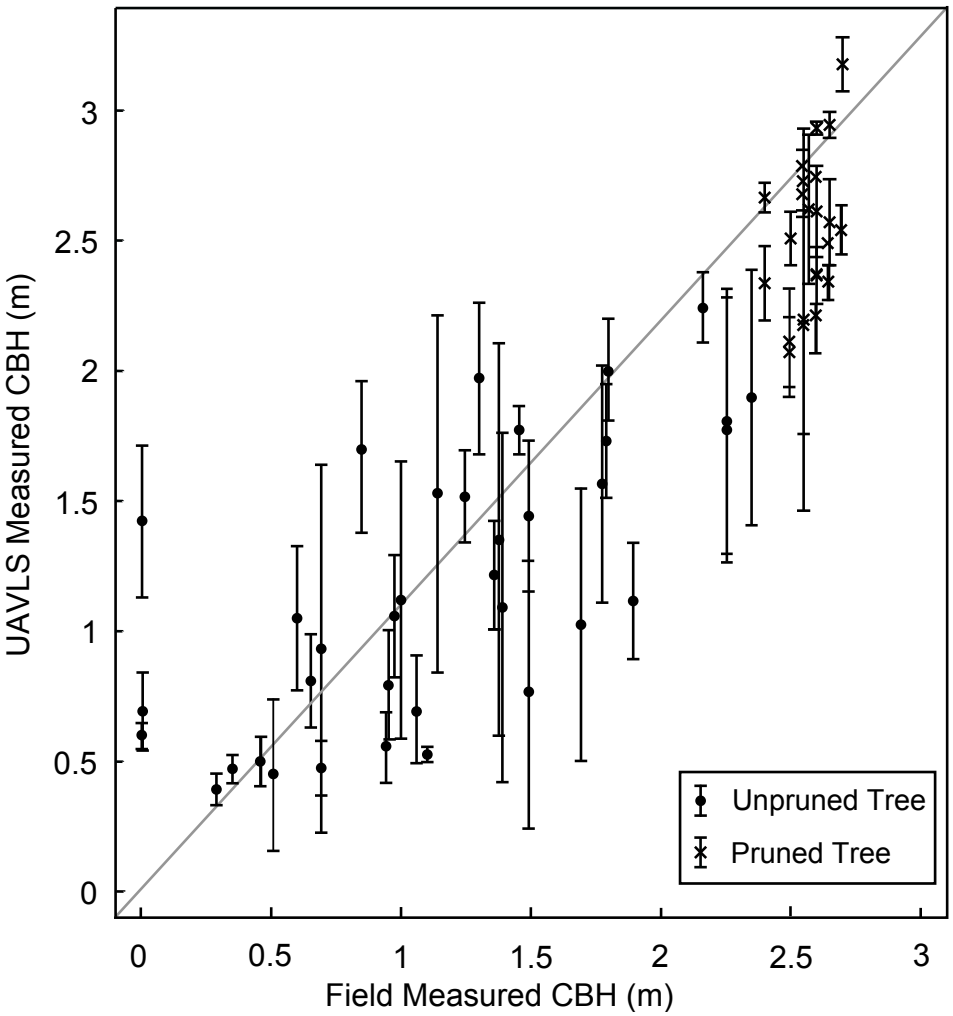

Figure 6.5: Laser-derived crown base heights plotted against ground-truth crown base heights for unpruned (dots) and pruned (crosses) stems. The error bars represent the standard deviations; error bars for trees with fewer than three measurements are represented by the mean standard deviation.

was +/−0.31 m. This reached a maximum of +/−1.41 m in any one segment (Table 6.2). In comparison, the CBH of pruned stems was found to be determined with greater repeatability (σ = +/−0.16 m). Observations of volume were highly variable, with σ (+/−5.6 m^3) being up to one third of the overall mean crown volume for most trees. The variability of the lower AGH percentiles (AGH10 to AGH50) was greater than for the higher percentiles, suggesting that measuring change in this part of the crown is likely to be more difficult than monitoring tree growth. The standard deviation for the return type proportions were all within +/−4 %. This is significant for % last returns as the mean proportion of last returns was only 9 %.

Wilcoxon signed rank tests indicated that only CBH, AGH5, AGH10 and % last returns were significantly different between the B and P5 datasets at $p < 0.01$. Other statistics

Table 6.2: Standard deviations and Wilcoxon sign rank test p-values of measurements made on unpruned and pruned tree segments for which no change had occurred. Significant p-values ($p < 0.01$) are highlighted in bold.

	mean			$\sigma(+/-)$			
Variable	unpruned	pruned	all	unpruned	pruned	all	p-value
CBH	**1.14**	**2.53**	**1.66**	**0.31**	**0.16**	**0.26**	**0.00**
volume	39.94	33.11	37.39	6.56	4.37	5.74	0.80
AGH5	**1.90**	**3.04**	**2.33**	**0.38**	**0.28**	**0.34**	**0.00**
AGH10	**2.53**	**3.48**	**2.88**	**0.34**	**0.23**	**0.30**	**0.00**
AGH20	3.34	4.09	3.62	0.34	0.26	0.31	0.02
AGH30	3.98	4.69	4.25	0.34	0.28	0.32	0.02
AGH40	4.55	5.20	4.79	0.36	0.26	0.32	0.20
AGH50	5.11	5.65	5.31	0.36	0.24	0.31	0.83
AGH60	5.70	6.13	5.86	0.33	0.24	0.29	0.92
AGH70	6.27	6.56	6.38	0.30	0.21	0.27	1.00
AGH80	6.85	7.08	6.94	0.23	0.19	0.21	1.00
AGH90	7.47	7.68	7.55	0.17	0.16	0.16	1.00
AGH99	8.38	8.51	8.43	0.11	0.12	0.12	1.00
mean	5.05	5.59	5.25	0.26	0.20	0.24	0.43
σ_{AGH}	1.86	1.59	1.76	0.10	0.09	0.10	0.02
skewness	0.11	0.18	0.14	0.16	0.17	0.17	1.00
kurtosis	0.26	0.53	0.44	0.23	0.34	0.27	1.00
% First Returns	72	75	73	4	3	4	0.14
% Last Returns	**42**	**35**	**40**	**3**	**2**	**3**	**0.01**
% Canopy Returns	72	69	71	4	4	4	0.06

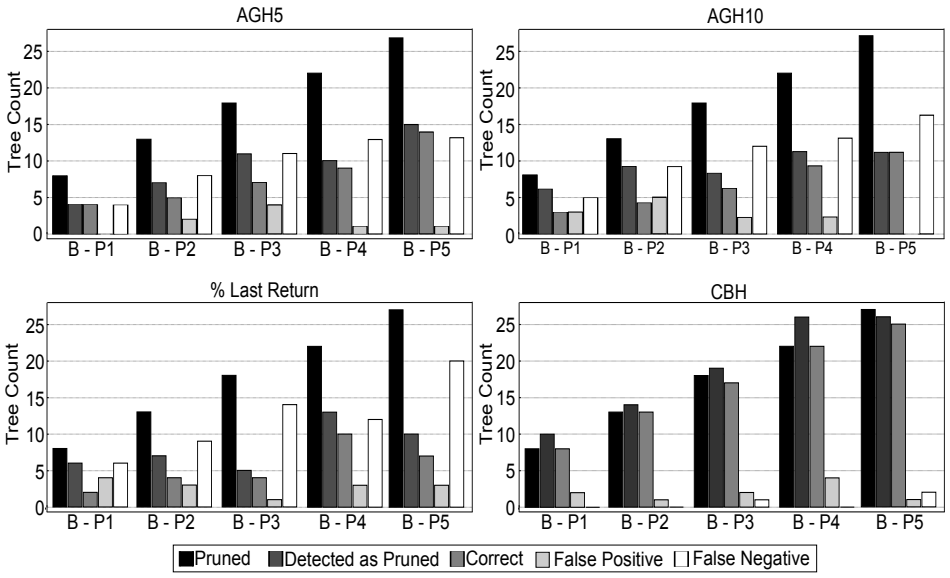

Figure 6.6: Detection of pruned trees for the four identified statistics (AGH5, AGH10, % last returns and CBH) for comparisons between baseline dataset (B) and each stage of pruning (P1 to P5). Each panel shows the true count of pruned trees, the UAVLS detected count, false positives and false negatives

such as AGH20, AGH30, σ_{AGH} and % of canopy returns showed moderately significant differences, however, were not considered in any further analysis. Volume was not found to show significant differences. This can be attributed to the high levels of variance in the measurement of volume.

6.3.2 Tree Level Change Detection

Analysis of change detection was performed using the CBH, AGH5, AGH10 and % last returns metrics, assessing each independently. Using the statistics based on the properties of the returns (AGH5, AGH10 and % last returns) each gave similarly poor change detection results with a high number of false negative identifications (Figure 6.6). These false negatives are caused by an overestimation of these statistics for most segments from the baseline point clouds. This is potentially due to the interaction between the understory and canopy elements not being adequately resolved in this dataset.

The rate of false negatives and false positives in the change detection varied between sequential comparisons (Figure 6.7). This is due to the measurement variability being greater than the change caused in the individual statistic by pruning. The incorrect detection of pruning was found to occur within the same tree and comparison for all three statistics. This suggests that these segments were inadequately capturing the

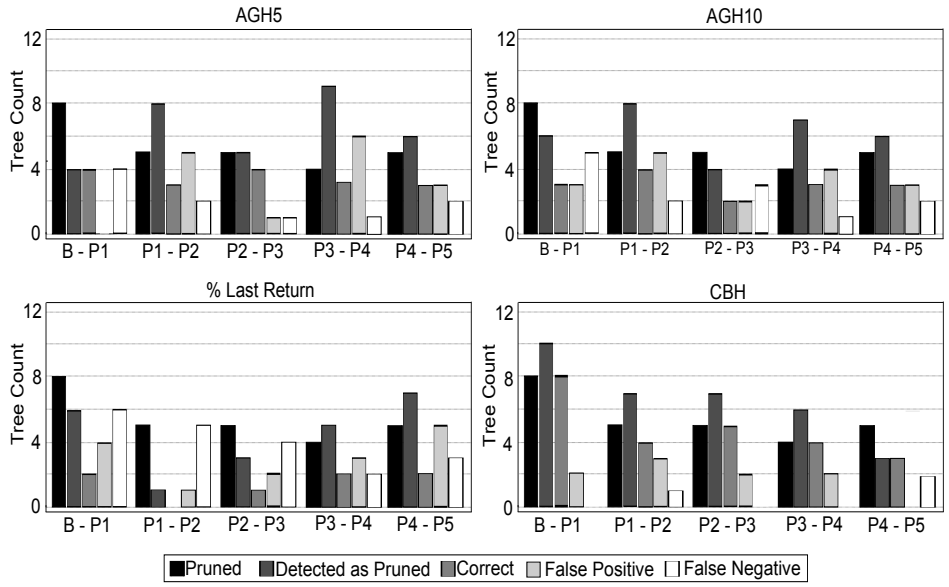

Figure 6.7: Detection of pruned trees for the four identified statistics (AGH5, AGH10, % last returns and CBH) for comparisons between the baseline (B) and each stage of prunning (P1 to P5) sequentially. Showing the true count of pruned trees, the UAVLS detected count, false positives and false negatives

foliage or lack thereof in the lower half of the crown. No correlation between the location of a segment and incorrect identification was found.

Using UAVLS CBH for change detection gave significantly better detection results. When comparing the baseline data set to all other datasets, the detected pruning rate was between 96 % and 125 % of the actual rate of pruning. The variability in the measurement of CBH was a source of both false positive (mean rate of 11 %) and false negative (3.5 %) results. For instance, tree 10 (baseline UAVLS CBH = 1.1 m) was correctly detected at pruning rates of 200 (UAVLS CBH = 2.50 m), 300 (2.45 m) and 400 (2.35 m), but was not detected in the final stage where the CBH was 2.15 m. The variation of CBH was caused by a number of factors including variations in the point density due to slight changes in flying height or viewing angle as well as change occurring in neighbouring segments.

Examining the spatial distribution of errors in the results reveals that false positive detections typically occurred when one or more neighbouring trees had been pruned (Figure 6.8). This was caused by points from pruned stems being included in the neighbouring unpruned segments resulting in an increase in CBH between datasets. Similarly, false negatives occurred when neighbouring trees remained unpruned. No correlation between plot location and correct or incorrect detection could be identified due to the

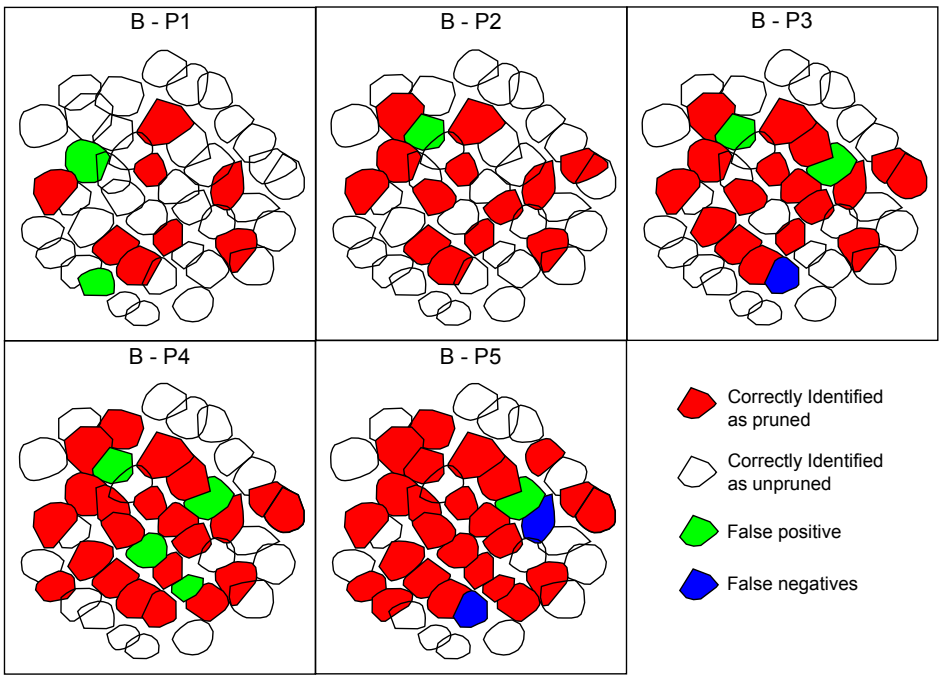

Figure 6.8: Plot showing correctly detected trees along with false positives and false negatives when the stages of pruning (P1 to P5) are compared to the baseline (B) dataset

limited dataset.

Similar patterns in false positive and false negative detection due to neighborhood pruning were also observed when comparing the datasets sequentially (Figure 6.9). Variability in the measurement of CBH, however, resulted in a more random spatial distribution of false positive and false negative detections.

6.4 Discussion

Significant change in AGH5, AGH10 and % last returns at the plot-level highlights that the change due to pruning is represented within the high density UAVLS data. Deriving CBH from the point cloud allowed reliable detection of pruning (96 % to 125 %) to be achieved. False positive (mean rate of 11 %) and false negative (3.5 %) detections were caused by the variability in the measurement of CBH. These results suggest that using a UAV to monitor silvicultural activities to ensure treatments are applied following best practice is feasible. This added level of accounting combined with other potential uses of the UAVLS system, such as the collection of inventory or monitoring canopy closure (Wallace 2013), highlight the potential economic benefits of these systems.

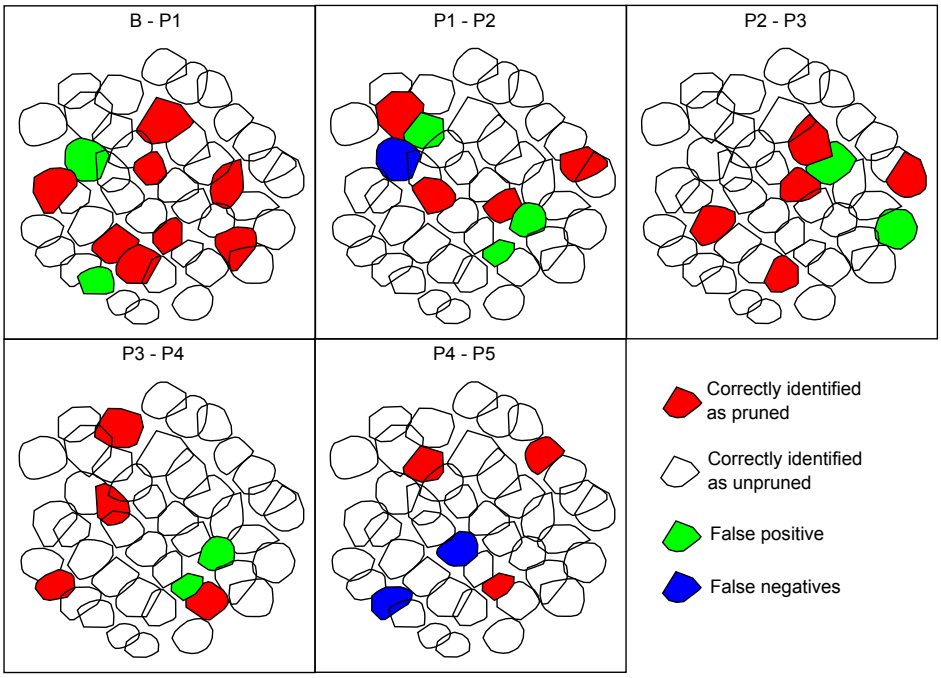

Figure 6.9: Plot showing correctly detected trees along with false positives and false negatives when the stages of pruning are compared sequentially

The accuracy of CBH was found to be similar if not improved, to that found in other studies using similar techniques such as (Holmgren and Persson 2004) and (Vauhkonen 2010b). In these studies, CBH was often determined with a positive bias, which has been suggested to be due to a lack of penetration through the crown (Dean et al. 2009). Although the initial CBH of most trees was close to the ground, only a small negative bias was observed in this study. Higher point density, the use of higher scan angles (up to 30°) and the properties of the study area are all likely to have contributed to this lower bias. It is notable that the RMSE and bias reduced further once pruning had occurred suggesting that at other stages of growth, when there is no interaction between canopy and understory elements, UAVLS CBH determination may offer further improved estimates of CBH. It is necessary to note that previous studies focussed on more mature forests where the overall crown depth is likely to be greater (Dean et al. 2009; Vauhkonen 2010b; Maltamo et al. 2010) .Further work is required to determine the applicability of UAVLS determined CBH in other forest age classes and species.

A key component of detecting correct CBH from a UAVLS point cloud is the correct attribution of individual points to a tree segment. The normalised cut segmentation procedure allowed accurate detection of trees within the point cloud. As the space between trees approached the point spacing of the collected datasets, inconsistencies in the description of tree boundaries occurred. This resulted in errors in the change

detection procedure, highlighted by the number of false positives occurring close to pruned stems.

Although it was possible to detect pruning using CBH, the magnitude of noise in the measurement of return statistics in comparison to the magnitude of change due to pruning was not sufficient to allow individual pruned stems to be easily identified. As such, it can be suggested that the magnitude of the change induced by manual pruning was at the detectable limit in regards to the data collection methodology. Therefore, more subtle change due to the death of lower canopy limbs due to changing light conditions or mild insect infestation are unlikely to be detected (in this species and age class) using this technique until irreparable damage has been inflicted.

The noise in the return statistics is likely a function of errors in the segmentation procedure, variations in the flying track, height and speed and the properties of the scanner. The low-cost IbeoLUX scanner was only able to collect three discrete returns per pulse and has a relatively large footprint (0.69 m along track and 0.07 m across track) in comparison to modern airborne scanners (0.3 m) (Glennie 2007). This and the ‘dead spaceâĂŹ (approx 0.8 m) between returns limit the information available describing the canopy where change had occurred. Full-waveform information, which has shown potential for use on full-scale platforms (Reitberger et al. (2009) for instance), would overcome this restriction. This technology is not yet available in a form factor suitable for mini-UAV platforms.

This study was limited by the small number of pruned and unpruned trees within a single plot. A clear extension of this work is to include a greater number of plots within a stand. This would enable the use design-based inference methods that could provide an indication of the overall pruning rates within an entire stand. Furthermore, collecting a greater number of samples would allow a more rigorous classification algorithm such as support vector machines or random forest to be employed using the return statistics, and remove the reliance on a modelled variable such as CBH.

This study has outlined one potential use for UAVLS data within forested environments. The first lift of pruning within a *Eucalypt* stand represents a low impact activity. The successful detection of this activity and the use of UAVLS for assessing other individual tree attributes as shown in Jaakkola et al. (2010) and Wallace et al. (2012b) suggest other activities, including later stages of pruning or thinning, will be readily detected allowing UAVLS data to be utilised throughout a plantations rotation. Furthermore, the high spatial resolution data, relatively low-cost deployment and multi-sensor attributes

of UAV remote sensing systems in general suggest that there are several more potential opportunities to exploit these platforms for forestry management purposes.

6.5 Conclusions

This study investigated the use of Laser Scanning data collected from a Unmanned Aerial Vehicle (UAV) to detect change induced by pruning within a 4-year old *Eucalyptus* stand. The high density UAV laser scanning (UAVLS) data showed significant differences in the above ground return height distribution between unpruned and pruned stems indicating the change due to pruning had been captured in the data. To map this change at the individual tree-level, Canopy Base Height (CBH) was derived from the UAVLS data. Using CBH a detection rate of 96 to 125 % was achieved with only a small number of false positive (11 %) and false negative (3 %) detections. This study highlights the potential of UAVLS data, which can be collected at high resolution with low survey costs, to be integrated with the current remote sensing tools deployed by forest managers.

6.6 Thesis context

Based on the findings of the previous chapters, this chapter outlines the use of UAVLS for monitoring change in a forested environment. This chapter demonstrates that the information captured by the UAVLS is sufficient to monitor change within the lower part of the crown as caused by pruning.

7 | Conclusions

In this study, a mini-Unmanned Aerial Vehicle Laser Scanning (UAVLS) system has been developed. The use of low-cost and lightweight sensors combined with a novel position and orientation algorithm allowed the required georeferencing accuracy to be achieved. The application of this UAVLS system to the collection of forest metrics was investigated within two four-year old *Eucalyptus* plantations. Automatic methods for the extraction of metrics describing the 3D structure of individual trees were developed, demonstrating that these metrics were measured both accurately, in comparison to field measurements, and with high repeatability. Based on these results, the UAVLS system was used to map change induced by pruning, demonstrating that this change could be reliably mapped at the individual tree level.

7.1 System development

Objective 1 - *Assess existing approaches and technologies for collecting georeferenced laser scanner data from a mini-UAV and adapt these methods to provide a workflow for accurately georeferencing the data captured by UAVLS.*

The successful integration of low-cost off-the-shelf sensors both in hardware and software and the development of an accurate georeferencing solution have been fundamental to the success of this study. The development of an error budget indicated that the traditional Airborne Laser Scanning (ALS) processing workflow based on an Inertial Measurement Unit (IMU)/GPS Kalman smoother was infeasible primarily due to the low accuracy of the lightweight MEMs-based IMUs on the UAVLS system. The use of a vision-based sensor, deriving orientation estimates using Structure-from-Motion (SfM) to overcome this issue has advanced investigations into direct-georeferencing from mini-UAV platforms. The horizontal and vertical accuracies of this system were assessed in the field and shown to be ± 0.30 m (root mean square error (RMSE)) and ± 0.15 m (RMSE) respectively. Achieving comparable accuracies to modern full-scale systems is considered a significant achievement, particularly given that sensors were chosen based on strict criteria of low cost and low weight for use with the mini-UAV.

7.2 Forest inventory mapping

Objective 2 - *Adapt existing and develop new processing methods for processing very high resolution point clouds generated by a UAV platform to accurately assess the structural attributes of typical Tasmanian Eucalyptus plantation forests at the individual tree level.*

Initial investigations into the use of the UAVLS system in *Eucalyptus* forests demonstrated that flying height had to be restricted to below 50 m above ground level (AGL) in order to derive point clouds that adequately represented the vegetation structure. This resulted in a survey design utilising parallel or crossing transects in order to capture a forestry plot sized area. This method, which relied on the accuracy of the direct georeferencing algorithm, was shown to generate high-density point clouds with repeatable plot-level characteristics to be captured for plot-sized areas in a single flight.

A key requirement in the accurate estimation of tree-level metrics from laser scanning data is the detection and delineation of individual tree segments. This thesis demonstrates that high-density point clouds (up to 180 p/m^2) increase the likelihood of accurate tree detection and improve the accuracy of the crown delineation. This improvement was shown for five different tree detection and delineation methods tested. Chapter 4 demonstrated that utilising the full 3D structure within the point cloud enabled more accurate and repeatable delineation of individual trees compared to full-scale LiDAR based tree detection techniques. The best performing method, which utilised both a Canopy Height Model and the point cloud, resulted in 98% of trees being repeatedly and correctly delineated from the point cloud.

Achieving accurate and repeatable tree-level segments allowed the repeatability of key inventory metrics to be assessed. Chapter 5 demonstrated that tree location (mean absolute deviation (MAD) of 0.48 m), height (0.35 m) and crown area (3.3 m^2), as well as terrain height (0.15 m), can be derived with high levels of repeatability. Tree-level metrics were shown to be highly correlated with field measurements, allowing tree height to be measured with insignificant bias. In addition, Chapter 5 described the development of new approaches for generating understory height maps by separating canopy and understory returns and for deriving canopy cover. The method developed for the derivation of canopy cover was shown to improve repeatability in this metric (MAD of 2.3%), in comparison to other commonly used techniques, while allowing for the generation of spatially explicit canopy cover maps.

Objective 3 *- Determine the capabilities of the UAVLS for measuring change in forest conditions..*

The final chapter of the thesis demonstrated the use of UAVLS to monitor change caused by the silvicultural application of pruning. The successful detection of pruning (at rates of between 96 and 125%) highlights the amount of information available within a UAVLS point cloud. This serves to emphasise the success of the previous work in generating a spatially accurate point cloud, from which repeatable tree level segments and metric estimates could be made. Change due to thinning (or loss of stems) and variations in tree height (from growth or damage) have been previously demonstrated using ALS systems. The repeatability of metrics such as tree height and tree count suggest that change due to thinning or forest growth can also be accurately monitored with this system.

7.3 Contributions to knowledge

The development of a mini-UAV based laser scanning system and associated methods for the extraction and monitoring of forest metrics developed in this thesis represents significant progress in the fields of UAV remote sensing and remote sensing of forested environments. This section summarises the key scientific contributions to knowledge within these sub-disciplines.

UAV remote sensing

- Integration of low-cost off-the-shelf sensors capable of observing position, orientation and laser scanner range and scan angle enabling accurately time synchronised data streams to be logged on-board a mini-UAV.

- A novel sigma-point Kalman smoother utilising observations from HD-video based on SfM in order to constrain the error in attitude measurements in the MEMs-based IMU, allowing accurate estimate of UAV position and orientation for the robust georeferencing of UAVLS point clouds.

- A UAVLS surveying and processing workflow to produce point clouds that accurately represent the 3D characteristics of the underlying geography.

Remote sensing of forested environments

- Proof-of-concept for the use of mini-UAVs for mapping and monitoring the 3D structure of trees within a *Eucalyptus* plantation forest.

- Improvements in tree detection and crown delineation accuracy of established methods through the use of high resolution point clouds

- A methodology for the segmentation of canopy and understory in UAVLS or other high density point clouds.

- A new spatially explicit method to estimate canopy cover from high density point clouds.

- Improve the capability for tree-level metrics to be captured with high repeatability from airborne remote sensing systems

- First successful detection of change occurring in the lower half of tree crowns from an airborne remote sensing system making it possible to accurately monitor pruning treatments

7.4 Limitations and future research directions

Eucalyptus plantations were chosen as the forest type for this thesis because the genus is widely planted throughout the world and requires managed silvicultural intervention at several stages during a rotation to produce quality timber. The use of two similar age class monoculture forests, however, limited this study in terms of assessing the effect of different forest structure on the repeatability of metric estimates from the UAVLS. Although plots were selected subjectively to ensure that a variety of stocking densities were examined, individual trees within the study area typically had similar properties. The results from studies analysing data collected from ALS systems suggest that vegetation structure can have a significant effect on the derivation of individual tree-level metrics (Vauhkonen et al. 2008). In particularly, the delineation of suppressed trees from mixed species forests is an on-going challenge for the use of ALS data, which may in part be addressed by higher resolution point clouds. In order for this to be assessed with a UAVLS system, the interaction between the properties of lightweight low-cost scanners (in this case the Ibeo-LUX) and more complex vegetation structures found in multilayered and mixed species forests requires further investigation. Future work should focus on the deployment of the system within alternative forest types (particularly mixed

species forests) and the assessment of inventory metrics at all key management stages of a *Eucalyptus* rotation.

A general limitation of the mini-UAV platform for the collection of remotely sensed data is the limited coverage area of a single flight. The combination of the weight of the laser scanning system, the required flying parameters, and battery life of the mini-UAV platform restricted the safe flight time of the OktoKopter AD-8 platform to between 3 and 4 minutes. This allowed for a maximum of two to four swaths over a plot-sized area depending on the initial distance from the take-off location. Current and future developments in battery and UAV technology as well as the further miniaturisation of sensors should allow the flight time to be significantly increased. As ALS has maturated as a forest measurement technique in-depth discussion around the advantages of a number of different sampling regimes has continued. Similar research and discussion is required for the use of UAV platforms, particularly given the restricted area of coverage. In this study, plot-based sampling methods were presented; however, further research should examine the advantages of other sampling regimes.

The laser scanner deployed in this study was designed for use in the automotive industry and does not have the optimal properties required for mapping purposes. The development of a dedicated laser scanner for UAVLS purposes would be expected to significantly improve the results found in this study. Increases in laser power, lower beam divergence and more sensitive triggering mechanisms would provide greater measurement range and allow for increased flying heights. The use of technological advances such as the collection of full-wave form data or the use of dual wavelength and hyperspectral laser scanners are ongoing and the potential for this technology to be miniaturised will present further opportunities for UAVLS in forested environments.

UAVLS systems previously presented in the literature have focused on the use of more stable and accurate IMU technology, such as fiber optic gyroscopes to achieve the required mapping accuracy. The weight of this technology, however, limited the range of UAV platforms on which these laser scanning systems could be deployed. A primary prerequisite for the sensor package of the UAVLS outlined in this thesis was to allow deployment on a commercially available mini-UAV. The gross weight of this system (2.4 kg) highlights further opportunities for UAVLS, by widening the available platforms on which a laser scanning system could be deployed. The repeatability of plot level metrics at flying heights of up to 50 m AGL highlights the flexibility of the system design for use in alternative sampling methodologies and fields. In this study, an OktoKopter was chosen due to its ability to fly low and slow and thus collect dense data,

however, deployment on lightweight fixed wing UAVs would offer greater coverage and should be investigated.

The accuracy of the direct georeferencing method developed in the thesis presents opportunities for use in direct georeferencing of other sensors to support forest inventory applications. Sensors such as visual, multispectral, and thermal cameras as well as hyperspectral cameras have all shown potential for monitoring forest conditions. Future research should focus on the simultaneous data collection of UAVLS with additional sensors to characterise the forest environment. Finally, the combination of UAVLS point clouds with complementary SfM point clouds should be investigated as an innovative tool for 3D mapping and monitoring purposes.

7.5 Final remarks

Although laser scanning has evolved into a common and reliable source of information within forest inventories, a low-cost method for the collection of data on-demand has not been available. Forest managers therefore often rely on information that is small in regards to the sample size, out-of-date or potentially suffers from bias and subjective interpretation. In meeting the three objectives of this thesis, it has been demonstrated that UAVLS surveys can overcome these limitations by offering an on-demand high resolution 3D sampling of forest structure.

The novel low-cost UAVLS system developed here, combined with methods for extracting forest metrics, enables high-density point clouds to be obtained that accurately represent current forest conditions. The efficiency, accuracy, and repeatability of this tool and associated processing methods have surpassed that of traditional field sampling techniques. The reliable non-subjective mapping and monitoring techniques presented in this thesis will provide forest managers with high resolution information on the 3D structure of forests when assessment of inventory is required. Although reliant on the ability to predict growth responses, the application of targeted silvicultural treatments based on the information provided by UAVLS systems will contribute to more precise forestry practices. This has the potential to allow for increases in timber quality and yield and contribute to future sustainable plantation forestry practices.

Improvements in the technology in the design of this UAVLS systems have already taken place at the time of writing, with the reported accuracies of new MEMs based IMUs improving by an order of magnitude. These improvements will enable similar UAVLS

systems to be developed commercially, providing researchers and forest managers with increasing capacity to map forest conditions on-demand and at key stages of growth throughout a rotation. The work presented in this thesis contributes to the evolution of UAV and laser scanning technology and its application to forest management.

References

Akay, A. E., Oğuz, H., Karas, I. R., and Aruga, K. (2009). Using LiDAR technology in forestry activities. *Environmental Monitoring and Assessment* 151 (1-4), pp. 117–125.

Alcorn, P. J., Forrester, D. I., Smith, R. G. B., Thomas, D. S., James, R., Nicotra, A. B., and Bauhus, J. (2013). The influence of site quality on timing of pruning in Eucalyptus pilularis and Eucalyptus cloeziana plantations. *Australian Forestry* 76 (1), pp. 25–36.

Alcorn, P. J., Bauhus, J., Thomas, D. S., James, R. N., Smith, R. G. B., and Nicotra, A. B. (2008). Photosynthetic response to green crown pruning in young plantation-grown Eucalyptus pilularis and E. cloeziana. *Forest Ecology and Management* 255 (11), pp. 3827–3838.

Alexander, C. (2009). Delineating tree crowns from airborne laser scanning point cloud data using Delaunay triangulation. *International Journal of Remote Sensing* 30 (14), pp. 3843–3848.

Andersen, E. and Taylor, C. (2007). Improving MAV pose estimation using visual information. *In Proceedings of IEEE/RSJ International Conference on Intelligent Robots and Systems*. San Diego, CA, USA, pp. 3745–3750.

Andersen, H.-E., Strunk, J., and Temesgen, H. (2011). Using airborne light detection and ranging as a sampling tool for estimating forest biomass resources in the upper Tanana Valley of Interior Alaska. *Western Journal of Applied Forestry* 26 (4), pp. 157–164.

Anderson, K. and Gaston, K. J. (2013). Lightweight unmanned aerial vehicles will revolutionize spatial ecology. *Frontiers in Ecology and the Environment* 11 (3), pp. 138 –146.

Axelsson, P. (1999). Processing of laser scanner data algorithms and applications. *ISPRS Journal of Photogrammetry and Remote Sensing* 54 (2-3), pp. 138–147.

Baltsavias, E. (1999). Airborne laser scanning: basic relations and formulas. *ISPRS Journal of Photogrammetry and Remote Sensing* 54 (2), pp. 199 –214.

Barazzetti, L, Remondino, F, and Scaioni, M (2010). Automation in 3D reconstruction: results on different kinds of close-range blocks. *In Proceedings of ISPRS - International Archives of the Photogrammetry, Remote Sensing and Spatial Information Sciences*. Vol. XXXVIII. 5. Newcastle upon Tyne, UK.

Bater, C. and Wulder, M. (2011). Stability of sample-based scanning-LiDAR-derived vegetation metrics for forest monitoring. *IEEE Transactions on Geoscience and Remote Sensing* 49 (6), pp. 2385–2392.

Bay, H., Tuytelaars, T., and Van Gool, L. (2006). Surf: Speeded up robust features. *Computer Vision–ECCV 2006*. Springer, pp. 404–417.

Ben-Arie, J. R., Hay, G. J., Powers, R. P., Castilla, G., and St-Onge, B. (2009). Development of a pit filling algorithm for LiDAR canopy height models. *Computers & Geosciences* 35 (9), pp. 1940–1949.

Berni, J. A. J., Zarco-Tejada, P. J., Suárez, L., and Fereres, E. (2009). Thermal and Narrowband Multispectral Remote Sensing for Vegetation Monitoring From an Unmanned Aerial Vehicle. *IEEE Transactions on Geoscience and Remote Sensing* 47 (3), pp. 722–738.

Bi, H., Fox, J., Li, Y., Lei, Y., and Pang, Y. (2012). Evaluation of nonlinear equations for predicting diameter from tree height. *Canadian Journal of Forest Research* 42 (4), pp. 789–806.

Bollandsas, O. (2013). Detection of biomass change in a Norwegian mountain forest area using small footprint airborne laser scanner data. *Statistical Methods and Applications* 22 (1), pp. 113–129.

Boudreau, J. and Nelson, R. (2008). Regional aboveground forest biomass using airborne and spaceborne LiDAR in Québec. *Remote Sensing of Environment* 112 (10), pp. 3876–3890.

Bouget, J.-Y. (2010). *Camera Calibration Toolbox for Matlab*.

Brandtberg, T (2003). Detection and analysis of individual leaf-off tree crowns in small footprint, high sampling density lidar data from the eastern deciduous forest in North America. *Remote Sensing of Environment* 85 (3), pp. 290–303.

Bryson, M. and Sukkarieh, S. (2011). A comparison of feature and pose-based mapping using vision, inertial and GPS on a UAV. *In Proceedings of 2011 IEEE/RSJ International Conference on Intelligent Robots and Systems (IROS)*. San Francisco, CA, USA, pp. 4256–4262.

Cassidy, M., Palmer, G., Glencross, K., Nichols, J., and Smith, R. (2012). Stocking and intensity of thinning affect log size and value in Eucalyptus pilularis. *Forest Ecology and Management* 264, pp. 220 –227.

Chiabrando, F., Nex, F., Piatti, D., and Rinaudo, F. (2011). UAV and RPV systems for photogrammetric surveys in archaelogical areas: two tests in the Piedmont region (Italy). *Journal of Archaeological Science* 38 (3), pp. 697–710.

Chiang, K.-W., Chang, H.-W., Li, C.-Y., and Huang, Y.-W. (2009). An Artificial Neural Network Embedded Position and Orientation Determination Algorithm for Low Cost MEMS INS/GPS Integrated Sensors. *Sensors* 9 (4), pp. 2586–2610.

Choi, K., Lee, I., Hong, J., Oh, T., and Shin, S. (2009). Developing a UAV-based rapid mapping system for emergency response. *In Proceedings of SPIE, Unmanned Systems Technology XI*. Orlando, Fl., USA.

Clark, M. L., Roberts, D. A., and Clark, D. B. (2005). Hyperspectral discrimination of tropical rain forest tree species at leaf to crown scales. *Remote Sensing of Environment* 96, pp. 375–398.

Coops, N. C., Black, T. A., Jassal, R. S., Trofymow, J. A., and Morgenstern, K. (2007). Comparison of MODIS, eddy covariance determined and physiologically modelled gross primary production (GPP) in a Douglas-fir forest stand. *Remote Sensing of Environment* 107 (3), pp. 385–401.

Corona, P., Kohl, M., and Marchetti, M. (2003). *Advances in Forest Inventory for Sustainable Forest Management and Biodiversity Monitoring*. Dordrecht: Kluwer Academic Publishers.

Crassidis, J. (2006). Sigma-point Kalman filtering for integrated GPS and inertial navigation. *IEEE Transactions on Aerospace and Electronic Systems* 42 (2), pp. 750–756.

Dandois, J. P. and Ellis, E. C. (2010). Remote Sensing of Vegetation Structure Using Computer Vision. *Remote Sensing* 2 (4), pp. 1157–1176.

— (2013). High spatial resolution three-dimensional mapping of vegetation spectral dynamics using computer vision. *Remote Sensing of Environment* 136, pp. 259 –276.

Dean, T., Cao, Q., Roberts, S., and Evans, D. (2009). Measuring heights to crown base and crown median with LiDAR in a mature, even-aged loblolly pine stand. *Forest Ecology and Management* 257 (1), pp. 126 –133.

Dellaert, F., Seitz, S. M., Thorpe, C. E., and Thrun, S. (2000). Structure from motion without correspondence. *In Proceedings of the IEEE International Conference on Computer Vision and Pattern Recognition (CVPR)*. Hilton Head, SC, USA, pp. 2557–2564.

Disney, M., Kalogirou, V., Lewis, P., Prieto-Blanco, a., Hancock, S., and Pfeifer, M. (2010). Simulating the impact of discrete-return lidar system and survey characteristics over young conifer and broadleaf forests. *Remote Sensing of Environment* 114 (7), pp. 1546–1560.

Donoghue, D. N., Watt, P. J., Cox, N. J., and Wilson, J. (2007). Remote sensing of species mixtures in conifer plantations using LiDAR height and intensity data. *Remote Sensing of Environment* 110 (4), pp. 509 –522.

Du, S. (2010). Integration of Precise Point Positioning and Low Cost MEMS IMU. Unpublished masters dissertation. University of Calgary, Calgary.

Dunford, R., Michel, K., Gagnage, M., Piegay, H., and Tremelo, M.-L. (2009). Potential and constraints of Unmanned Aerial Vehicle technology for the characterization of Mediterranean riparian forest. *International Journal of Remote Sensing* 30 (19), pp. 4915–4935.

Edelsbrunner, H. and Mücke, E. P. (1994). Three-dimensional alpha shapes. *ACM Transactions on Graphics* 13 (1), pp. 43–72.

Edson, C. and Wing, M. G. (2011). Airborne Light Detection and Ranging (LiDAR) for Individual Tree Stem Location, Height, and Biomass Measurements. *Remote Sensing* 3 (11), pp. 2494–2528.

Eisenbeiss, H. (2009). UAV Photogrammetry. PhD thesis. Institute of Geodesy and Photogrammetry, ETH Zurich.

El-Sheimy, N. (2009). Georeferencing Component of LiDAR Systems. *Topographic Laser Ranging and Scanning: Principles and Processing*. Ed. by J. Shan and C. Toth. Florida: Boca Raton.

El-Sheimy, N., Chiang, K.-W., and Noureldin, A. (2006). The Utilization of Artificial Neural Networks for Multisensor System Integration in Navigation and Positioning Instruments. *IEEE Transactions on Instrumentation and Measurement* 55 (5), pp. 1606–1615.

El-sheimy, N. (2009). Emerging MEMS IMU and Its Impact on Mapping Applications. *In Proceedings of Photogrammetric Week*. Stuttgart, Germany, pp. 203–216.

Ene, L., Næ sset, E., and Gobakken, T. (2012). Single tree detection in heterogeneous boreal forests using airborne laser scanning and area-based stem number estimates. *International Journal of Remote Sensing* 33 (16), pp. 37–41.

Erdody, T. L. and Moskal, L. M. (2010). Fusion of LiDAR and imagery for estimating forest canopy fuels. *Remote Sensing of Environment* 114 (4), pp. 725–737.

Ferraz, A., Bretar, F., Jacquemoud, S., Gonçalves, G., Pereira, L., Tomé, M., and Soares, P. (2012). 3-D mapping of a multi-layered Mediterranean forest using ALS data. *Remote Sensing of Environment* 121, pp. 210–223.

Fonstad, M. A., Dietrich, J. T., Courville, B. C., Jensen, J. L., and Carbonneau, P. E. (2013). Topographic structure from motion: a new development in photogrammetric measurement. *Earth Surface Processes and Landforms* 38 (4), pp. 421–430.

Forrester, D. I., Elms, S. R., and Baker, T. G. (2013a). Tree growth-competition relationships in thinned Eucalyptus plantations vary with stand structure and site quality. *European Journal of Forest Research* 132 (2), pp. 241–252.

Forrester, D., Wiedemann, J. C., Forrester, R. I., and Baker, T. G. (2013b). Effects of planting density and site quality on mean tree size and total stand growth of Euca-

lyptus globulus plantations. *Canadian Journal of Forest Research* 43 (9), pp. 846–851.

Frazer, G., Magnussen, S., Wulder, M., and Niemann, K. (2011). Simulated impact of sample plot size and co-registration error on the accuracy and uncertainty of LiDAR-derived estimates of forest stand biomass. *Remote Sensing of Environment* 115 (2), pp. 636 –649.

Gajdamowicz, K., Öhman, D., and Horemuz, M. (2007). Mapping and 3D modelling of urban environment based on lidar, gps/imu and image data. *In Proceedings of the 5th International Symposium on Mobile Mapping Technology*. Padova, Italy.

Gavrilets, V. (2003). Autonomous Aerobatic Maneuvering of Miniature Helicopters. PhD thesis. Massachusetts Institute of Technology, Massachusetts, USA.

Gerrand, A., Neilsen, W., and Medhurst, J. (1997). Thinning and pruning eucalypt plantations for sawlog production in Tasmania. *TasForests* 9, pp. 15 –34.

Gillis, M. D. (2001). Canada's National Forest Inventory (Responding to current information needs). *Environmental Monitoring and Assessment* 67 (1), pp. 121–129.

Glennie, C. (2007). Rigorous 3D error analysis of kinematic scanning LIDAR systems. *Journal of Applied Geodesy* 1, pp. 147–157.

Goodwin, N. R., Coops, N. C., and Culvenor, D. S. (2006). Assessment of forest structure with airborne LiDAR and the effects ofplatform altitude. *Remote Sensing of Environment* 103 (2), pp. 140–152.

Goulden, T. and Hopkinson, C. (2010). The Forward Propagation of Integrated System Component Errors within Airborne Lidar Data. *Photogrammetric Engineering & Remote Sensing* 5 (76), pp. 589–601.

Gupta, S., Weinacker, H., and Koch, B. (2010). Comparative Analysis of Clustering-Based Approaches for 3-D Single Tree Detection Using Airborne Fullwave Lidar Data. *Remote Sensing* 2 (4), pp. 968–989.

Habib, A., Bang, K., Kersting, A., and Chow, J. (2010). Alternative Methodologies for LiDAR System Calibration. *Remote Sensing* 2 (3), pp. 874 –907.

Hastie, T., Tibshirani, R., and Friedman, J. (2009). *The elements of statistical learning*. 2nd ed. Springer Series in Statistic. Springer, p. 268.

Heinzel, J. N., Weinacker, H., and Koch, B. (2011). Prior-knowledge-based single-tree extraction. *International Journal of Remote Sensing* 32 (17), pp. 4999–5020.

Hilker, T., Frazer, G., Coops, N., Wulder, M., Newnham, G., Stewart, J., Leeuwen, M. van, and Culvenor, D. (2013). Prediction of Wood Fiber Attributes from LiDAR-Derived Forest Canopy Indicators. *Forest Science* 59 (2), pp. 231–242.

Hol, J. D., Schon, T. B., and Gustafsson, F. (2010). Modeling and Calibration of Inertial and Vision Sensors. *International Journal of Robotics Research* 29 (2-3), pp. 231–244.

Holmgren, J and Persson, A (2004). Identifying species of individual trees using airborne laser scanner. *Remote Sensing of Environment* 90 (4), pp. 415–423.

Holmgren, J, Persson, Å, and Söderman, U (2008). Species identification of individual trees by combining high resolution LiDAR data with multi-spectral images. *International Journal of Remote Sensing* 29 (5), pp. 1537–1552.

Holmgren, J. (2004). Prediction of tree height, basal area and stem volume in forest stands using airborne laser scanning. *Scandinavian Journal of Forest Research* 19 (6), pp. 543–553.

Holopainen, M., Mäkinen, A., Rasinmäki, J., Hyyppä, J., Hyyppä, H., Kaartinen, H., Viitala, R., Vastaranta, M., and Kangas, A. (2010). Effect of tree-level airborne

laser-scanning measurement accuracy on the timing and expected value of harvest decisions. *European Journal of Forest Research* 129 (5), pp. 899–907.

Holopainen, M., Kankare, V., Vastaranta, M., Liang, X., Lin, Y., Vaaja, M., Yu, X., Hyyppä, J., Hyyppä, H., Kaartinen, H., Kukko, A., Tanhuanpää, T., and Alho, P. (2013). Tree mapping using airborne, terrestrial and mobile laser scanning - A case study in a heterogeneous urban forest. *Urban Forestry & Urban Greening*.

Hopkinson, C (2008). The uncertainty in conifer plantation growth prediction from multi-temporal lidar datasets. *Remote Sensing of Environment* 112 (3), pp. 1168–1180.

Hopkinson, C., Chasmer, L., Young-Pow, C., and Treitz, P. (2004). Assessing forest metrics with a ground-based scanning lidar. *Canadian Journal of Forest Research* 34 (3), pp. 573–583.

Horcher, A. and Visser, R. (2004). Unmanned Aerial Vehicles: Applications for Natural Resource Management and Monitoring. *In Council on Forest Engineering Proceedings 2004: Machines and People*.

Hudak, A. T., Crookston, N. L., Evans, J. S., Hall, D. E., and Falkowski, M. J. (2008). Nearest neighbor imputation of species-level, plot-scale forest structure attributes from LiDAR data. *Remote Sensing of Environment* 112 (5), pp. 2232–2245.

Hunt Jr, E., Hively, W., Fujikawa, S., Linden, D., Daughtry, C., and McCarty, G. (2010). Acquisition of NIR-Green-Blue Digital Photographs from Unmanned Aircraft for Crop Monitoring. *Remote Sensing* 2 (1), pp. 290–305.

Hyyppä, J. and Inkinen, M. (1999). Detection and estimating attributes for single trees using laser scanner. *Photogrammetric Journal of Finland* 16, pp. 27–42.

Hyyppä, J., Schardt, M., Haggrén, H., Koch, B., Lohr, U., Scherrer, H., Paananen, R., Luukkonen, H., Ziegler, M., Hyyppä, H., Pyysalo, U., Friedländer, H., Uuttera, J., Wagner, S., Inkinen, M., Wimmer, A., Kukko, A., Ahokas, E., and Karjalainen, M. (2001). HIGH-SCAN: The first European-wide attempt to derive single-tree information from laserscanner data. *The Photogrammetric Journal of Finland* 17, pp. 58–68.

Hyyppä, J., Hyyppä, H., Leckie, D., Gougeon, F., Yu, X., and Maltamo, M. (2008). Review of methods of small-footprint airborne laser scanning for extracting forest inventory data in boreal forests. *International Journal of Remote Sensing* 29 (5), pp. 1339–1366.

Hyyppä, J., Yu, X., Hyyppä, H., Vastaranta, M., Holopainen, M., Kukko, A., Kaartinen, H., Jaakkola, A., Vaaja, M., Koskinen, J., and Alho, P. (2012a). Advances in Forest Inventory Using Airborne Laser Scanning. *Remote Sensing* 4 (5), pp. 1190–1207.

Hyyppä, J., Holopainen, M., and Olsson, H. k. (2012b). Laser Scanning in Forests. *Remote Sensing* 4 (10), pp. 2919–2922.

Innes, T., Greaves, B., Washusen, R., and Nolan, G. (2008). *Determining the economics of processing plantation eucalypts for solid timber products. Forest and Wood Products*. Tech. rep. Forest and Wood Products Australia.

Isenberg, M. (2011). *LAStools - efficient tools for LiDAR processing*. Available online: http://www.cs.unc.edu/ isenburg/lastools/ (accessed on 15 December 2011).

Jaakkola, A., Hyyppä, J., Kukko, A., Yu, X., Kaartinen, H., Lehtomäki, M., and Lin, Y. (2010). A low-cost multi-sensoral mobile mapping system and its feasibility for tree measurements. *ISPRS Journal of Photogrammetry and Remote Sensing* 65 (6), pp. 514–522.

Kaartinen, H., Hyyppä, J., Yu, X., Vastaranta, M., Hyyppä, H., Kukko, A., Holopainen, M., Heipke, C., Hirschmugl, M., Morsdorf, F., Næsset, E., Pitkänen, J., Popescu,

S., Solberg, S., Wolf, B. M., and Wu, J.-C. (2012). An International Comparison of Individual Tree Detection and Extraction Using Airborne Laser Scanning. *Remote Sensing* 4 (4), pp. 950–974.

Kelly, J. and Sukhatme, G. (2009). Visual-inertial simultaneous localization, mapping and sensor-to-sensor self-calibration. *In Proceedings of 2009 IEEE International Symposium on Computational Intelligence in Robotics and Automation*. Daejeon,Korea, pp. 360 –368.

Kitahara, F., Mizoue, N., and Yoshida, S. (2010). Effects of training for inexperienced surveyors on data quality of tree diameter and height measurements. *Silva Fennica* 44 (4), pp. 6–10.

Koch, B., Heyder, U., and Weinacker, H. (2006). Detection of individual tree crowns in airborne LiDAR data. *Photogrammetric engineering & Remote Sensing* 72 (4), pp. 357 –363.

Korhonen, L., Vauhkonen, J., Virolainen, A., Hovib, A., and Korpela, I. (2013). Estimation of tree crown volume from airborne lidar data using computational geometry. *International Journal of Remote Sensing* 34 (20), pp. 7236–7248.

Lahivaara, T., Seppanen, A., Kaipio, J. P., Vauhkonen, J., Korhonen, L., Tokola, T., and Maltamo, M. (2012). Bayesian approach to tree detection with airborne laser scanning. *In Proceeding of the 2012 IEEE International Geoscience and Remote Sensing Symposium*. Munich, Germany, pp. 1641–1644.

Laliberte, A. S., Goforth, M. A., Steele, C. M., and Rango, A. (2011). Multispectral Remote Sensing from Unmanned Aircraft: Image Processing Workflows and Applications for Rangeland Environments. *Remote Sensing* 3 (11).

Larsen, M., Eriksson, M., and Descombes, X. (2011). Comparison of six individual tree crown detection algorithms evaluated under varying forest conditions. *International Journal of Remote Sensing* 32 (20), pp. 5827–5852.

Lee, D.-J., Merrell, P., Wei, Z., and Nelson, B. E. (2010). Two-frame structure from motion using optical flow probability distributions for unmanned air vehicle obstacle avoidance. *Machine Vision and Applications* 21 (3), pp. 229–240.

Lefsky, M., Cohen, W., Parker, G., and Harding, D. (2002). Lidar remote sensing for ecosystem studies. *Bioscience* 52 (1), pp. 19–30.

Li, J., Hu, B., and Noland, T. (2013). Classification of tree species based on structural features derived from high density LiDAR data. *Agricultural and Forest Meteorology* 171-172, pp. 104–114.

Li, W. and Guo, Q. (2012). A new method for segmenting individual trees from the lidar point cloud. *Photogrammetric Engineering & Remote Sensing* 78 (1), pp. 75–84.

Liang, X., Hyyppä, J., Kaartinen, H., Holopainen, M., and Melkas, T. (2012). Detecting changes in forest structure over time with bi-temporal terrestrial laser scanning data. *ISPRS International Journal of Geo-Information* 1 (3), pp. 242–255.

Lichti, D. and Gordon, S. J. (2004). Error Propagation in Directly Georeferenced Terrestrial Laser Scanner Point Clouds for Cultural Heritage Recording. *In Proceedings of FIG Working Week 2004*. Athens, Greece.

Lim, K. S. and Treitz, P. M. (2004). Estimation of above ground forest biomass from airborne discrete return laser scanner data using canopy-based quantile estimators. *Scandinavian Journal of Forest Research* 19 (6), pp. 558 –570.

Lim, K., Treitz, P., Wulder, M., St-Onge, B., and Flood, M. (2003). LiDAR remote sensing of forest structure. *Progress in Physical Geography* 27 (1), pp. 88–106.

Lin, Y., Hyyppä, J., Kukko, A., Jaakkola, A., and Kaartinen, H. (2012). Tree height growth measurement with single-scan airborne, static terrestrial and mobile laser scanning. *Sensors* 12 (9), pp. 12798–12813.

Lin, Y., Hyyppä, J., and Jaakkola, A. (2011). Mini-UAV-borne LIDAR for fine-scale mapping. *IEEE Transactions on Geoscience and Remote Sensing* 8 (99), pp. 426–430.

Lovell, J., Jupp, D., Newnham, G., Coops, N., and Culvenor, D. (2005). Simulation study for finding optimal lidar acquisition parameters for forest height retrieval. *Forest Ecology and Management* 214 (1-3), pp. 398–412.

Lowe, D. (2004). Distinctive image features from scale-invariant keypoints. *International Journal of Computer Vision* 60 (2), pp. 91–110.

Lucieer, A., Turner, D., King, D. H., and Robinson, S. A. (2014). Using an Unmanned Aerial Vehicle (UAV) to capture micro-topography of Antarctic moss beds. *International Journal of Applied Earth Observation and Geoinformation* 27, pp. 53–62.

Maas, H., Bienert, A., Scheller, S., and Keane, E. (2008). Automatic forest inventory parameter determination from terrestrial laser scanner data. *International Journal of Remote Sensing* 29 (5), pp. 1579–1593.

Macfarlane, C., Grigg, A., and Evangelista, C. (2007). Estimating forest leaf area using cover and fullframe fisheye photography: Thinking inside the circle. *Agricultural and Forest Meteorology* 146 (1-2), pp. 1–12.

Maclean, G. A. and Martin, G. L. (1984). Merchantable timber volume estimation using cross-sectional photogrammetric and densitometric methods. *Canadian Journal of Forest Research* 6 (6), pp. 803–810.

Magnussen, S., Næsset, E., and Gobakken, T. (2010). Reliability of LiDAR derived predictors of forest inventory attributes: A case study with Norway spruce. *Remote Sensing of Environment* 114 (4), pp. 700 –712.

Magnussen, S., Næsset, E, Gobakken, T, and Frazer, G (2012). A fine-scale model for area-based predictions of tree-size-related attributes derived from LiDAR canopy heights. *Scandinavian Journal of Forest Research* 27 (3), pp. 312–322.

Maltamo, M., Packalén, P., Yu, X., Eerikäinen, K., Hyyppä, J., and Pitkänen, J. (2005). Identifying and quantifying structural characteristics of heterogeneous boreal forests using laser scanner data. *Forest Ecology and Management* 216 (1-3), pp. 41–50.

Maltamo, M., Bollandsas, O. M., Vauhkonen, J., Breidenbach, J., Gobakken, T., and Næsset, E. (2010). Comparing different methods for prediction of mean crown height in Norway spruce stands using airborne laser scanner data. *Forestry* 83 (3), pp. 257–268.

Maltamo, M., Mehtätalo, L., Vauhkonen, J., and Packalén, P. (2012). Predicting and calibrating tree attributes by means of airborne laser scanning and field measurements. *Canadian Journal of Forest Research* 42 (11), pp. 1896 –1907.

Maltamo, M., Peuhkurinen, J., Malinen, J., Vauhkonen, J., Packalén, P., and Tokola, T. (2009). Predicting tree attributes and quality characteristics of Scots pine using airborne laser scanning data. *Silva Fennica* 43 (3), pp. 507–521.

Mandallaz, D. (2007). *Sampling techniques for forest inventories*. Taylor & Francis.

May, N. and Toth, C. (2007). Point positioning accuracy of airborne LiDAR systems: A rigorous analysis. *International Archives of Photogrammetry, Remote Sensing and Spatial Information Sciences* 36 (pt 3), pp. 107–111.

McRoberts, R. E., Gobakken, T., and Næsset, E. (2012). Post-stratified estimation of forest area and growing stock volume using lidar-based stratifications. *Remote Sensing of Environment* 125, pp. 157–166.

Medhurst, J. L. and Beadle, C. L. (2001). Crown structure and leaf area index development in thinned and unthinned Eucalyptus nitens plantations. *Tree Physiology* 21 (12–13), pp. 989–999.

Meng, X., Currit, N., and Zhao, K. (2010). Ground Filtering Algorithms for Airborne LiDAR Data: A Review of Critical Issues. *Remote Sensing* 2 (3), pp. 833–860.

Miller, R. and Amidi, O. (1998). 3-D Site Mapping with the CMU Autonomous Helicopter 3-D Site Mapping with the CMU Autonomous Helicopter. *In Proceedings of the 5th International Conference on Intelligent Autonomous Systems*. Sapparo, Japan.

Montagu, K., Kearney, D., and Smith, R. (2003). The biology and silviculture of pruning planted eucalypts for clear wood production: a review. *Forest Ecology and Management* 179 (1-3), pp. 1–13.

Morin, K. W. (2002). Calibration of airborne laser scanners. MA thesis. University of Calgary, Calgary.

Morsdorf, F., Kötz, B., Meier, E., Itten, K., and Allgöwer, B. (2006). Estimation of LAI and fractional cover from small footprint airborne laser scanning data based on gap fraction. *Remote Sensing of Environment* 104 (1), pp. 50–61.

Morsdorf, F., Meier, E., Allgöwer, B., and Nüesch, D. (2003). Clustering in airborne laser scanning raw data for segmentation of single trees. *International Archives of Photogrammetry, Remote Sensing and Spatial Information Sciences* 34 (part 3), pp. 27–33.

Morsdorf, F., Nichol, C., Malthus, T., and Woodhouse, I. H. (2009). Assessing forest structural and physiological information content of multi-spectral LiDAR waveforms by radiative transfer modelling. *Remote Sensing of Environment* 113 (10), pp. 2152–2163.

Muñoz, F., Rubilar, R., Espinosa, M., Cancino, J., Toro, J., and Herrera, M. (2008). The effect of pruning and thinning on above ground aerial biomass of Eucalyptus nitens (Deane & Maiden) Maiden. *Forest Ecology and Management* 255 (3-4), pp. 365–373.

Musk, R. and Osborn, J. (2007). Timber inventory in wet eucalypt forest using small footprint LiDAR. *In Proceedings of Spatial Science Institute Biennial International Conference*. Hobart, Australia, pp. 987–1001.

Næsset, E. (1997). Estimating timber volume of forest stands using airborne laser scanner data. *Remote Sensing of Environment* 61 (2), pp. 246–259.

Næsset, E. and Gobakken, T. (2005). Estimating forest growth using canopy metrics derived from airborne laser scanner data. *Remote Sensing of Environment* 96 (3-4), pp. 453–465.

Næsset, E., Bollandsas, O., Gobakken, T., Gregoire, T., and Ståhl, G. (2013). Model-assisted estimation of change in forest biomass over an 11 year period in a sample survey supported by airborne LiDAR: A case study with post-stratification to provide 'activity data'. *Remote Sensing of Environment* 128, pp. 299–314.

Næsset, E. (2002). Predicting forest stand characteristics with airborne scanning laser using a practical two-stage procedure and field data. *Remote Sensing of Environment* 80, pp. 88–99.

Nagai, M., Shibasaki, R., Kumagai, H., and Ahmed, A. (2009). UAV-borne 3-D mapping system by multisensor integration. *IEEE Transactions on Geoscience and Remote Sensing* 47 (3), pp. 701–708.

Nelson, R., Krabill, W., and Tonelli, J. (1988). Estimating forest biomass and volume using airborne laser data. *Remote Sensing of Environment* 24, pp. 247–267.

Nelson, R., Valenti, M., Short, A., and Keller, C. (2003). A multiple resource inventory of delaware using airborne laser data. *BioScience* 53 (10), pp. 981 –992.

Niethammer, U, James, M., Rothmund, S, Travelletti, J, and Joswig, M (2012). UAV-based remote sensing of the Super-Sauze landslide: Evaluation and results. *Engineering Geology* 128, pp. 2–11.

Nistér, D. (2004). An efficient solution to the five-point relative pose problem. *IEEE Transactions on Pattern Analysis and Machine Intelligence* 26 (6), pp. 756–770.

Nyström, M., Holmgren, J., and Olsson, H (2013). Change detection of mountain birch using multi-temporal ALS point clouds. *Remote Sensing Letters* 4 (2), pp. 37–41.

Ørka, H., Gobakken, T., Næsset, E., Ene, L., and Lien, V. (2012). Simultaneously acquired airborne laser scanning and multispectral imagery for individual tree species identification. *Canadian Journal of Forest Research* 38 (2), pp. 125–138.

Packalén, P. and Maltamo, M. (2007). The k-MSN method for the prediction of species-specific stand attributes using airborne laser scanning and aerial photographs. *Remote Sensing of Environment* 109 (3), pp. 328–341.

Persson, A., Holmgren, J., and Soderman, U. (2002). Detecting and Measuring Individual Trees Using an Airborne Laser Scanner. *Photogrammetric Engineering & Remote Sensing* 68 (9), pp. 925–932.

Petrie, G. and Toth, C. (2009). Airborne and Spaceborne Laser Profilers and Scanners. *Topographic Laser Ranging and Scanning: Principles and Processing*. Ed. by J. Shan and C. Toth. Florida: Boca Raton.

Peuhkurinen, J., Mehtätalo, L., and Maltamo, M. (2011). Comparing individual tree detection and the area-based statistical approach for the retrieval of forest stand characteristics using airborne laser scanning in Scots pine stands. *Canadian Journal of Forest Research* 41 (3), pp. 583–598.

Pinkard, E. and Beadle, C. L. (1998). Effects of green pruning on growth and stem shape of Eucalyptus nitens(Deane and Maiden) Maiden. *New Forests* 15, pp. 107 –126.

Pinkard, E. (2002). Effects of pattern and severity of pruning on growth and branch development of pre-canopy closure Eucalyptus nitens. *Forest Ecology and Management* 157 (1-3), pp. 217–230.

Pinkard, E., Mohammed, C., Beadle, C., Hall, M., Worledge, D., and Mollon, A. (2004). Growth responses, physiology and decay associated with pruning plantation-grown Eucalyptus globulus Labill. and E. nitens (Deane and Maiden) Maiden. *Forest Ecology and Management* 200 (1-3), pp. 263–277.

Pitkanen, J, Maltamo, M., Hyypp, and Yu, X (2004). Adaptive Methods for Individual Tree Detection on Airborne Laser Based Canopy Height Model. *In Proceedings of ISPRS Workshop Laser-Scanners for Forest and Landscape Assessment*. Freiburg, Germany, pp. 187–191.

Popescu, S. C. (2007). Estimating biomass of individual pine trees using airborne lidar. *Biomass and Bioenergy* 31 (9), pp. 646–655.

Popescu, S. C. and Zhao, K. (2008). A voxel-based lidar method for estimating crown base height for deciduous and pine trees. *Remote Sensing of Environment* 112 (3), pp. 767–781.

Pyysalo, U and Hyyppa, H (2002). Reconstructing tree crowns from laser scanner data for feature extraction. *The International Archives of the Photogrammetry, Remote Sensing and Spatial Information Science, vol. XXXIV, Part 3AISPRS Commission III Symposium*. Graz, pp. 218–221.

Raber, G., Jensen, J., Hodgson, M. E., Tullis, J., Davis, B., and Berglund, J (2007). Impact of LiDAR nominal post-spacing on DEM accuracy and flood zone delineation. *Photogrammetric Engineering & Remote Sensing* 73 (7), pp. 793–804.

Reitberger, J, Schnörr, C, Krzystek, P, and Stilla, U (2009). 3D segmentation of single trees exploiting full waveform LIDAR data. *ISPRS Journal of Photogrammetry and Remote Sensing* 64 (6), pp. 561–574.

Roberts, S. D., Dean, T. J., Evans, D. L., McCombs, J. W., Harrington, R. L., and Glass, P. A. (2005). Estimating individual tree leaf area in loblolly pine plantations using LiDAR-derived measurements of height and crown dimensions. *Forest Ecology and Management* 213 (1-3), pp. 54–70.

Rosenqvist, A., Milne, A., Lucas, R., Imhoff, M., and Dobson, C. (2003). A review of remote sensing technology in support of the Kyoto protocol. *Environmental Science & Policy* 6, pp. 441–455.

Rutzinger, M., Pratihast, A. K., Oude Elberink, S. J., and Vosselman, G. (2011). Tree modelling from mobile laser scanning data-sets. *The Photogrammetric Record* 26 (135), pp. 361–372.

Schaer, P., Skaloud, J., Landtwing, S., and Legat, K. (2007). Accuracy estimation for laser point cloud including scanning geometry. *In Proceedings of 5th International Symposium on Mobile Mapping Technology (MMT2007)*. Padua, Italy.

Schwarz, K. and El-Sheimy, N. (2004). Mobile Mapping Systems State of the art and future trends. *International Archives of Photogrammetry, Remote Sensing and Spatial Information Sciences* 35 (Part B), p. 10.

Shin, E. (2004). An unscented Kalman filter for in-motion alignment of low-cost IMUs. *In Proceedings of the Position Location and Navigation Symposium*. Huntsville, AL, USA, pp. 273 –279.

Shrestha, R. and Wynne, R. H. (2012). Estimating Biophysical Parameters of Individual Trees in an Urban Environment Using Small Footprint Discrete-Return Imaging Lidar. *Remote Sensing* 4 (2), pp. 484–508.

Snavely, N., Seitz, S. M., and Szeliski, R. (2006). Photo tourism: exploring photo collections in 3D. *ACM Transactions on Graphics* 25 (3), pp. 835–846.

Solberg, S., Næsset, E., Hanssen, K., and Christiansen, E. (2006a). Mapping defoliation during a severe insect attack on Scots pine using airborne laser scanning. *Remote Sensing of Environment* 102 (3-4), pp. 364–376.

Solberg, S., Næsset, E., and Bollandsas, O. (2006b). Single tree segmentation using airborne laser scanner data in a structurally heterogeneous spruce forest. *Photogrammetric Engineering & Remote Sensing* 72 (12), pp. 1369–1378.

Ståhl, G., Holm, S., Gregoire, T., Gobakken, T., Næsset, E., and Nelson, R. (2011). Model-based inference for biomass estimation in a LiDAR sample survey in Hedmark County, Norway. *Canadian Journal of Forest Research* 41 (1), pp. 96–107.

Sugiura, R, Noguchi, N, and Ishii, K (2005). Remote-sensing Technology for Vegetation Monitoring using an Unmanned Helicopter. *Biosystems Engineering* 90 (4), pp. 369–379.

Tao, W., Lei, Y., and Mooney, P. (2011). Dense point cloud extraction from UAV captured images in forest area. *In Proceedings of the 2011 IEEE International Conference on Spatial Data Mining and Geographical Knowledge Services*. Fuzhou, China, pp. 389–392.

Van Der Merwe, R. (2004). Sigma-point Kalman filters for probabilistic inference in dynamic state-space models. PhD thesis. Oregon Health and Science University, Oregon, USA.

Van Der Merwe, R. and Wan, E. (2004). Sigma-point Kalman filters for integrated navigation. *In Proceedings of the 60th Annual Meeting of the Institute of Navigation (ION)*. Dayton, Ohio, USA, pp. 641–654.

Vastaranta, M., Holopainen, M., Yu, X., Hyyppä, J., Mäkinen, A., Rasinmäki, J., Melkas, T., Kaartinen, H., and Hyyppä, H. (2011). Effects of Individual Tree Detection Error Sources on Forest Management Planning Calculations. *Remote Sensing* 3 (8), pp. 1614–1626.

Vastaranta, M., Kantola, T., Lyytikäinen-Saarenmaa, P., Holopainen, M., Kankare, V., Wulder, M., Hyyppä, J., and Hyyppä, H. (2013). Area-Based Mapping of Defoliation of Scots Pine Stands Using Airborne Scanning LiDAR. *Remote Sensing* 5 (3), pp. 1220–1234.

Vaughn, N. R., Moskal, L. M., and Turnblom, E. C. (2012). Tree Species Detection Accuracies Using Discrete Point Lidar and Airborne Waveform Lidar. *Remote Sensing* 4 (2), pp. 377–403.

Vauhkonen, H. (2010a). Estimating single-tree attributes by airborne laser scanning: methods based on computational geometry of the 3-D point data. PhD thesis. School of Forest Sciences, Faculty of Science and Forestry, University of Eastern Finland.

Vauhkonen, J. (2010b). Estimating crown base height for Scots pine by means of the 3D geometry of airborne laser scanning data. *International Journal of Remote Sensing* 31 (5), pp. 1213–1226.

Vauhkonen, J., Tokola, T., Maltamo, M., and Packalén, P. (2008). Effects of pulse density on predicting characteristics of individual trees of Scandinavian commercial species using alpha shape metrics based on airborne laser scanning data. *Canadian Journal of Remote Sensing* 34, S441–S459.

Vauhkonen, J., Mehtätalo, L., and Packalén, P (2011a). Combining tree height samples produced by airborne laser scanning and stand management records to estimate plot volume in Eucalyptus plantations. *Canadian Journal of Forest Research* 41 (8), pp. 1649–1658.

Vauhkonen, J., Ene, L., Gupta, S., Heinzel, J., Holmgren, J., Pitkanen, J., Solberg, S., Wang, Y., Weinacker, H., Hauglin, K. M., Lien, V., Packalen, P., Gobakken, T., Koch, B., Næsset, E., Tokola, T., and Maltamo, M. (2011b). Comparative testing of single-tree detection algorithms under different types of forest. *Forestry* 85 (1), pp. 27–40.

Vepakomma, U, St-Onge, B, and Kneeshaw, D (2008). Spatially explicit characterization of boreal forest gap dynamics using multi-temporal lidar data. *Remote Sensing of Environment* 112 (5), pp. 2326–2340.

Wallace, L. (2013). Assessing the stability of canopy maps produced from UAV-LiDAR data. *In Proceedings of of the IEEE International Geoscience and Remote Sensing Symposium*. Melbourne, Australia.

Wallace, L., Lucieer, A., and Watson, C. (2012a). Assessing the feasibility of UAV-based lidar for high resolution forest change detection. *In Proceedings of ISPRS - International Archives of the Photogrammetry, Remote Sensing and Spatial Information Sciences Vol. XXXIX-B7*, pp. 499–504.

Wallace, L., Lucieer, A., Watson, C., and Turner, D. (2012b). Development of a UAV-LiDAR System with Application to Forest Inventory. *Remote Sensing* 4 (6), pp. 1519–1543.

Wallace, L., Watson, C., and Lucieer, A. (2014). Detecting pruning of individual stems using Airborne Laser Scanning data captured from an Unmanned Aerial Vehicle.

International Journal of Applied Earth Observation and Geoinformation 30, pp. 76–85.

Wallace, L., Musk, R., and Lucieer, A. (Accepted for publication[a]). An assessment of the repeatability of automatic forest inventory metrics derived from UAV-borne laser scanning data. *IEEE Transactions on Geoscience and Remote Sensing*.

Wallace, L., Lucieer, A., and C., W. (Accepted for publication[b]). Evaluating tree detection and segmentation routines on very high resolution UAV LiDAR data. *IEEE Transactions on Geoscience and Remote Sensing*.

Wallace, L., Lucieer, A., Turner, D., and Watson, C. (2011). Error assessment and mitigation for hyper-temporal UAV-borne LiDAR surveys of forest inventory. *In Proceedings of Silvilaser 2011*. Hobart, Australia.

Wan, E. and Van Der Merwe, R. (2000). The unscented Kalman filter for nonlinear estimation. *In Proceedings of the IEEE 2000 Adaptive Systems for Signal Processing, Communications, and Control Symposium*. Lake Louise, Alberta, Canada, pp. 153–158.

Wang, Y., Weinacker, H., Koch, B., and Sterenczak, K (2008). Lidar point cloud based fully automatic 3D single tree modelling in forest and evaluations of the procedure. *International Archives of Photogrammetry, Remote Sensing and Spatial Information Sciences* XXXVII (B6b).

Watts, A. C., Ambrosia, V. G., and Hinkley, E. A. (2012). Unmanned Aircraft Systems in Remote Sensing and Scientific Research: Classification and Considerations of Use. *Remote Sensing* 4 (6), pp. 1671–1692.

Westoby, M., Brasington, J., Glasser, N., Hambrey, M., and Reynolds, J. (2012). âĂŸStructure-from-MotionâĂŹ photogrammetry: A low-cost, effective tool for geoscience applications. *Geomorphology* 179, pp. 300–314.

Wills, A. J., Burbidge, T. E., and Abbott, I. (2004). Impact of repeated defoliation on jarrah (Eucalyptus marginata) saplings. *Australian Forestry* 67 (3), pp. 194–198.

Wood, M., McLarin, M., Volker, P., and Syme, M. (2009). Management of eucalypt plantations for profitable sawlog production in Tasmania, Australia. *TasForests* 18, pp. 117–130.

Wulder, M., Bater, C., and Coops, N. (2008). The role of LiDAR in sustainable forest management. *The Forestry Chronicle* 84 (6).

Wulder, M., White, J., Nelson, R., Næsset, E., Ørka, H., Coops, N., Hilker, T., Bater, C., and Gobakken, T. (2012). Lidar sampling for large-area forest characterization: A review. *Remote Sensing of Environment* 121, pp. 196–209.

Xie, Y., Sha, Z., and Yu, M. (2008). Remote sensing imagery in vegetation mapping: a review. *Journal of Plant Ecology* 1 (1), pp. 9–23.

Xing, Y., Gier, A. de, Zhang, J., and Wang, L. (2010). An improved method for estimating forest canopy height using ICESat-GLAS full waveform data over sloping terrain: A case study in Changbai mountains, China. *International Journal of Applied Earth Observation and Geoinformation* 12 (5), pp. 385–392.

Yao, W., Krzystek, P., and Heurich, M. (2012). Tree species classification and estimation of stem volume and DBH based on single tree extraction by exploiting airborne full-waveform LiDAR data. *Remote Sensing of Environment* 123, pp. 368–380.

Yu, X., Hyyppä, J., Kaartinen, H., Maltamo, M., and Hyyppä, H. (2008). Obtaining plotwise mean height and volume growth in boreal forests using multi-temporal laser surveys and various change detection techniques. *International Journal of Remote Sensing* 29 (5), pp. 1367–1386.

Yu, X., Hyyppä, J., Vastaranta, M., Holopainen, M., and Viitala, R. (2011). Predicting individual tree attributes from airborne laser point clouds based on the random forests technique. *ISPRS Journal of Photogrammetry and Remote Sensing* 66 (1), pp. 28–37.

Zhang, H., Wu, Y., Wu, W., Wu, M., and Hu, X. (2010). Improved multi-position calibration for inertial measurement units. *Measurement Science and Technology* 21 (1), pp. 15107–15117.